Thermal properties of reservoir rocks, role of pore fluids, minerals and digenesis. A comparative study of two differently indurated chalks

by

Tijana Voake

Thesis submitted in fulfilment of
the requirements for the degree of
PHILOSOPHIAE DOCTOR
(PhD)

University
of Stavanger

Faculty of Science and Technology
Institute of Energy Resources
2020

Acknowledgements

I would like to express my deep gratitude and appreciation to my supervisors Dr. Anders Nermoen and Prof. Ida Lykke Fabricius for their guidance, assistance and support. Thank you for the trust you put in me and encouraged me to present my work at different conferences around the world. I would also like to thank Reidar Inge Korsnes and Kim Andre N. Vorland for their guidance and help in the laboratory works.

I would like to thank my parents, Mirjana and Branko Livada, for always being by my side and their full support along my long educational path. I thank my husband Alexander for making me apply for this opportunity, believe in myself, cheering me on, proof reading and making this journey an unforgettable one. And finally, I would like to thank out little daughter Martha for making this experience even more meaningful.

Summary

Carbonate rocks are distressed by temperature fluctuations, most commonly observed in marble monuments and cladding exposed to varying outdoor temperatures. Similarly, reservoir rocks are cooled on periodic basises during oil production by injecting cold fluid, locally cooling the surrounding reservoir rock. The rock will then reheat to its original temperature when the injection stops. These temperature fluctuations can potentially cause deformation to the reservoir and change its mechanical properties, which must be taken into consideration during the recovery.

This body of work focuses on chalk reservoirs, where the proposed effect could be of importance because the main building agent of chalk is calcite, which has a highly anisotropic thermal expansion coefficient. Thus, temperature fluctuations could strain the grain contacts between neighbouring particles. To gain a better understanding of stress accumulation at the contact level, two chalks with differing degrees of contact cement are compared; higher indurated chalk from a quarry in Kansas (USA) and a low indurated chalk originating from Mons (Belgium). The interpretation of temperature dependence is based upon the analysis of three different series of experiments, each providing different mechanical parameter estimates relating to: tensile strength, elasto-plastic partitioning during hydrostatic stress cycles, and elastic moduli (Bulk modulus, Young's modulus and shear modulus).

The influence of temperature cycling on tensile strength was tested using samples from the two chalk types in dry and water saturated states, and then exposed to 0, 15, and 30 temperature cycles. The dry samples were not influenced by temperature cycling for either of the chalk types. However, in the water saturated state, tensile strength is increasingly reduced with a progressive number of temperature cycles for both chalks.

The effect of temperature cycling was further examined by hydrostatic stress cycling in order to compare their mechanical responses. The two types of chalk were saturated by two different fluids to additionally determine the importance of water weakening. During a hydrostatic stress cycle, the total volumetric strain is partitioned into a reversible (elastic) and irreversible (plastic) component. Here, the fraction of irreversible strain during each stress cycle is reported and compared for the two chalks and two saturating fluids. All tests exposed to temperature cycling between each stress cycle accumulated more irreversible strain, the biggest difference was observed for the water saturated, highly indurated, Kansas chalk.

Using the samples from the two types of chalks, the dependence of elastic moduli on temperature cycling was investigated. The bulk modulus tested under hydrostatic conditions did not show significant dependence on increasing numbers of temperature cycles for Kansas chalk, but the modulus for Mons chalk demonstrated a decreasing trend with increasing numbers of temperature cycles. Young's modulus and compression modulus measured under confined constant overburden

stress showed no effect with increasing numbers of temperature cycles. Thermal linear expansion coefficient had a decreasing trend with increasing number of temperature cycles.

In response to temperature variation, the anisotropic thermal expansion of calcite crystals induces thermal stress that resulted in the accumulation of irreversible strain and decrease of tensile strength. This was especially pronounced in water saturated samples. Water is a polar fluid and has an electrical charge, so an electrical exchange with the calcite surface occurs. This creates a so called electrical double layer, whose thickness is assumed to be directly proportional to the Debye length. The thickness of Debye length is seen to depend on temperature, increasing with increasing temperature. When the temperature is increased, due to the increase of the double layer, the area of repulsion between two neighbouring particles is also increased. It is proposed that fluctuating the length of charged double layer has a permanent damage on chalk through increasing the number of micro fractures.

Another contributing factor as to why temperature cycling enhances weakening in water saturated chalk samples rather than dry or Isopar H saturated samples, is that the surface energy γ_s of the main calcite cleavage plane $\{10\bar{1}4\}$ depends on the presence of water. The surface energy of dry and fully hydrated calcite surfaces are 0.32 J/m^2 and 0.15 J/m^2 respectively. Hence, the energy necessary to form a dry surface (fracture) is double the energy required for a formation of wet surface.

List of publication

Papers:

Paper I:

Voake, T., Nermoen, A., Ravnas, C., Korsnes, R.I., Fabricius, I.L. (2019).

Influence of temperature cycling and pore fluid on tensile strength of chalk. *Journal of Rock Mechanics and Geotechnical Engineering* 11(2): 277-288.

Paper II:

Voake, T., Nermoen, A., Korsnes, R.I., Fabricius, I.L. (2019).

Temperature cycling and its effect on mechanical behaviours of high-porosity chalks. *Journal of Rock Mechanics and Geotechnical Engineering* 11(4): 749-759.

Paper III:

Voake, T., Nermoen, A., Korsnes, R.I., Fabricius, I.L. (In review).

Elastic moduli dependence on temperature cycling in high porosity chalks. *Journal of Rock Mechanics and Geotechnical Engineering*

Paper IV:

Voake, T., Nermoen, A., Korsnes, R.I., Fabricius, I.L. (2017)

Induced shear failure by temperature reduction at uni-axial strain conditions. *EAGE - 19ᵗʰ European Symposium on Improved Oil Recovery/IOR Norway*, Stavanger.

Paper V:

Voake, T., Nermoen, A., Korsnes, R.I., Fabricius, I.L. (2016).

To what degree thermal cycles affect chalk strength. *SCA annual symposium.* Snowmass Colorado.

Conference contributions:

Meireles, L., Nermoen, A., Voake, T., Welch, M., Fabricius, I.L. (2018)

Compaction driven IOR in chalk reservoirs. *39th Annual workshop & symposium, IEA-EOR*. Copenhagen. (Presentation)

Voake, T., Nermoen, A., Korsnes, R.I., Fabricius, I.L. (2018).

Temperature cycling and its effect on stress-strain relationships in high porosity chalks. *EGU*, Vienna. (Poster)

Voake, T., Nermoen, A., Korsnes, R.I., Fabricius, I.L. (2018).

Temperature cycling and its effect on stress-strain relationships in high porosity chalks. *IOR Norway 2018*, Stavanger. (Poster)

Voake, T., Nermoen, A., Korsnes, R.I., Fabricius, I.L. (2017)

Induced shear failure by temperature reduction at uni-axial strain conditions*. EAGE - 19th European Symposium on Improved Oil Recovery/IOR Norway*, Stavanger. (Poster)

Voake, T., Nermoen, A., Korsnes, R.I., Fabricius, I.L. (2016).

To what degree thermal cycles affect chalk strength. *SCA annual symposium.* Snowmass Colorado. (Poster)

Table of Contents

Table of Figures

List of Tables

1   Introduction

Recurring cold-water injection into a hot reservoir during oil production periodically cools the reservoir rock and could potentially thermally degrade the formation surrounding an injection well. Thermal strain may destabilise a rock and cause permanent damage, especially if a rock is composed of an anisotropic mineral phase. This project focuses on chalk reservoirs, where the proposed effect could be high because chalk is composed of calcite which has a highly anisotropic thermal expansion coefficient.

1.1   Physical properties of chalk

1.1.1   Calcite anisotropic thermal expansion

Freshly deposited calcareous ooze has a porosity of approximately 70%, but it is mechanically compacted by the overburden stress, resulting in a reduction of pore volume. As the ooze is buried deeper, stress at particle contacts builds up, resulting in pressure dissolution and contact cement, forming chalk (Fabricius, 2014).

Calcite crystals and carbonate rocks have large anisotropic thermal expansion coefficients, which could induce stresses at cemented particle contacts caused by temperature variations (Table 1). Marble is a metamorphosed rock also composed of calcite, and experiments have shown that its strength is greatly influenced by temperature fluctuations. For example, marble monuments experience degradation and some marble façades tend to experience concave bowing when exposed to outdoor temperature variation (Figure 1) (Luque et al., 2011; Weiss, Siegesmund, & Fuller, 2003). Hansen, Leksø, and Grelk (2003) found that naturally exposed marble weakens relative to the number of years exposed, and that the marble laboratory tested at 100% relative humidity weakens respectively with number of cooling and heating cycles.

Table 1 - Limestone and calcite anisotropic thermal expansion coefficient reported in literature

Reference – limestone	Limestone region	α (10^{-6} K^{-1})
Harvey (1967)	Illinois	5.2 - 5.7
Johnson and Parsons (1944)	Mille Roche, Canada	3.8 - 4.1
	St Louis Cp., MO	3.8 - 4.4
	Bethany Falls, MO	3.0 - 4.3
	Jordanville, NY	4.0 - 4.4
	North le Roy, NY	5.6 - 5.8
	Paso Pobles, CA	8.6 - 9.4
Goncalves and Brito (2017)	Anca, Portugal	4.6
Reference – calcite	$\alpha \parallel c$ (10^{-6} K^{-1})	$\alpha \perp c$ (10^{-6} K^{-1})
Rosenholtz and Smith (1949)	23.8	-5.2
Markgraf and Reeder (1985)	32.3	-2.8
Wu, Shen, Weathers, Bassett, and Chou (1995)	28.798	-5.371
Rao, Naidu, and Murthy (1968)	25.10	-3.68

Figure 1- Marble displaying flakes and granular disintegration in Granada, Spain (Luque et al., 2011)

Other minerals with different mineralogical components also show weakening due to temperature cycling. Tensile strength of sandstone specimens is dependent upon cyclical saturation of water and drying at

105°C cycles, with 50% of strength lost just after seven repeated cycles (Hua, Dong, Li, Xu, & Wang, 2015). Quartz, the main component of sandstone, has an anisotropic thermal expansion coefficient with 14.4×10^{-6} K^{-1} perpendicular and 7.8×10^{-6} K^{-1} parallel to the principle axis (Jay, 1934). The thermal anisotropy of quartz is not as pronounced as of calcite, but still believed significant for stress to be accumulated at particle contacts.

1.1.2 Chalk water weakening

Water presence has been shown to play an important role on rock mechanics. In the experiment by Hansen et al. (2003) mentioned previously, marble did not show any weakening effects due to temperature cycling when tested at 0% humidity. Saturation with a polar pore fluid generally reduces the strength of porous rocks – as seen in sandstone (Baud, Zhu, & Wong, 2000; Wasantha & Ranjith, 2014), limestone (Lebedev, Wilson, & Mikhaltsevitch, 2014), and chalk (Risnes, Madland, Hole, & Kwabiah, 2005). Wasantha and Ranjith (2014) found that water saturation led to a 13-38% reduction of the initial dry strength of Hawkesbury sandstone, which is further enhanced at higher confining pressures. Baud, et al. (2000) studied effects of water saturation on four different sandstones, and found brittle strength reduction of 5-17%, where sandstone with the lowest porosity had the highest reduction. In the same study, samples with higher contents of altered feldspar and clay had greater weakening by water saturation.

Water weakening of chalks has gained a lot of attention since the development of the Ekofisk oil field on the Norwegian continental shelf. Madland, Korsnes, and Risnes (2002) found a reduction in chalk tensile strength and hydrostatic yield stress due to water saturation. By altering water activity as a pore fluid, Risnes et al. (2005) concluded that chalk strength is more reduced with higher water activity. Similarly, Megawati, Hiorth, and Madland (2013) found that the weakening is enhanced with an increasingly negative surface charge of chalk in the

presence of different pore fluids. Greater negative charge on pore walls would lead to the greater overlap of the electrical double layers between the neighbouring particles and hence results in a rise in disjoining pressure.

Subcritical fracturing is considered the main mechanism responsible for propagation of pre-existing fractures, and would be the dominant mode for rock failure (Atkinson, 1984). The fracture velocity was found to be much higher in water than air, and also influenced by the chemical composition of the saturating fluid (Atkinson & Meredith, 1981). Lisabeth and Zhu (2015) demonstrated that limestone saturated with equilibrated water was stronger than the samples saturated with distilled water, and that the microcracking was a dominant deformation mechanism at lower pressures.

1.1.3 Calcite surface charge and the adsorption of surface-active ions

Calcite crystal surfaces have charged sites, with the principal cleavage plane $\{10\bar{1}4\}$ populated with partially charged Ca^{2+} and CO_3^{2-}, (Stipp, Brady, Ragnarsdottir, & Charlet, 1999). With an introduction of a polar pore fluid, its charge is absorbed onto the calcite surface, creating a repulsive double layer. The thickness of the double layer is described by Debye-Hückel theory (Andreassen & Fabricius, 2010), and is characterized by the Debye length κ^{-1} (Lyklema, 2000):

$$\kappa^{-1} = \left(\frac{\varepsilon_0 \varepsilon_r k_b T}{2 N_A e^2 I}\right)^{\frac{1}{2}} = \left(\frac{(8.85 \times 10^{-12})\varepsilon_r\,(1.38 \times 10^{-23})T}{2(6.02 \times 10^{23})(1.60 \times 10^{-19})^2 I}\right)^{\frac{1}{2}} \quad (1)$$

Where ε_0 is the permittivity of a vacuum, ε_r is relative permittivity of water (the saturating fluid), k_b is Boltzmann's constant, T is temperature, N_A is Avogadro's number, e is elementary charge, and I is ionic strength of the pore water. Relative permittivity of water also depends on temperature, where ε_r is 88.44 at 20°C and 55.43 at 100°C and 34.5 at

200°C (Yakaboylu, Harinck, Smit, & de Jong, 2013). Hence, the Debye length depends on temperature, and initially increases with increasing temperature (Figure 2).
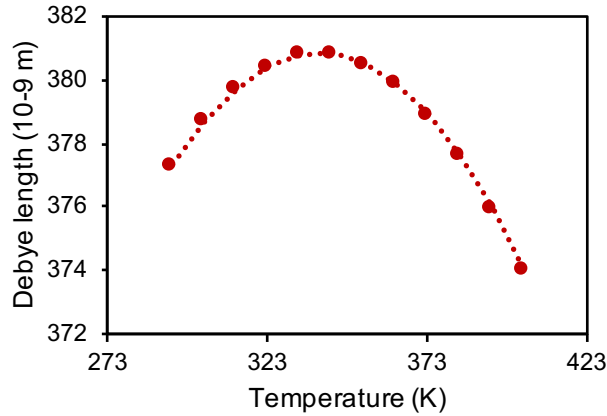
Figure 2 - Debye length increases with increasing temperature based on κ^{-1} equation (Eq (1)).

A thicker Debye length leads to an increase in the repulsive area between the particles at higher temperatures, which causes further weakening of the water saturated samples (Figure 3). The increased repulsion could facilitate the propagation of fractures that would not develop in the dry state, thereby creating greater repulsion and fracturing of the contact cement, thus weakening the samples as the number of temperature cycles are increased. Additionally, the increase of the repulsive area may be sufficient to pull particles farther apart, so water can then invade the fracture, reducing the attractive area between the two particles.
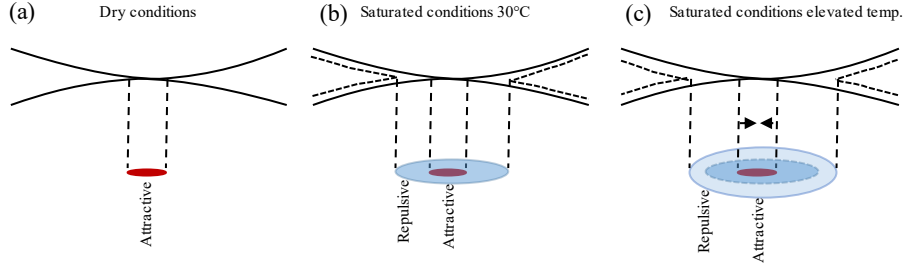
Figure 3 - Attractive and repulsive forces present between two calcite particles in (a) dry conditions, (b) water saturated conditions at 30°C, and (c) saturated conditions at elevated temperature, an extra area of repulsive forces occur at higher temperature associated with the increasing Debye length.

Once the fracture propagates, a new surface is generated. The energy required to create a surface $U_{surface}$ between two particles is a function of the cross-sectional area A of the contact cement between two particles:

$$U_{surface} = \gamma_s A \tag{2}$$

For calcite, the surface energy γ_s of the cleavage plane $\{10\bar{1}4\}$ depends on the presence of water, where the surface energy of a dry calcite surface is 0.32 J/m² and the surface energy of a fully hydrated calcite surface is 0.15 J/m² (Røyne, Bisschop, & Dysthe, 2011). Since two surfaces are created with each fracture, calculated energies of the dry and saturated surface are:

$$U_{surf,dry} = 2 \cdot 0.32 \frac{J}{m^2} \cdot (10 \ \mu m)^2 \cdot \left(10^{-12} \cdot \frac{m^2}{\mu m^2}\right) \tag{3}$$
$$= 6.4 \cdot 10^{-11} J$$
$$U_{surf,sat} = 2 \cdot 0.15 \frac{J}{m^2} \cdot (10 \ \mu m)^2 \cdot \left(10^{-12} \cdot \frac{m^2}{\mu m^2}\right) \tag{4}$$
$$= 3.0 \cdot 10^{-11} J$$

It is observed that the energy necessary to generate a dry surface (fracture) is double the energy required for a wet one.

1.2 Mechanical properties and how they are measured

1.2.1 Brazilian testing and tensile strength

The Brazilian tests subject a cylindrical shaped sample to load applied by two loading plates until the sample fails and splits in half (Figure 4).
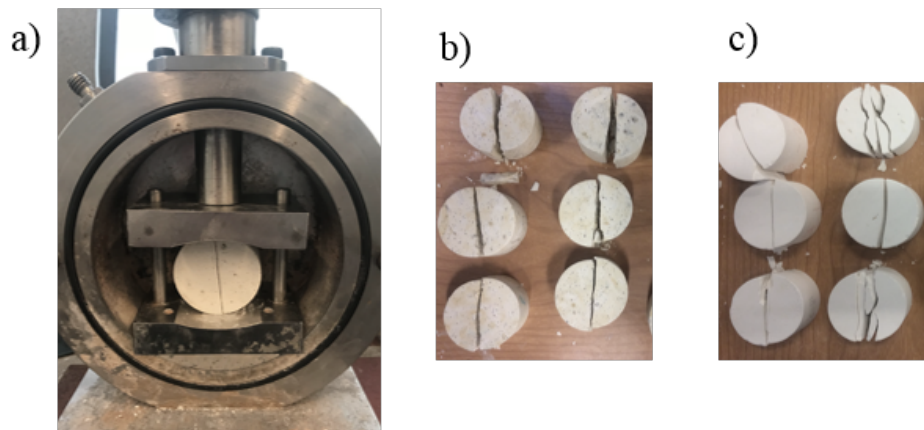
Figure 4 – (a) Brazilian test set up with a cylindrical chalk sample fractured under the load of the two parallel plate. (b) and (c) Cylindrical fractured samples for Kansas and Mons chalk.

From the peak force (F) at which the sample fails, tensile strength (T_0) was calculated from the equation below, where D and t are diameter and thickness of the disk respectively:

$$T_0 = \frac{2F}{\pi D t} \qquad (5)$$

1.2.2 Stress, strain and elastic and plastic moduli determination

The principles of this section were used for hydrostatic (bulk modulus and elasto-plastic partitioning) and uniaxial (Young's and uniaxial compressibility moduli) stress tests interpretation.

Deformation of a rock sample is caused when it is exposed to stress. This deformation, strain ε, of a rock sample is calculated form the differences between the newly obtained length L and diameter D and their original dimensions, L_0 and D_0, according to,

$$\varepsilon_z = -\frac{L-L_0}{L} \text{ and } \varepsilon_r = -\frac{(D-D_0)}{D} \tag{6}$$

1.2.2.1 Bulk Modulus

The elastic bulk modulus K is tested on samples under hydrostatic stress conditions according to,

$$K = \frac{\Delta\sigma'_{hyd}}{\Delta\varepsilon_{vol}} \tag{7}$$

Where it is assumed that the sample is isotropic, and the volumetric strain is estimated as $\varepsilon_{vol} \simeq 2\varepsilon_r + \varepsilon_z$. The effective stress, σ'_{hyd}, is dependent on pore pressure and pore connectivity in porous material, and was determined by $\sigma'_{hyd} = \sigma_{hyd} - \beta P_{pore}$, where β is the Biot coefficient.

1.2.2.2 Young's Modulus and uniaxial compressibility modulus

The axial and radial stresses applied to a sample are not the same in a uniaxial test, $\sigma_z \neq \sigma_r$. If a sample is assumed linearly elastic, homogeneous and isotropic, in this experimental set-up Young's modulus E and Poisson's ratio ν can be measured. The effective stress σ'_i in radial and axial direction is determined as $\sigma'_i = \sigma_i - \beta P_{pore}$, where $i = r, z$. For cylindrical samples, Hook's law relates stress and strain as:

$$E\varepsilon_r = (1 - v)\sigma_r' - v\sigma_z' \tag{8}$$
$$E\varepsilon_z = \sigma_z' - 2v\sigma_r' \tag{9}$$

The elastic coefficients can be estimated from incremental changes, Δ, in the effective stresses and measured changes of the strains. Assuming that E and v are constant:

$$E\Delta\varepsilon_r = (1 - v)\Delta\sigma_r' - v\Delta\sigma_z' \tag{10}$$
$$E\Delta\varepsilon_z = \Delta\sigma_z' - 2v\Delta\sigma_r' \tag{11}$$

A large difference between vertical stress and lateral stress may result in very low strain in one direction, and hence a very low Poisson's ratio v. In this case, the uniaxial compressibility modulus H is calculated,

$$H = \frac{\Delta\sigma_r}{\Delta\varepsilon_r} \tag{12}$$

1.2.2.3   Elasto-plastic partitioning

When exposed to a stress cycle within its elastic region, a perfectly elastic rock should not accumulate any strain. If a rock is not perfectly elastic, after a stress cycle completion, the strain that is reversed is the elastic element of the material, and the irreversible strain represents the plastic behaviour of the material (Figure 5). The total strain reached at the highest stress point is expressed as:

$$\varepsilon_{tot} = \varepsilon_{rev} + \varepsilon_{irr} \tag{13}$$

The percentage of the irreversible strain during a stress cycle is calculated as:

$$\varepsilon_{irr}(\%) = \frac{\varepsilon_{irr}}{\varepsilon_{tot}} \times 100\% \tag{14}$$
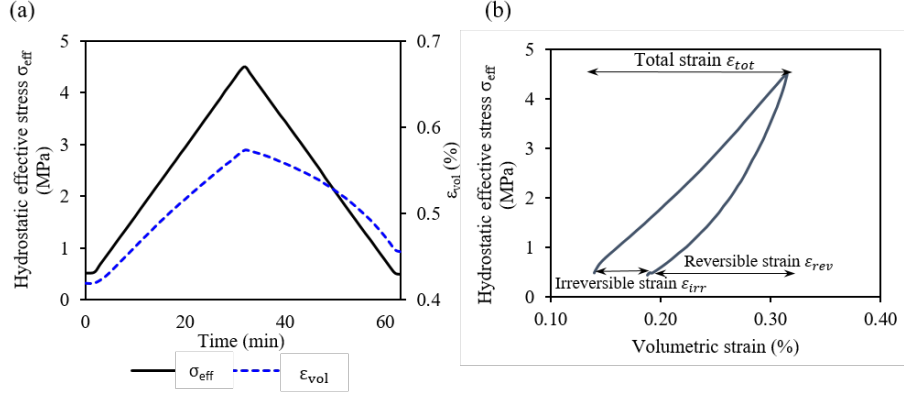
Figure 5 – Stress-strain relation during a stress cycle. (a) Strain response to stress changes. (b) After a complete stress cycle, strain is partitioned into elastic/reversible stain and plastic/irreversible strain.

1.2.3 Coefficient of thermal expansion

The coefficient of thermal expansion α is determined from the sample's strain during temperature change, ΔT,

$$\varepsilon = -\alpha \Delta T \qquad (15)$$

1.2.4 $p' - q$ diagram

The pq diagrams are very useful in visualizing the elastic stress boundaries of a rock. The pq diagram in a cylindrical geometry is expressed as:

$$q = \sigma_z - \sigma_r \qquad (16)$$
$$p' = \frac{1}{3}\,(2\sigma_r' + \sigma_z') \qquad (17)$$

Different modes of failure are used to plot the pq diagram (Figure 6). Tensile failure is obtained from the Brazilian tests, shear failure from the uniaxial deviatoric loading, and the pore collapse line is estimated from the hydrostatic yield stress.

10
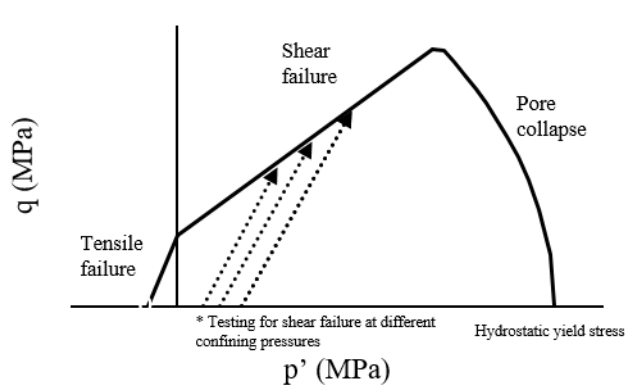
Figure 6 – $p' - q$ diagram indicating different modes of failure. The arrows represent the direction of deviatoric loading at different confining pressures until shear failure line is reached and the sample fails.

2   Material and Methods

2.1   Description of chalk materials studied

2.1.1   Kansas chalk

Kansas chalk is from the Niobrara Formation, Fort Hays Member (Late Cretaceous) in Niobrara, Kansas, USA. The Niobrara formation has undergone a high degree of diagenesis, with a burial depth of up to 7000m in some locations (Finn & Johnson, 2016). However, the induration of H3 and porosity of approximately 33% indicates burial of less than 1000m for the chalk tested. Kansas chalk has a carbonate content of 96.9% and a Biot coefficient of 0.91 (Figure 7).
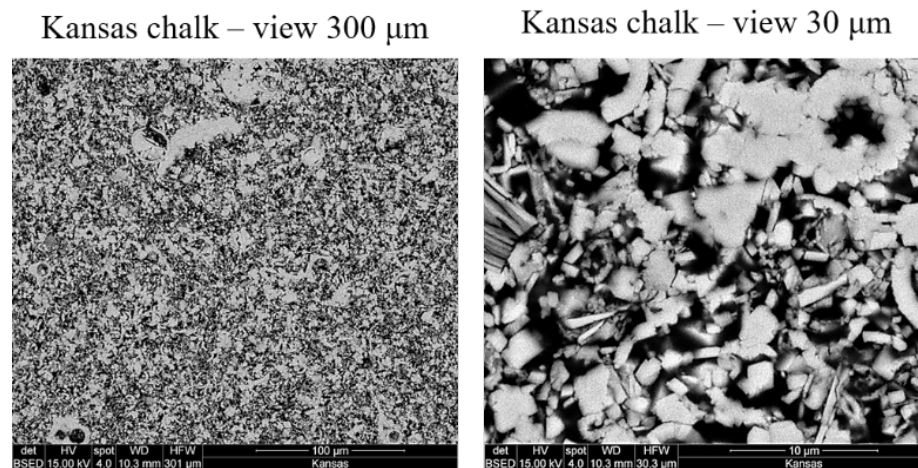
Figure 7 - Backscatter electronic micrographs of Kansas chalk with two magnifications

2.1.2   Mons chalk

Mons chalk is from the Trivières Formation (Late Cretaceous) in Harmignies, Belgium. Mons chalk has low amounts of diagenesis as it has been buried to shallow depths, less that 500m (Pirson et al., 2008). The Mons chalk has a carbonate content of 99.8% and Biot coefficient

of 0.95. A higher Biot coefficient indicates a smaller area of contact cement between neighboring grains, and this is reflected in Mons chalk's lower induration of H2.

Mons chalk – view 300 μm   Mons chalk – view 30 μm
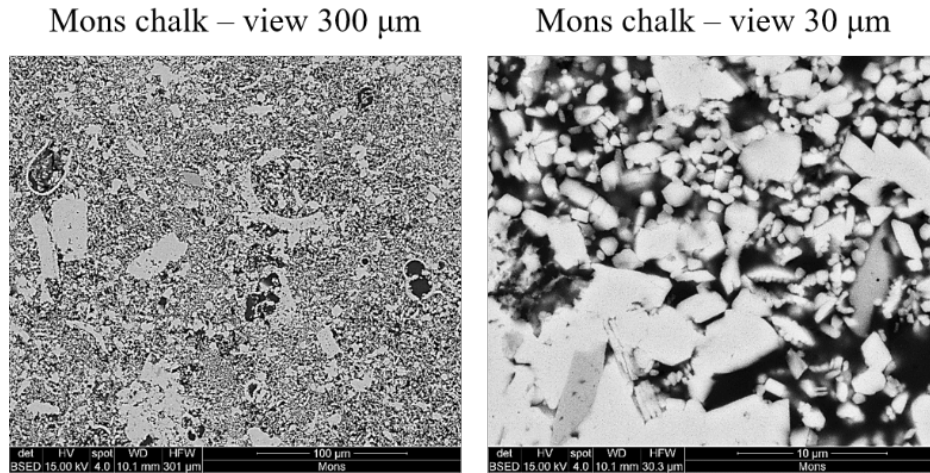
Figure 8 - Backscatter electronic micrographs of Mons chalk with two magnifications

2.1.3 Saturating fluids

The chalk samples were tested dry (i.e. saturated by air), saturated with equilibrated calcite water (polar fluid), or saturated with Isopar H (non-polar fluid). The equilibrium water was made by dissolving chalk pieces in distilled water, and after settling filtered using a 0.65 μm filter. The activity of the water was measured to be 0.652 mmol/L.

The two fluids were selected in order to minimise the impact of chemical reactions, and to focus on studying the rock-fluid interactions related to ion adsorption on mineral surfaces.

13

2.2   Sample preparation

2.2.1   Tensile stress tests using Brazilian setup

Each chalk block had cylindrical shaped cores drilled of approximately 200 mm long and 40 mm in diameter. The cores were radially adjusted to 38.1 mm, and then cut into disk-shaped samples of length from 20 to 25 mm.

For each chalk type, the disk-shaped samples were randomly divided into two groups, where half of the samples remained dry, and the other half saturated with calcite equilibrated water. They were further randomly divided in the experimental subcategories for testing after 0, 15, and 30 temperature cycles.

2.2.2   Strain, elastic moduli, thermal expansion coefficient and shear failure tests using the triaxial setup

Similarly to the Brazilian test sample preparation, drilled cores were adjusted to 38.1 mm, but were cut into cylindrical samples of approximately 70 mm. For shear failure, thermal expansion coefficient and elastic moduli experiments, the samples were saturated with calcite equilibrated water. For elasto-plastic partitioning, half of the samples were saturated with calcite equilibrated water, and the other half with Isopar-H.

2.3   Mechanical testing

2.3.1   Tensile strength using Brazilian setup

The force of the parallel plates was applied by injecting hydraulic oil with a Gilson 307 pump at flow rate of 0.5 ml/min. The applied force

was measured with an NTT Transducer 1 ton (type C2S) and logged in a LabView routine. The maximum force a sample could sustain before fracturing was used to calculate the tensile strength of a sample using Eq. (5). Once the sample was fractured, the applied force experienced a rapid drop (Figure 9).
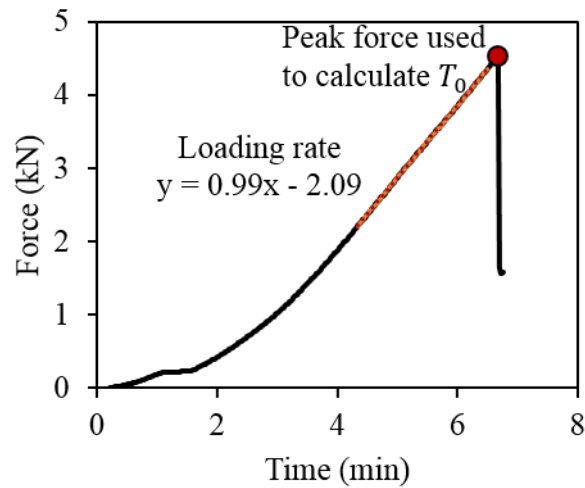
Figure 9 - A typical loading curve obtained during a Brazilian test (dry Kansas chalk sample). The peak force (red dot) was used to calculate the tensile strength of a sample.

A single temperature cycle lasted 24h and consisted of heating the samples to 130°C and cooling them back to room temperature. It is important to note that even though the cooling took a long time, the desired starting temperature was always reached (Figure 10).
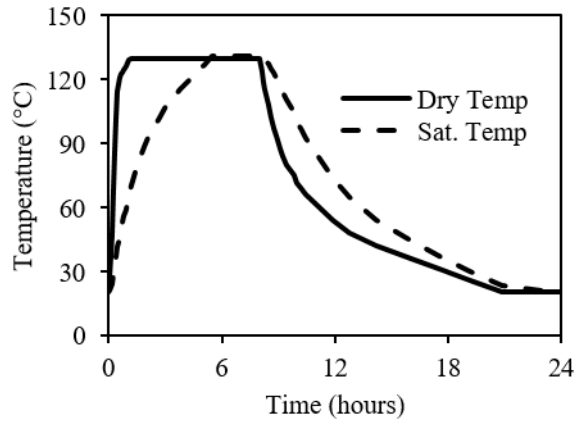
Figure 10 - A single temperature cycle for dry and saturated samples.

2.3.2 Description of the triaxial cell

The experiments for strain partitioning, elastic properties, shear failure, and thermal expansion coefficient, were performed using a triaxial cell (Figure 11). Radial and axial stresses were independently controlled by two different pumps connected to the cell. A Hydraulic Quizix pump, model QX-20000 HC is equipped with two cylinders, both cylinder were used for controlling radial confining pressure, and the Teledyne ISCO model 260D pump controlled the movement of the piston that acted as the axial stress. The radial deformation was measured using an extensometer, where the circumference changes were detected by LVDT MHR 100 from Measurements Specialties™. The axial deformation was measured internally by LVDT MHR 250 from Measurements Specialties™. Both LVDTs have a precision of 0.15% of the measurement. The constant pore pressure of 0.7 MPa was controlled by the Gilson Pump (model 307 HPLC), that injected a desired saturating fluid, and the back pressure regulator connected to the outlet side of the sample. All pumps were individually operated through a LabVIEW routine. The cell was wrapped with a 1000 W heating jacket, which was

controlled by an Omron E5CN PID for temperature control (±0.1°C precision).
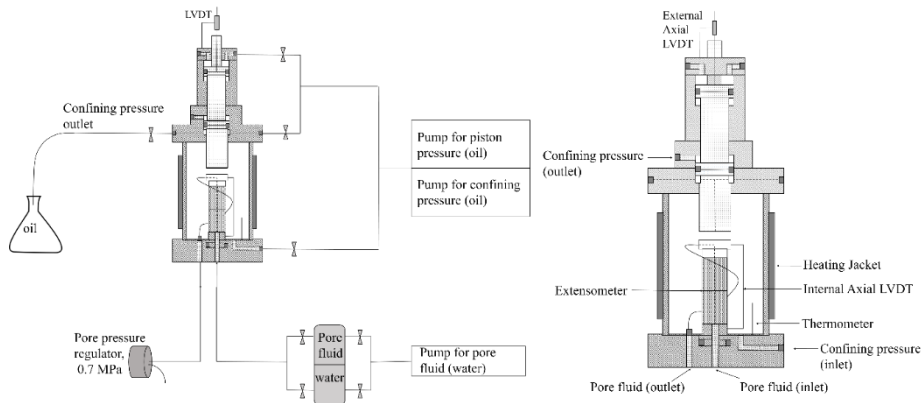
Figure 11 - Triaxial cell and its set up

2.3.2.1   Description of hydrostatic stress tests

The hydrostatic test method was used in two studies, for elasto-plastic partitioning and temperature cycling influence on the elastic bulk modulus K.

Elasto-plastic partitioning experiments compared the strain accumulation during stress cycles between the samples that have been tested at the constant temperature to those exposed to a temperature cycle between each stress cycle (30°C – 130°C – 30°C). Two chalk types, Kansas and Mons chalk, and two saturating fluids were used, equilibrated water (polar) and non-polar Isopar-H oil. Each sample was exposed to 10 hydrostatic stress cycles from 1.2 MPa to 5.2 MPa. The stress cycles were always performed at 30°C, regardless of temperature cycling. Even for the samples exposed to temperature cycling, 24h between stress cycles was enough for temperature to stabilize at 30°C (Figure 12). For the samples exposed to temperature cycling, an additional 11th hydrostatic stress cycle was performed without a

temperature cycle in order confirm consistency of the chalk behaviour between the experiments. The total accumulated strain during a stress cycle and its irreversible fraction are reported. At the end of each experiment, the samples were hydrostatically loaded to hydrostatic yield stress.
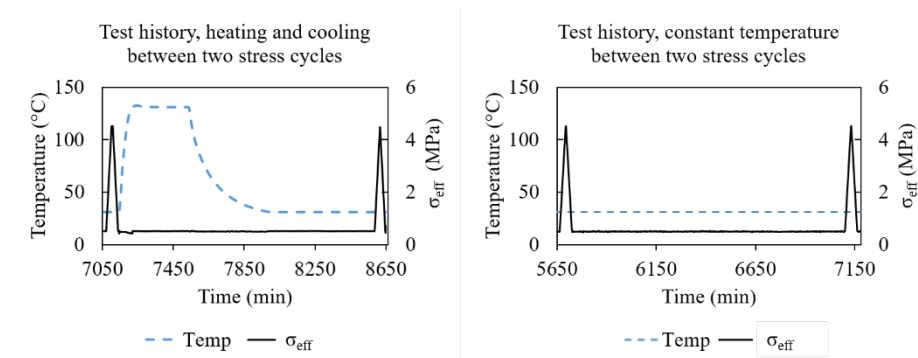
Figure 12 - Test history for samples tested with temperature cycling and samples tested at the constant temperature of 30°C.

In the other set of experiments, the bulk modulus, K was measured at 30˚C during reduction of the hydrostatic stress from 4 MPa to 0.8 MPa. Two Kansas chalk samples and two Mons chalk samples saturated with calcite equilibrated water were tested. Each sample was exposed to three temperature cycles of 30˚C to 90˚C and back to 30˚C, where K was measured following each temperature cycle once the sample stabilized. The thermal expansion coefficient was measured during cooling from 90°C to 30°C.

2.3.2.2   Uniaxial stress tests

Uniaxial stress tests were used to determine two properties for the chalks tested, the shear failure limits and temperature cycling influence on the elastic Young's modulus E.

Kansas and Mons chalk samples saturated with calcite equilibrated water had their axial stress increased until failure at four different radial

18

stresses (0.8, 1.2, 2, and 3 MPa). The shear failure line is estimated for the two chalks at 30°C.

In the experiments where Young's modulus E was calculated, it was aimed to mimic reservoir conditions, and the vertical overburden stress was kept constant, while the radial stress was varied. One Mons chalk sample and one Kansas chalk sample saturated with equilibrated water were tested. The deviatoric unloading, during which the elastic modulus and Poisson's ratio were estimated, was repeated three times for each sample following a temperature cycle 30˚C to 90˚C and back to 30˚C. The axial stress was kept constant at 70% of the stress required to induce shear failure at 2 MPa, 11.8 MPa for Kansas chalk, and 5.3 MPa for Mons chalk. With $\Delta\sigma_z' = 0$, and the radial stress $\Delta\sigma_r' \neq 0$, and the Eq. 10 and Eq. 11 simplify to:

$$\Delta\sigma_r' = \frac{E\Delta\varepsilon_r}{(1-v)}, \text{and} \tag{18}$$

$$\Delta\sigma_r' = -\frac{E\Delta\varepsilon_z}{2v}. \tag{19}$$

The equations are further rearranged to express Poisson's ratio in terms of measured strains:

$$E = \frac{\Delta\sigma_r(1-v)}{\Delta\varepsilon_r} \tag{20}$$

$$E = -\frac{2\Delta\sigma_r v}{2\Delta\varepsilon_z} \tag{21}$$

$$\frac{\Delta\sigma_r(1-v)}{\Delta\varepsilon_r} = -\frac{2\Delta\sigma_r v}{2\Delta\varepsilon_z} \tag{22}$$

$$v = \frac{-\Delta\varepsilon_z}{2\Delta\varepsilon_r - \Delta\varepsilon_z} \tag{23}$$

In order to express Young's modulus E in only stress and strain terms, Eq. 23 is substituted into either Eq. 20 or 21,

$$E = \frac{2\Delta\sigma_r}{2\Delta\varepsilon_r - \Delta\varepsilon_z} \qquad (24)$$

However, as the testing was performed near failure conditions (70% to failure), permanent deformation of the samples may have occured. A large difference between high vertical (overburden) stress and low lateral stress may result in very low lateral strain, resulting in apparent very low Poisson's ratio. A cut off value of apparent Poisson's ratio of 0.1 was selected. In this case, the uniaxial compressibility modulus H is calculated (Eq. 12).

3   Results and discussion

Temperature cycling effects have been analysed on different mechanical properties of chalk, tensile strength, elastic bulk and Young's modulus, elasto-plastic partitioning, and thermal expansion. The results of all tests have been combined in a p-q diagram. In addition, the tests have been performed on two different chalks of different burial history and induration in order to analyse if the area of contact cement plays a role. In addition, one polar and one non-polar (or dry) saturating fluid have been used in order to quantify the water weakening of chalk.

3.1   Tensile strength

The tensile strength was calculated as an average of 10-15 samples for each chalk type (Kansas and Mons chalk), saturating state (dry and water saturated), and the number of temperature cycles (0, 15, and 30 cycles) (Table 2).

Table 2 - Average values and standard deviations for the tensile strength measurements.

Chalk locality	State	No. of cycles	No. of samples	T_0 (MPa)	Stand. Dev. (MPa)
Kansas	Dry	0	10	3.0	0.4
		15	13	3.3	0.6
		30	10	3.3	0.6
	Saturated	0	14	1.4	0.2
		15	12	1.1	0.2
		30	12	0.8	0.2
Mons	Dry	0	13	1.6	0.3
		15	15	1.3	0.4
		30	15	1.4	0.4
	Saturated	0	13	0.9	0.2
		15	14	0.6	0.2
		30	15	0.4	0.1

For the visual representation of the data, each line represents the results of the tensile strength from 10-15 samples in each series, arranged in ascending order, starting from the weakest samples on the left, and ending with the strongest on the right (Figure 13 a and b). The average and standard deviation of the data measurements were used to estimate the Gaussian distribution (Figure 13 c and d).
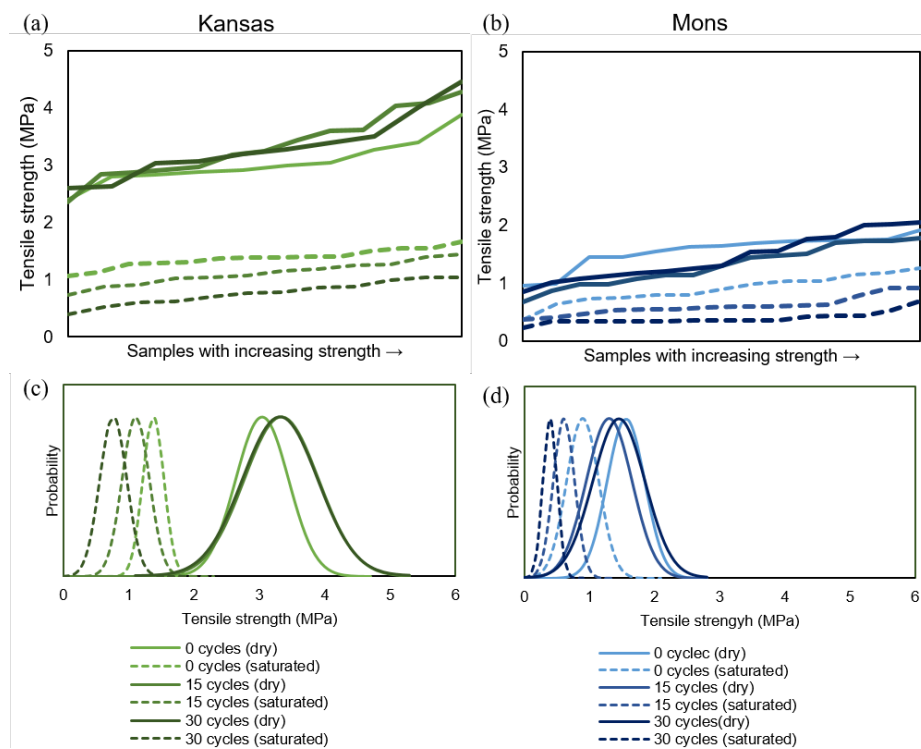
Figure 13 - Tensile strength for the Kansas (green) and Mons chalk (blue) samples in dry (solid line), and water saturated (dashed line). (a) and (b) represent individual samples for each group in increasing order from low (left) to high tensile strength. (c) and (d) display the Gaussian distributions of each data set.

The more indurated Kansas chalk has an initial tensile strength higher than Mons chalk. Comparing the dry and saturated tensile strength at 0 cycles, Kansas chalk had a bigger absolute drop of 1.6 MPa than Mons chalk of 0.7 MPa. However, proportional strength reduction by

saturation was similar for the two chalks, 47% for Kansas chalk and 56% Mons chalk, indicating that the initially stronger Kansas chalk was similarly susceptible to water weakening as Mons chalk at 0 cycles (Figure 14 a). Reduction of tensile strength by water saturation observed here agrees with previous research (Madland et al., 2002; Risnes et al., 2005).

The tensile strength of Kansas and Mons chalk showed no dependence on the number of temperature cycles tested in dry state. The seeming increasing trend in strength due to temperature cycling for dry Kansas chalk is not significant when the standard deviation is taken into account.

However, the measurements of the tensile strength for the water saturated chalk indicate weakening with increasing number of temperature cycles. Even when standard deviation is taken into an account, there is a descending trend for the average measurements. The two chalks weaken by the same absolute value (0.3 MPa) from 0 to 15 cycles, and the tensile strength reduction rate from 15 to 30 temperature cycles remained 0.3 MPa following an additional 15 cycles for Kansas chalk, but was lowered for Mons chalk (0.2 MPa/15 cycles). After 30 cycles the proportion of strength reduction in saturated samples was similar for the two chalk types (Figure 14 b).
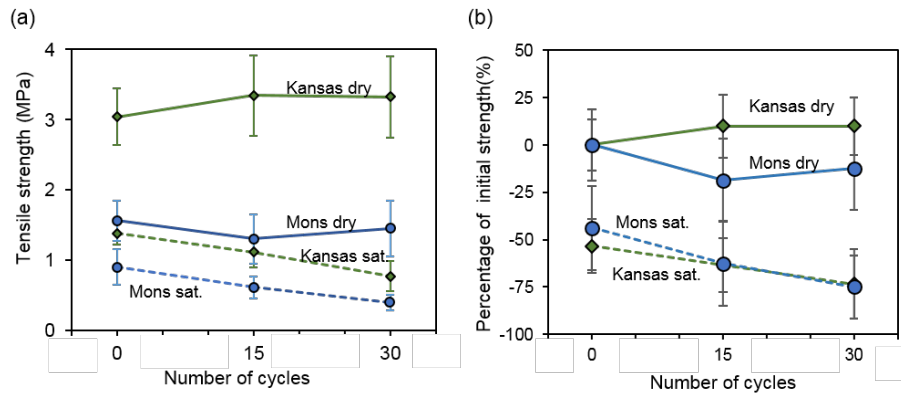
Figure 14 - (a) Average tensile strength and standard deviation as a function of number of temperature cycles in absolute measurements. (b) Tensile strength difference (in percent) as function of temperature cycling, reference is the dry and 0 cycles for each chalk type.

The difference in behaviour between the dry and saturated samples suggest that the contact cement bonds break in water saturated state but not in dry. Furthermore, the fact that the samples continued to weaken after the first 15 cycles implies that not all the bonds are broken initially, but continuously. This implies that the bond breakage is a relatively rare event compared to the number of bonds found in a sample. Since Kansas samples had a constant weakening rate up to 30 cycles, whereas Mons sample the rate was reduced for 15-30 cycles, it could indicate that the overall number of bonds holding the sample together is smaller for Mons chalk than Kansas chalk.

When theoretically calculated, the tensile elastic energy between two neighboring particles with c-axis parallel to each other, caused by 100°C heating would be $2.3 \cdot 10^{-11}$J, and insufficient to create either a dry or a saturated calcite surface (Eq. 3 and Eq. 4). Alternatively, if two particles had a perpendicular orientation to each other, the shear energy caused by 100°C heating is $2.2 \cdot 10^{-9}$J, and is more than sufficient to generate surfaces in both dry and saturated states. However, the parallel or perpendicular orientation of c-axis of the two neighboring particles is extremely rare, and since no weakening in dry samples is observed it

would indicate that the tensile and shear energies due to anisotropic thermal expansion are not sufficient to generate dry surfaces, but are sufficient to generate water saturated surfaces.

3.2 Hydrostatic stress tests

3.2.1 Bulk modulus

The effects of temperature cycling on bulk modulus have been measured in two separate experiments, both measured at 30°C.

During three stress cycles with a temperature cycle in-between, the elastic bulk modulus K was not significantly impacted for Kansas chalk, while there is a decrease of the bulk modulus with additional temperature cycles for Mons chalk. Kansas chalk has higher bulk modulus than Mons chalk (Figure 15).
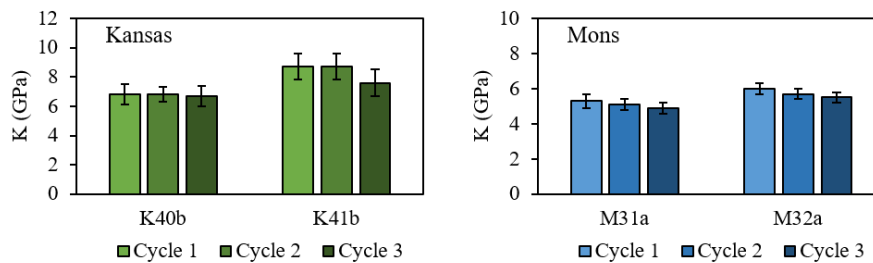
Figure 15 - Elastic bulk modulus K estimated from hydrostatic stress reduction from 4 MPa to 0.8 MPa.

Bulk modulus was also measured during 10 stress cycles in the experiments for elasto-plastic partitioning. Here, the bulk modulus K displayed no dependence on additional stress cycles for either samples tested at constant temperature or with temperature cycling, regardless of the chalk type or saturating fluid (Figure 16). Kansas chalk again had a higher estimated bulk modulus than Mons chalk.
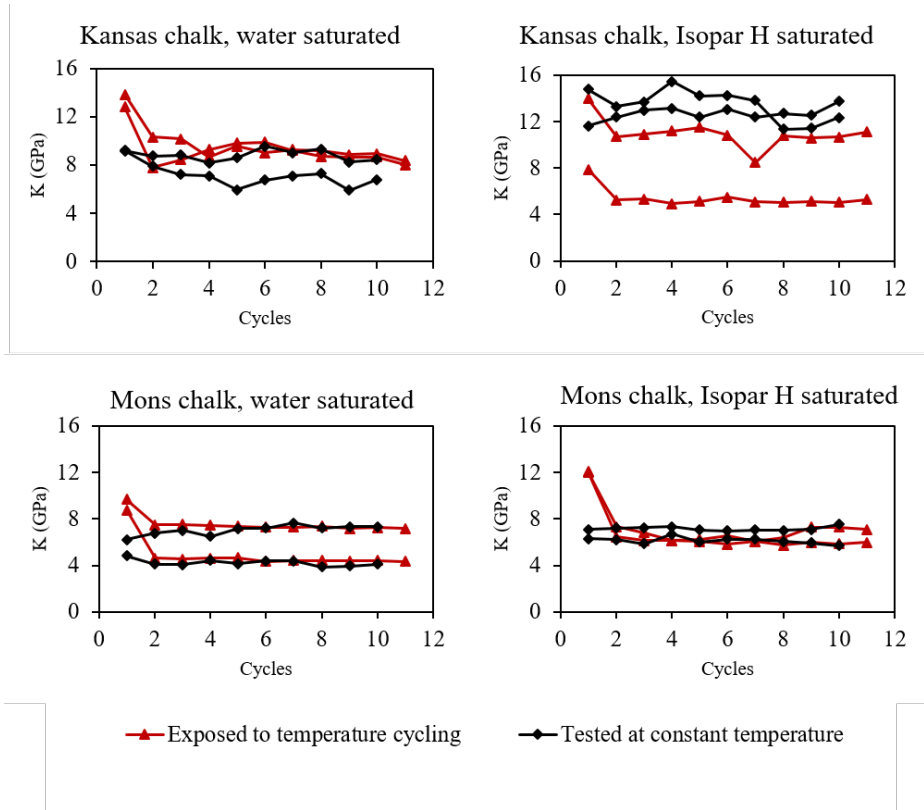
Figure 16 - Elastic bulk modulus *K* through a number of hydrostatic stress cycles. Red lines represent samples exposed to temperature variation between each stress cycle, and black lines correspond to samples held at a constant temperature.

3.2.2 Elasto-plastic partitioning

A significant difference was found between samples tested at a constant temperature and those exposed to a temperature cycle between each stress cycle. More strain was accumulated in the samples that were exposed to temperature variations, even though all stress cycles were performed at 30˚C. (Figure 17 and Figure 18). For each individual stress cycle, approximately double the irreversible strain was accumulated if temperature cycling was performed, as opposed to experiments at a constant temperature of 30°C. The greatest accumulation of irreversible

strain was found in the water saturated Kansas chalk, where the strain accumulated during only a single cycle is approximately equal to the strain accumulated after all ten cycles in a sample tested at constant temperature. The duplicated experiments had a consistent irreversible strain accumulation (Figure 19).

For the samples tested at the temperature cycling, an additional 11th stress cycle performed without a prior temperature cycle, the irreversible strain dropped to the value observed in samples tested at the constant temperature (Figure 19). This indicates that a temperature cycle of 30-130-30°C causes the material to behave less elastically. This behaviour was seen in all samples tested, regardless of chalk type or saturating fluid.

Different behaviour was observed between the two chalk types when saturated with water, but no significant difference was observed in Isopar H saturated samples. When saturated with water, the more indurated Kansas chalk accumulated more irreversible strain within each stress cycle than Mons chalk. The greater amount of contact cementation seems more susceptible to the anisotropic thermal expansion and contraction of calcite particles when saturated with a polar fluid (water in this case).

This further confirms the theory that polar saturating fluid has electrical charge exchange with the calcite surface, creating an electrical double layer. Increasing this area of repulsion between particles by increasing temperature, would stress the areas of contact cementation and thus more indurated samples would be more influenced during temperature cycling.
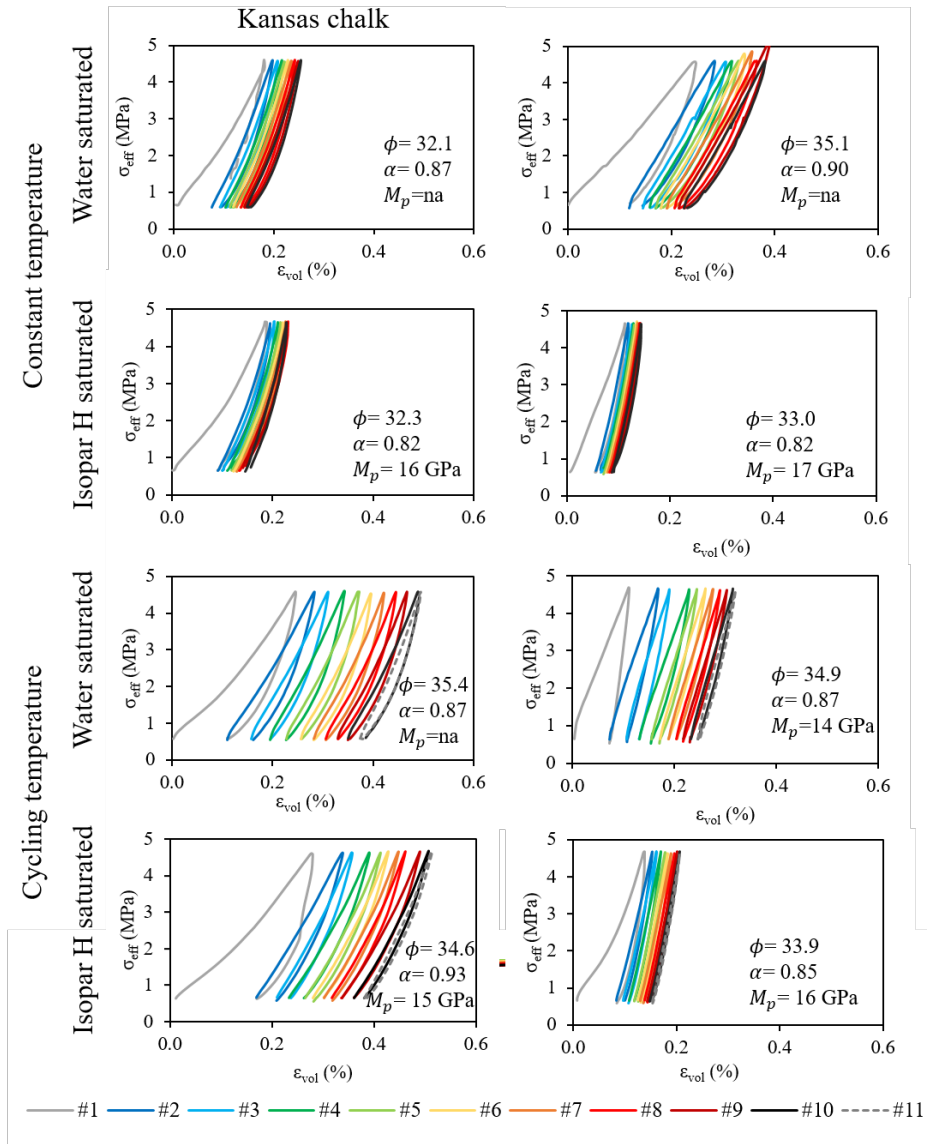
Figure 17 - Stress-strain curves for 10 or 11 cycles for Kansas chalk tested at constant temperature (top two rows) and with a temperature cycle in between stress cycles (bottom two rows).

28
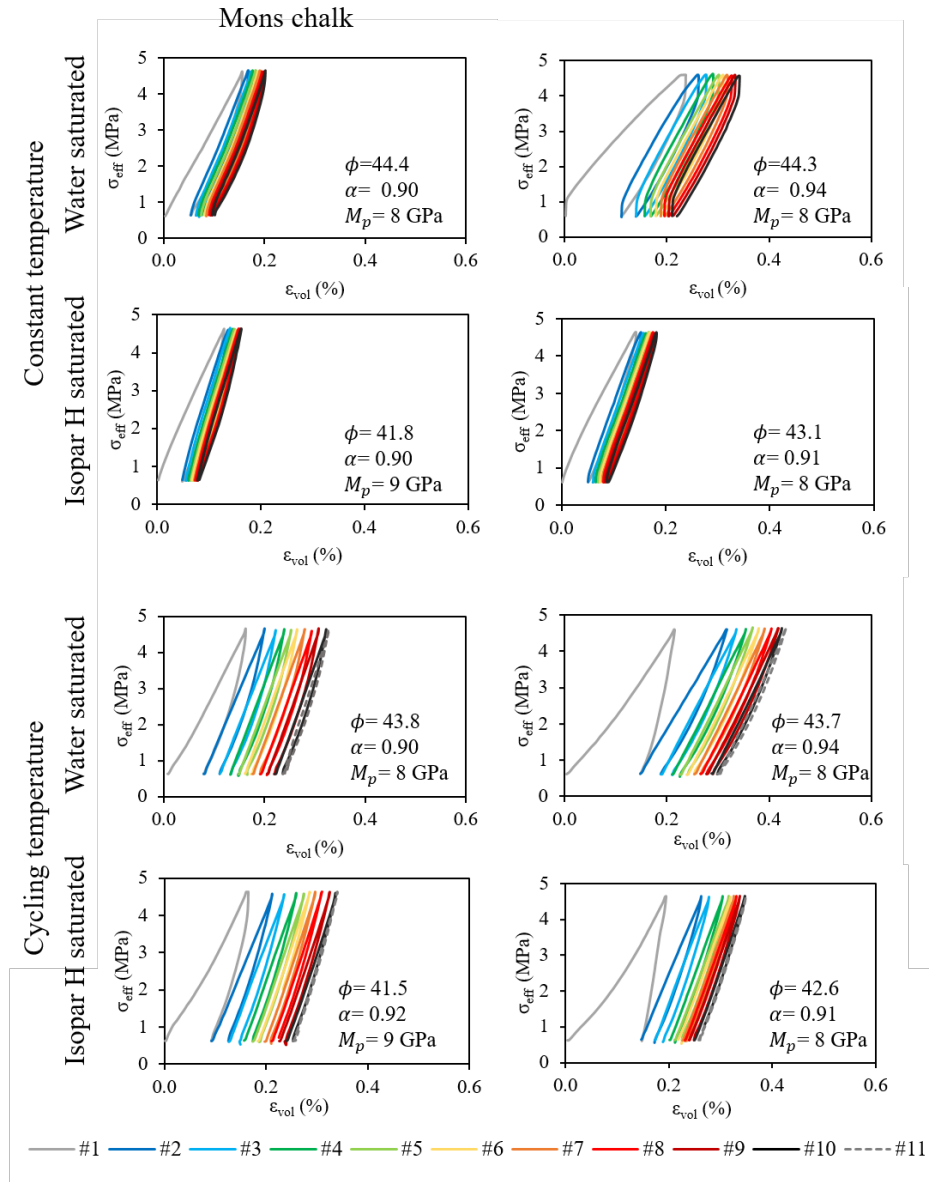
Figure 18 - Stress-strain curves for 10 or 11 cycles for Mons chalk tested at constant temperature (top two rows) and with a temperature cycle in between stress cycles (bottom two rows).

29
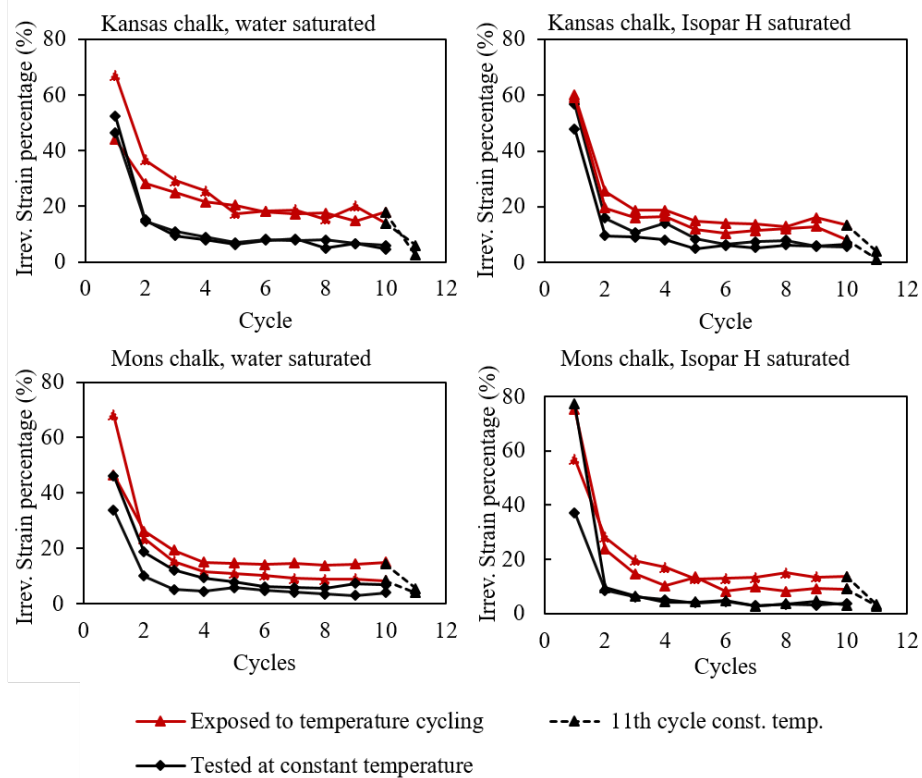
Figure 19- Irreversible strain for individual stress cycles. The red lines illustrate the test results for samples that have been exposed to temperature cycling, and black lines the samples tested at a constant temperature. The dashed line represents the result for the 11th cycle, which was only performed on samples exposed to temperature cycling. This cycle did not include a temperature cycle.

3.2.3 Yield stress during hydrostatic loading

The samples tested for elasto-plastic partitioning were hydrostatically loaded to failure following the last stress cycle. Similar to tensile strength tests, the more indurated Kansas chalk was stronger than Mons chalk (Table 3). Pore fluid also played a role, where samples saturated with the polar fluid were much weaker than samples saturated with non-polar fluid. The effect of water weakening was significant, as the hydrostatic

yield stress reduced from between 13.2-16.3 MPa for Isopar H to 7.9-10.3 MPa for the water saturated Mons chalk, and from 32.2-36.8 MPa to 12.9-18.7 MPa for Kansas chalk.

Table 3 - Yield failure of samples. The maximum stress during stress cycling of 5.2 is well below the yield failure in all cases.

Sample	Saturating fluid and constant/cycled temperature	Yield failure (MPa)	Percentage of stress cycle maximum (5.2 MPa) to yield stress (%)
K19a	Water/cycle	12.9 ± 2.8	40
K40	Water/cycle	15.9 ± 3.2	33
K17a	Water/const.	18.7 ± 4.4	28
K18b	Water/const.	16.7 ± 4.5	31
K44a	Isopar H/cycle	35.2 ± 6.8	15
K22	Isopar H/cycle	34.4 ± 4.6	14
K25	Isopar H/const.	36.8 ± 6.4	16
K44b	Isopar H/const	32.2 ± 4.7	15
M36b	Water/cycle	8.5 ± 1.9	62
M31b	Water/cycle	7.9 ± 2.2	66
M13	Water/const.	10.3 ± 2.6	51
M24	Water/const.	9.7 ± 2.0	53
M30	Isopar H/cycle	15.2 ± 5.7	34
M36a	Isopar H/cycle	16.3 ± 5.4	32
M18	Isopar H/const.	13.2 ± 4.0	39
M32b	Isopar H/const.	15.5 ± 5.3	33

For both chalk types and saturating fluids, the temperature cycles had no significant influence on the yield strength, as no weakening could be observed between the samples that had been exposed to temperature cycling and those that had not. Increasing the length of the electrical double layer had no influence on yield stress, and hence it is concluded that the electrical double layer enhances the number of micro fractures. This would not affect the overall strength, which depends on the strength of the weakest bond rather than the number of weak bonds.

3.3 Uniaxial stress tests

3.3.1 Shear failure stress

Eight samples for Kansas chalk and eight samples for Mons chalk, saturated with equilibrated water, were axially loaded at four different confining pressures in order to obtain shear failure limits for the two chalks. The results are presented in Table 4, with p and q values representative of the peak stress points before samples failed.

Table 4 - Test results for shear failure for Mons and Kansas chalk.

σ_r	Kansas chalk			Mons chalk		
	Sample	***p***	***q***	**Sample**	***p***	***q***
0.8	K20a	4.4	12.5	M10a	1.8	5.1
0.8	K21b	4.1	11.6	M8	1.9	5.1
1.2	K30a	4.7	12.3	M4b	2.7	6.2
1.2	K29b	5.7	15.2	M9b	2.6	5.9
2.0	K19b	6.8	16.2	M5a	3.5	6.3
2.0	K25a	6.3	14.6	M5b	3.2	5.2
3.0	K25b	8.2	17.4	M3	4.7	6.8
3.0	K29a	8.2	17.4	M7	4.6	6.7
			Stan. dev			Stan. dev
	Slope	1.375	0.128	Slope	0.534	0.144
	Cohesion	6.344	0.796	Cohesion	4.236	0.471

3.3.2 Young's and uniaxial compressibility modulus

The strain dependence on applied stress is shown in Figure 21, along with the highlighted intervals from which Poisson's ratio v was calculated. During unloading of radial stress from 4 to 0.8 MPa, q is increased and the stress path almost reaches the shear failure limit (Figure 20). This could explain why in almost all cases, the apparent

Poisson's ratio significantly drops after the first unloading. Small axial strain during subsequent loading indicates that the sample lost strength to push back against the overburden and has been permanently damaged. If the strain is only observed in lateral direction, and not in axial, then the uniaxial compression modulus is used as elastic modulus rather than Young's modulus.

This situation could be applicable to reservoir conditions during water injection and cooling of the reservoir, causing the surrounding rock to contract. The weight of the overburden is constant, but the reservoir is able to be deformed axially, but is constrained laterally. In order to maintain horizontal strain constant, horizontal stress must be reduced and as a result the deviatoric stress is increased. The increased deviatoric stress could lead to permanent damage of a rock.

There is no clear trend of the moduli dependence with additional temperature cycles (Figure 22).
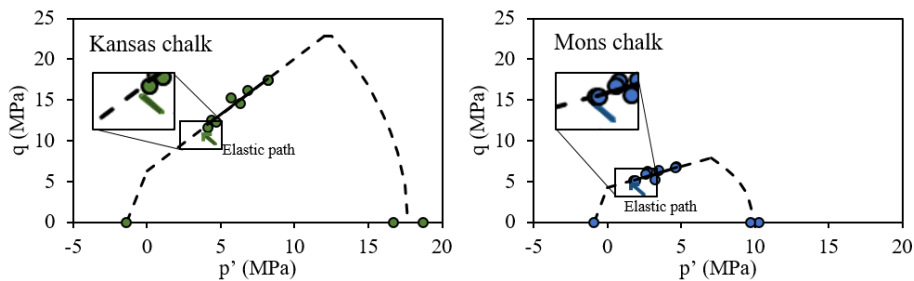
Figure 20 - Elastic path of the two chalks during unloading, indicates that the deviatoric stress gets almost high enough to induce shear failure of the sample and potentially permanently damages it.
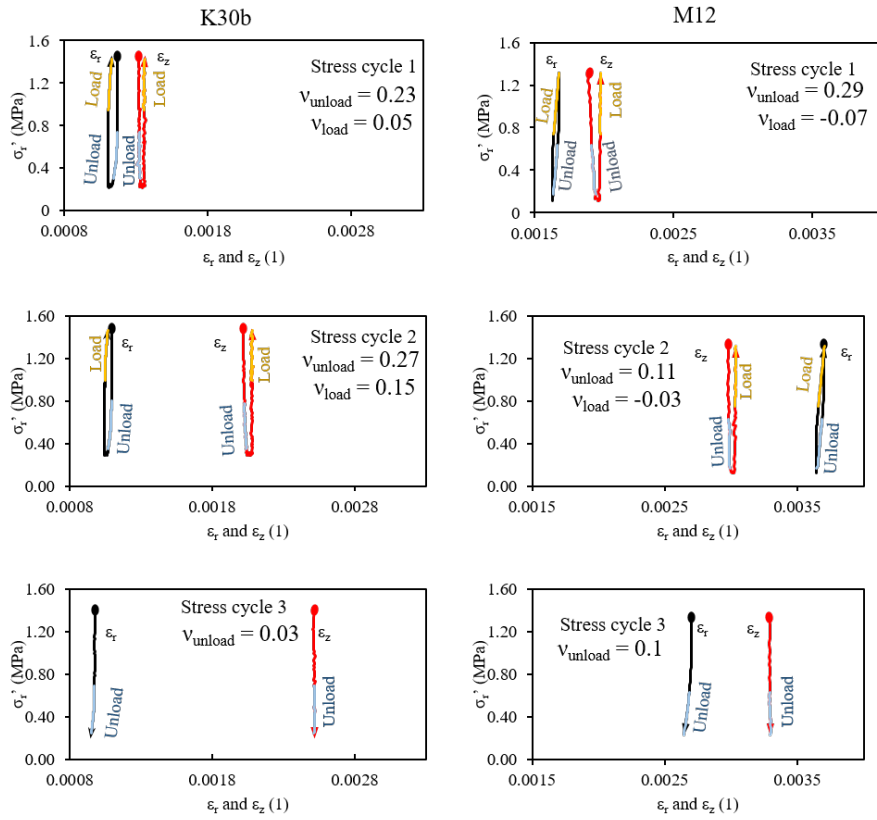
Figure 21 - Stress- strain relationship during the three stress cycles for Kansas chalk (left) and Mons chalk (right), highlighting the intervals at which ν was measured.
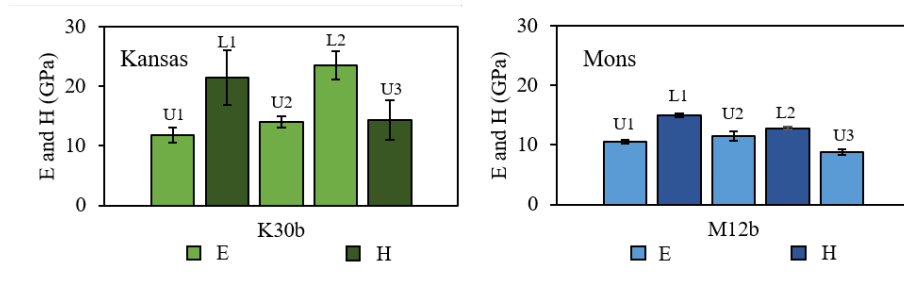
Figure 22 - Young´s modulus E (lighter colour) and uniaxial compression modulus H (darker colour) measured during unloading (U) and loading (L) under constant overburden experiments.

3.4 Thermal expansion

The coefficient of linear thermal expansion α was calculated using radial strain during cooling from 90 to 30°C (page 25). The values measured are similar between two chalk types and in line with an average thermal expansion of the c-axis and two perpendicular axes for calcite (Table 1). Temperature cycling had an impact on the thermal expansion coefficient, where both chalks demonstrated a decrease by approximately 10% by the third cycle (Figure 23).
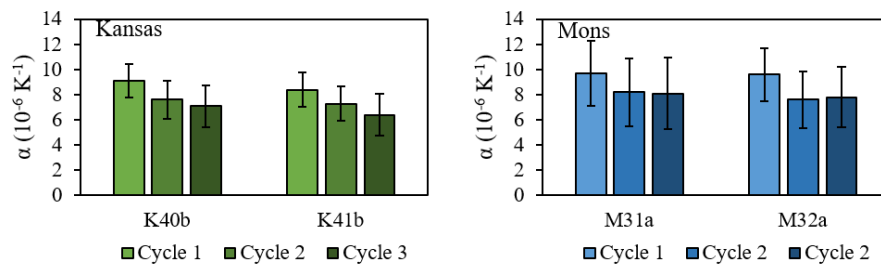
Figure 23 - Thermal expansion coefficient α evolution through temperature cycles for Kansas chalk samples (green) and Mons chalk samples (blue).

Thermal expansion was also measured with the constant overburden conditions (Figure 24). This meant that the samples were not allowed to expand freely in all directions. In this case, the thermal expansion of Kansas and Mons chalk differ, where thermal expansion of Mons chalk is almost double that of Kansas chalk, or in other words, Kansas chalk only contracted half as much as Mons chalk during cooling from 90°C to 30°C. This could correlate to the fact that the axial load applied on Kansas chalk samples is almost twice of that applied on the Mons samples, $\sigma_z'=11.8$ MPa for Kansas chalk and $\sigma_z'=5.3$ MPa for Mons chalk (70% of the shear failure strength).
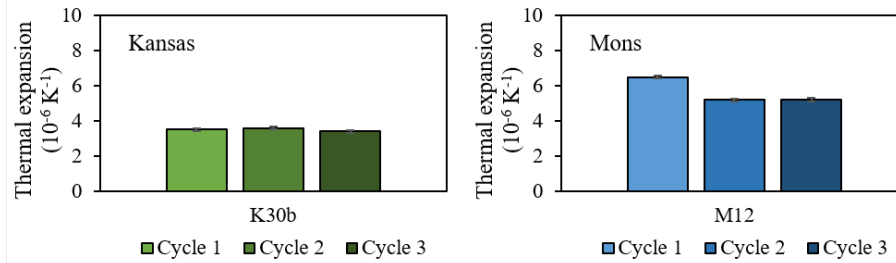
Figure 24 - Thermal expansion through temperature cycles under constant overburden stress for Kansas chalk samples (green) and Mons chalk samples (blue), where σ_z'=11.8 MPa for Kansas chalk and σ_z'=5.3 MPa for Mons chalk.

3.5 $p' - q$ diagram

Combining the shear failure information with data from tensile failure and hydrostatic yield, a $p - q$ failure envelop for Kansas and Mons chalks saturated with calcite equilibrated water at 30°C is produced (Figure 25), indicating the higher strength of the more indurated Kansas chalk.
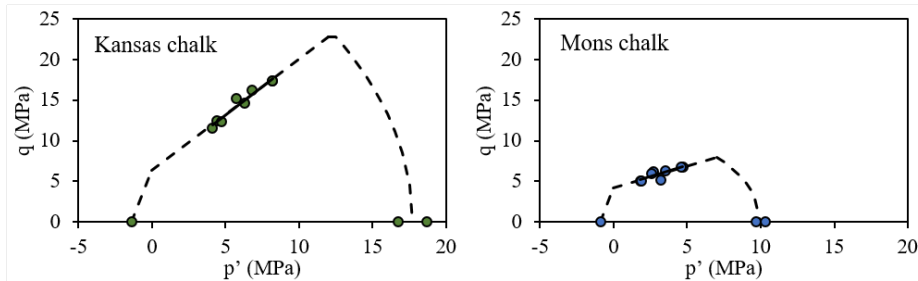
Figure 25 - $p - q$ failure limits for Kansas and Mons chalks saturated with calcite equilibrated water at 30°C.

4 Conclusion and future work

4.1 Conclusion and summery

The presented study provides a comprehensive analysis investigating the effects of temperature cycling on mechanical properties of chalks. The mechanical properties include tensile strength, elasto-plastic partition and irreversible strain accumulation, elastic moduli tested under hydrostatic and uniaxial stress conditions, and thermal expansion. To assess the importance of induration, two chalks of different diagenesis and contact cement amount were tested. In addition, the samples have been saturated with polar and non-polar fluid in order to gain better understanding of how of surface-ative ions absorb on mineral surfaces, and thus be related to water weakening mechanisms for chalk. For the oil and gas-industry, the implication of the experiments is to better understand how mechanical stability of chalk reservoirs are affected during sea-water injection.

Tensile strengths for dry chalk samples were not weakened by temperature cycles. However, for both chalks, the initial tensile strength was halved when saturated by water, and then a further reduction in tensile strength were observed with increasing number of temperature cycles. After 30 temperature cycles, water saturated samples had their strength reduced to only 25% of the dry samples not exposed to any temperature cycling.

Temperature cycles led to greater accumulation of irreversible strain during hydrostatic stress cycles than samples tested at constant temperature. Remark that the hydrostatic stress cycles were all performed at 30C, and the comparison of plastic component were compared the experiments kept at 30C throughout the test program, and those exposed to a temperature variation between each stress cycle. The irreversible strain accumulation was especially pronounced for the water

saturated and more indurated Kansas chalk than the Mons chalk. It was concluded that the anisotropic thermal expansion of calcite crystals resulted in more thermal stress accumulation when greater amount of contact cement is present. Thus, the polarity of the saturating fluid played a greater role on more indurated chalk when exposed to temperature cycling. However, temperature cycling did not have a weakening effect on the hydrostatic yield stress of the sample; leading to conclusion that even the temperature cycling resulted in an increase in the number of micro fractures, this did not influence the overall compression strength of the samples.

The elastic bulk moduli dependence on temperature cycling was less pronounced. The bulk modulus tested under hydrostatic condition was decreased for Mons but not Kansas chalk. The Young´s modulus and compression modulus tested under uniaxial stress conditions were not impacted by temperature cycling.

The coefficient of thermal expansion measured in the experiments is similar for the two chalk types and agrees with an average thermal expansion of calcite. Increasing the number of temperature cycles caused a decreasing trend in thermal expansion coefficients.

The results of this project are presented in academic papers as following:

Paper I -   Characterization of the two types of chalk tested is presented in this paper, including carbonate and other minerals content from XRD analysis, and P-wave modulus from p-wave velocity. Porosity, permeability, specific surface area and pore size estimation were tested for dry samples at 0 and 15 temperature cycles.

This paper further analyses tensile strength measurements, and its dependence on temperature cycles and water weakening.

Paper II - This paper compares the total accumulated strain during hydrostatic stress cycles and its irreversible fraction for the two types of chalk tested at a constant temperature to those tested with temperature cycling. The samples were saturated with equilibrated calcite water (polar) and non-polar Isopar-H oil in order to quantify the importance of water weakening

Paper III - Bulk moduli tested under hydrostatic condition, and Young´s moduli and compression moduli tested under uniaxial stress conditions are analysed for their dependence on temperature cycling. The effect of increasing temperature cycles is also analysed for thermal expansion.

Paper IV - Keeping the overburden stress constant, this study measures the amount of radial stress reduction needed to re-establish zero radial strain caused by 60°C cooling, and weather the increase in deviatoric stress would be sufficient to trigger shear failure.

Paper V - Preliminary report of tensile strength and irreversible fraction for more indurated chalk.

4.2 Future work

Much research is based on increasing recovery of oil from reservoirs, but few look into the effect they may have. It is important to understand how oilfield production practices in the form of EOR affect reservoir rocks and ultimate recovery from oilfields.

The results of the experiments presented in this work prove that temperature cycling has an effect on chalk mechanical behaviour. To

gain a deeper perception, some of the experiments could be enhanced, or altered.

For the tensile strength experiments, additional temperature cycles would show if the weakening rate drops or if it remains the same. It would also be beneficial to perform velocity measurements, v_p and v_s, after temperature cycling to see if the Biot coefficient changes with an increasing number of temperature cycles.

For the strain partitioning, experiments could be repeated at the constant temperature of 130°C to investigate if the strain would have accumulated with the enhanced double layer only, or if the accumulated strain was due to the temperature cycling.

In the experiments measuring the elastic moduli, the starting confining pressure could be set higher, and then one could measure the amount of side stress that needs to be reduced in order to maintain the sample's dimensions prior cooling, and if the stress reduction would be sufficient to induce shear failure.

In addition, it would be interesting to repeat these experiments on samples representing other types or reservoir and rocks within the reservoir units, such as sandstone or claystone. This would give us a better understanding to which extent anisotropic thermal expansion plays a role in rock weakening due to temperature cycling.

References

Andreassen, K. A., & Fabricius, I. L. (2010). Biot critical frequency applied to description of failure and yield of highly porous chalk with different pore fluids. *GEOPHYSICS, 75*(6), E205-E213. Retrieved from https://library.seg.org/doi/abs/10.1190/1.3504188

Atkinson, B. K. (1984). Subcritical crack growth in geological materials. *Journal of geophysical Research, 89*(B6), 4077-4114.

Atkinson, B. K., & Meredith, P. G. (1981). Stress corrosion cracking of quartz: a note on the influence of chamical environment. *Tectonophys, 77*, T1-T11.

Baud, P., Zhu, W. L., & Wong, T. F. (2000). Failure mode and weakening effect of water on sandstone. *Journal of Geophysical Research-Solid Earth, 105*(B7), 16371-16389. doi:Doi 10.1029/2000jb900087

Fabricius, I. L. (2014). Burial stress and elastic strain of carbonate rocks. *Geophysical Prospecting, 62*(6), 1327-1336. doi:10.1111/1365-2478.12184

Finn, T. M., & Johnson, R. C. (2016). Niobrara Total Petroleum System (503703) in the Southwestern Wyoming Province. In *Petroleum Systems and Geologic Assessment of Oil and Gas in the Southwestern Wyoming Province, Wyoming, Colorado, and Utah*: USGS.

Goncalves, T. D., & Brito, V. (2017). Differential thermal expansion as a cause of salt decay: literature review, experiments, and modelling of micro and macro effects on Anca limestone. *Studies in Conservation, 62*(6), 310-328. doi:10.1080/00393630.2016.1140860

Hansen, K. K., Leksø, H., & Grelk, B. (2003). Assessment of the Durability of Marble Cladding by Laboratory Exposure compared to Natural Exposure.

Harvey, R. (1967). Thermal expansion of certain Illinois limestones and dolomites. *Illinois State Geological Survey Circular*.

Hua, W., Dong, S. M., Li, Y. F., Xu, J. G., & Wang, Q. Y. (2015). The influence of cyclic wetting and drying on the fracture toughness of sandstone. *International Journal of Rock Mechanics and Mining Sciences, 78*, 331-335. Retrieved from <Go to ISI>://WOS:000360637800032

Jay, A. H. (1934). The thermal expansion of bismuth by X-ray measurements. *Proceedings of the Royal Society of London. Series A, 143*(849), 465-472. Retrieved from http://rspa.royalsocietypublishing.org/content/royprsa/143/849/465.full.pdf

Johnson, W. H., & Parsons, W. H. (1944). *Thermal expansion of concrete aggregate materials*. Washington,: U. S. Govt. print. off.

Lebedev, M., Wilson, M. E. J., & Mikhaltsevitch, V. (2014). An experimental study of solid matrix weakening in water-saturated Savonnieres limestone. *Geophysical Prospecting, 62*(6), 1253-1265. doi:10.1111/1365-2478.12168

Lisabeth, H. P., & Zhu, W. L. (2015). Effect of temperature and pore fluid on the strength of porous limestone. *Journal of Geophysical Research-Solid Earth, 120*(9), 6191-6208. doi:10.1002/2015jb012152

Luque, A., Leiss, B., Alvarez-Lloret, P., Cultrone, G., Siegesmund, S., Sebastian, E., & Cardell, C. (2011). Potential thermal expansion of calcitic and dolomitic marbles from Andalusia (Spain). *Journal of Applied Crystallography, 44*, 1227-1237. doi:Doi 10.1107/S0021889811036910

Lyklema, J. (2000). *Fundamentals of interface and colloid science*. San Diego: Academic Press.

Madland, M. V., Korsnes, R. I., & Risnes, R. (2002). Temperature Effects In Brazilian, Uniaxial And Triaxial Compressive Tests With High Porosity Chalk. *Society of Petroleum Engineers*, SPE77761.

Markgraf, S. A., & Reeder, R. J. (1985). High-temperature structure refinements of calcite and magnesite. *American Mineralogist, 70*(5-6), 590-600. Retrieved from http://dx.doi.org/

Megawati, M., Hiorth, A., & Madland, M. V. (2013). The Impact of Surface Charge on the Mechanical Behavior of High-Porosity

Chalk. *Rock Mechanics and Rock Engineering, 46*(5), 1073-1090. doi:10.1007/s00603-012-0317-z

Pirson, S., Spagna, P., Baele, J. M., Damblon, F., Gerrienne, P., Vanbrabant, Y., & Yans, J. (2008). An overview of the geology of Belgium. *Memoirs of the Geological Survey of Belgium, 55*, 5-25.

Rao, K. V. K., Naidu, S. V. N., & Murthy, K. S. (1968). Precision lattice parameters and thermal expansion of calcite. *Journal of Physics and Chemistry of Solids, 29*(2), 245-248. doi:https://doi.org/10.1016/0022-3697(68)90068-1

Risnes, R., Madland, M. V., Hole, M., & Kwabiah, N. K. (2005). Water weakening of chalk - Mechanical effects of water-glycol mixtures. *Journal of Petroleum Science and Engineering, 48*(1-2), 21-36. Retrieved from <Go to ISI>://WOS:000231275000002

Rosenholtz, J. L., & Smith, D. Z. (1949). Linear thermal expansion of calcite, var. Iceland spar and Yule marble. *American Mineral*(34), 846–854.

Røyne, A., Bisschop, J., & Dysthe, D. K. (2011). Experimental investigation of surface energy and subcritical crack growth in calcite. *Journal of Geophysical Research: Solid Earth, 116*(B4), B04204. doi:10.1029/2010JB008033

Stipp, S., Brady, P. V., Ragnarsdottir, K. V., & Charlet, L. (1999). Geochemistry in aqueous systems - A special issue in honor of Werner Stumm - Preface. *Geochimica Et Cosmochimica Acta, 63*(7). Retrieved from <Go to ISI>://WOS:000083824200002

Wasantha, P. L. P., & Ranjith, P. G. (2014). Water-weakening behavior of Hawkesbury sandstone in brittle regime. *Engineering Geology, 178*, 91-101. doi:10.1016/j.enggeo.2014.05.015

Weiss, T., Siegesmund, S., & Fuller, E. R. (2003). Thermal degradation of marble: indications from finite-element modelling. *Building and Environment, 38*(9-10), 1251-1260. doi:10.1016/S0360-1323(03)00082-9

Wu, T. C., Shen, A. H., Weathers, R. S., Bassett, W. A., & Chou, I. M. (1995). Anisotropic Thermal-Expansion of Calcite at High-Pressures - an in-Situ X-Ray-Diffraction Study in a Hydrothermal Diamond-Anvil Cell. *American Mineralogist,*

80(9-10), 941-946. Retrieved from <Go to ISI>://WOS:A1995RY40300010

Yakaboylu, O., Harinck, J., Smit, K. G. G., & de Jong, W. (2013). Supercritical water gasification of manure: A thermodynamic equilibrium modeling approach. *Biomass & Bioenergy, 59*, 253-263. Retrieved from <Go to ISI>://WOS:000330910400024

Publications

Paper I: Influence of temperature cycling and pore fluid on tensile strength of chalk

Voake, T., Nermoen, A., Ravnas, C., Korsnes, R.I., Fabricius, I.L. (2019).

Full Length Article

Influence of temperature cycling and pore fluid on tensile strength of chalk

T. Voake [a,b,*], A. Nermoen [b,c], C. Ravnås [d], R.I. Korsnes [a,b], I.L. Fabricius [a,d]

[a] University of Stavanger, Stavanger, Norway
[b] The National IOR Center of Norway, University of Stavanger, Stavanger, Norway
[c] NORCE Norwegian Research Centre AS, Oslo, Norway
[d] Technical University of Denmark, Copenhagen, Denmark

ABSTRACT

Calcite has a highly anisotropic thermal expansion coefficient, and repeated heating and cooling cycles can potentially destabilize chalks by breaking cement bonds between neighboring particles. Based on tensile strength measurements, we investigated how temperature cycles induce weakening of chalk. Tensile strength tests were performed on chalk specimens sampled from Kansas (USA) and Mons (Belgium), each with differing amounts of contact cement. Samples of the two chalk types were tested in dry and water-saturated states, and then exposed to 0, 15, and 30 temperature cycles in order to find out under what circumstances thermally induced tensile strength reduction occurs. The testing results show that the dry samples were not influenced by temperature cycling in either of the chalk types. However, in the water-saturated state, tensile strength is increasingly reduced with progressive numbers of temperature cycles for both chalk samples, especially for the more cemented Kansas chalk. The Kansas chalk demonstrated higher initial tensile strength compared to the less cemented Mons chalk, but the strength of both chalks was reduced by the same relative proportion when undergoing thermal cycles in the water-saturated state.

© 2019 Institute of Rock and Soil Mechanics, Chinese Academy of Sciences. Production and hosting by Elsevier B.V. This is an open access article under the CC BY-NC-ND license (http://creativecommons.org/licenses/by-nc-nd/4.0/).

1. Introduction

Carbonates are important reservoir rocks, which account for 50%–60% of the world's petroleum reserves (Burchette, 2012). Mechanical integrity of chalk has triggered a significant interest in engineering and academic circles since it was noticed that the sea bed over the Ekofisk oil field on the Norwegian Continental shelf subsided due to reservoir depletion (Sulak and Danielsen, 1988). Besides the reduction of pore pressure and then the increase in effective stress, compaction was later found to be enhanced by flooding with water (Hermansen et al., 1997). This so-called water weakening has been widely studied, but the potential effect of repeated temperature cycling of an initially warm reservoir cooling down due to the injection of cold water and then re-warming to equilibrate when this injection stops during the production life of an oil field has attracted less attention.

Chalk is a sedimentary rock with the main component of diagenetically altered calcareous nannofossils, which have calcite as a main component. Marble is a metamorphosed rock also composed of calcite, and experiments have shown that its strength is significantly influenced by temperature fluctuations. For example, marble monuments experience degradation and some marble façades tend to experience concave bowing when exposed to outdoor temperature variation (Weiss et al., 2003). Hansen et al. (2003) explored this phenomenon by comparing flexural strengths of naturally exposed marble to that of laboratory tested marble at 0% and 100% relative humidity. They found that naturally exposed marble weakens with respect to the number of years exposed, and the marble tested at 100% relative humidity weakens with the number of cooling and heating cycles, whereas no such trend was observed on dry samples tested.

Freshly deposited calcareous ooze has porosity of approximately 70%, and as it gets buried in depth, the ooze is mechanically compacted by overburden stress, resulting in pore volume loss. As the ooze is buried deeper, the stress at particle contacts builds up, resulting in pressure dissolution and contact cement, forming chalk (Fabricius, 2014). However, the strength development of chalk is

* Corresponding author.
E-mail address: tijana.voake@uis.no (T. Voake).
Peer review under responsibility of Institute of Rock and Soil Mechanics, Chinese Academy of Sciences.

not fully understood, and two strength components are suggested: attractive van der Waals forces at the contact cement and repulsive electrostatic forces between particles separated by water (Nermoen et al., 2018). Calcite is a uniaxial crystal with large anisotropic thermal expansion coefficients, which could induce stresses at cemented particle contacts when temperatures vary (Table 1). Two scenarios are considered here where the crystallographic c-axis of two neighboring particles parallel and perpendicular to each other (Fig. 1). Crystallographic axis perpendicular to c-axis is referred to as a-axis. Upon heating, in scenario 1, the particles contract in the plane perpendicular to the c-axis, resulting in the two particles being pulled apart and creating tensile forces at their contact cement (Fig. 1a); in scenario 2, the contact cement experiences shear forces as the contact area on one particle is contracting and the area on the other particle is expanding (Fig. 1b). These are two end member scenarios that most contact in a porous rock would fall in between. Once the contact cement bond is broken, it cannot be readily re-established; hence the premise of this paper is to investigate to what extent temperature variation induces loss in tensile strength of two chalk types.

Subcritical fracturing is considered as the main mechanism for stress corrosion, and propagation of pre-existing fractures during rock failure (Atkinson, 1984). The fracture depends on rock fabric, surrounding environments, and levels of applied stress. During subcritical fracturing of quartz, the fracture velocity was found to be much higher when water instead of air is present nearby the fracture tip. Additionally, the chemical species dissolved in the water, making it more polar, also play a role (Atkinson and Meredith, 1981). For limestone in which the primary mineral constituent is calcite, Lisabeth and Zhu (2015) demonstrated that the samples tested with equilibrated water were stronger than those tested with distilled water, and microcracking was the dominant deformation mechanism at lower pressures, while chemical weakening and twinning were more important for elevated pressures.

To understand how the pore fluid alters sample strength, a closer look at the surface properties of the mineral and its interaction with the ions dissolved in the water phase is required. The calcite surface has charged sites (Stipp, 1999). The cleavage plane $\{10\bar{1}4\}$ is populated with partially charged Ca^{2+} and CO_3^{2-}, thus, when a polar fluid is introduced to pore space, such as water, it is absorbed on the calcite surface, and a repulsive double-layer is created, making the chalk weaker (Megawati et al., 2013; Nermoen et al., 2018). The thickness of the double-layer, as described by the Debye–Hückel theory, increases with temperature (Andreassen and Fabricius, 2010), and is characterized by the Debye length κ^{-1} (Lyklema, 2000):

$$\kappa^{-1} = \left(\frac{\varepsilon_0 \varepsilon_r k_b T}{2 N_A e^2 I}\right)^{1/2}$$
$$= \left[\frac{(8.85 \times 10^{-12})\varepsilon_r (1.38 \times 10^{-23}) T}{2 \times (6.02 \times 10^{23}) \times (1.6 \times 10^{-19})^2 I}\right]^{1/2} \quad (1)$$

where ε_0 is the permittivity of a vacuum, ε_r is the relative permittivity of water (the saturating fluid), k_b is the Boltzmann's constant,

T is the temperature, N_A is the Avogadro's number, e is the elementary charge, and I is the ionic strength of the pore water. The relative permittivity of water also depends on the temperature, which must be taken into account. ε_r is 88.44 at 20 °C and 51.17 at 130 °C (Yakaboylu et al., 2013). Repulsion increases with the thickness of the double-layer, because the volume in which the double layers overlap between two neighboring particles increases.

The surface energy γ_s of the cleavage plane $\{10\bar{1}4\}$ depends on the presence of water, and the surface energies of dry and fully hydrated calcite surfaces are 0.32 J/m² and 0.15 J/m², respectively (Royne et al., 2011). Hence, the energy necessary to form a dry surface (fracture) is double the energy required for the formation of a wet surface. The energy $U_{Surface}$ required to create a surface between two calcite particles is a function of the cross-sectional area A of the contact cement between two particles:

$$U_{Surface} = \gamma_s A \quad (2)$$

This can be compared to the elastic energy $U_{tensile}$ of the contact cement caused by thermal expansion/contraction. In scenario 1 (Fig. 1a) where neighboring particles pull apart during heating, a tensile fracture occurs when the elastic energy overcomes the surface energy. In one-dimension (1D) condition, the tensile energy is calculated as

$$U_{tensile} = \frac{1}{2}E(\alpha\Delta T)^2 V_p \quad (3)$$

where E is the calcite Young's modulus, and V_p is the volume of a particle. Hooke's law for general anisotropic materials linearly relates stress to strain by elastic constant c:

$$\sigma_{ij} = c_{ijkl}\varepsilon_{kl} \quad (4)$$

Using an abbreviated Voigt notation, four elastic subscripts for the elastic constant are reduced to two, so that each pair of $ij(kl)$ is replaced by IJ (Mavko et al., 2009). In a transversely isotropic case, which corresponds to a calcite crystal, the Young's modulus along c-axis, E_{33}, becomes

$$E_{33} = c_{33} - \frac{2c_{13}^2}{c_{11} + c_{12}} = 57.8 \text{ GPa} \quad (5)$$

where $c_{11} = 149.9$ GPa, $c_{33} = 85.2$ GPa, $c_{12} = 57.9$ GPa, and $c_{13} = 53.5$ GPa (Chen et al., 2001). The Young's modulus along the a-axis, E_{11}, is expressed as

$$E_{11} = c_{11} - \frac{c_{13}^2(-c_{11} + c_{12}) + c_{12}(-c_{33}c_{12} + c_{13}^2)}{c_{33}c_{11} - c_{13}^2}$$
$$= 110.9 \text{ GPa} \quad (6)$$

When heated in scenario 2, one particle expands along the contact cement and the other contracts, resulting in the creation of a shear stress τ (Fig. 1b). The strain energy U_{Shear} created by strain depends upon the shear stress τ, shear angle β, and contact volume V_c:

$$U_{Shear} = \frac{1}{2}\tau\beta V_c \quad (7)$$

$$\tau = G/\beta \quad (8)$$

where G is the shear modulus, which also depends on the crystal orientation. For calcite, G_{33} corresponds to the shear modulus parallel to c-axis with $\theta = 0°$, and G_{11} perpendicular to c-axis with $\theta = 90°$:

Table 1
Calcite anisotropic thermal expansion coefficient in the literature.

Reference	Thermal expansion coefficient, α (10^{-6} K^{-1})	
	Parallel to c-axis	Perpendicular to c-axis
Rosenholtz and Smith (1949)	23.8	−5.2
Markgraf and Reeder (1985)	32.3	−2.8
Wu et al. (1995)	28.798	−5.371
Rao et al. (1968)	25.1	−3.68
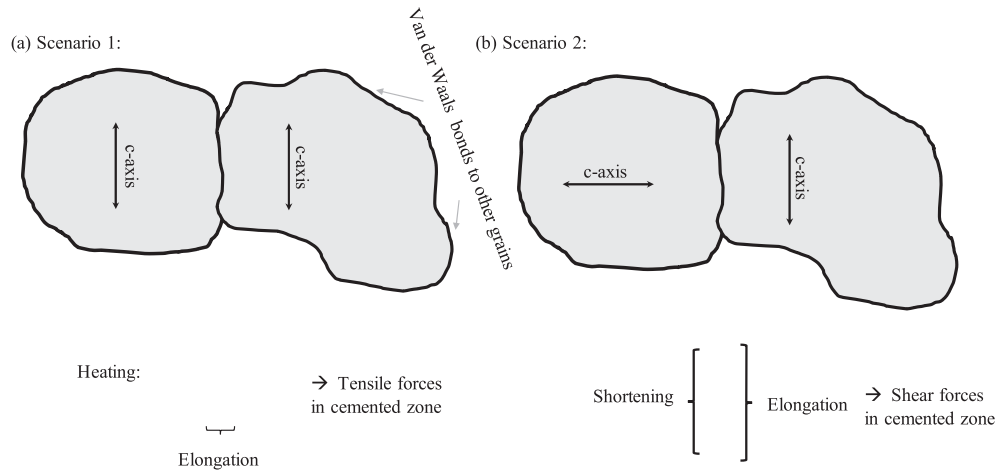
Fig. 1. Two scenarios in which the *c*-axis is (a) parallel and (b) perpendicular to each other dictate how the contact zone between neighboring calcite particles develop when the system is heated.

$$G = c_{66} \sin^2 \theta + c_{44} \cos^2 \theta \tag{9}$$

$$G_{33} = c_{66} \sin^2 0° + c_{44} \cos^2 0° = 34.1 \text{ GPa} \tag{10}$$

$$G_{11} = c_{66} \sin^2 90° + c_{44} \cos^2 90° = 45.8 \text{ GPa} \tag{11}$$

where $c_{44} = 34.1$ GPa (Chen et al., 2001), and $c_{66} = (c_{11} - c_{12})/2 = 45.8$ GPa.

As the tensile and shear energies depend on the particle volume, and the surface energy depends on the contact area between two particles, the elastic energy increases at a greater rate than the surface energy with increasing particle size. This would lead to larger particles breaking apart first, while smaller particles hold together.

Madland et al. (2002) experimentally studied how the tensile strength of highly porous chalk reduces when saturated with water or glycol at 130 °C compared with that tested at temperature 30 °C, while dry chalk showed no significant dependence of strength on temperature. Therefore, the temperature itself in the range of 30–130 °C is not likely to play a decisive role in determining the mechanical strength of chalks alone − for chalks it is the combination of pore fluid and temperature that together dictates sample strength within these temperature intervals. However, in the dry state, the dependence of strength on temperature has been observed in other materials including granite, gneiss, polymer mortars, as well as sandstone. They all demonstrated a strength reduction with increasing temperature (Jay, 1934; Lee et al., 1996; dos Reis, 2012; Huang and Xia, 2015).

Few studies have focused on how the material strength is affected by temperature cycles while performing strength tests at the same temperature. Hua et al. (2015) investigated how the tensile strength of sandstone samples depends on cyclical saturation with water for 48 h and drying at 105 °C for 24 h, and implied that 50% of strength was lost just after seven repeated cycles. Quartz, as the main component of sandstone, has an anisotropic thermal expansion coefficient of 14.4×10^{-6} K^{-1} and 7.8×10^{-6} K^{-1} in the direction perpendicular and parallel to the principal axis, respectively (Jay, 1934). Hence, the thermal anisotropy of quartz is not as pronounced as that of calcite.

In this paper, the effect of temperature cycling on chalks samples from two regions was studied by measuring tensile strength affected by 0, 15 and 30 temperature heating and cooling cycles. Furthermore, the tensile strengths of dry (air-saturated) and water-saturated samples are compared. The two chalks were selected due to their different degrees of induration and hence different degrees of contact cementation. Finally, the combined effects of pore fluid and temperature cycling on the two chalks are evaluated.

2. Materials and method

2.1. Materials

Chalks from two different quarries were used in this study: Kansas chalk from the Fort Hays Member of the Niobrara Formation (Late Cretaceous) located near Niobrara, Kansas, USA, and Mons chalk from the Trivières Formation (Late Cretaceous) located in Harmignies, Belgium. Kansas chalk has gone through a higher degree of diagenesis (Finn and Johnson, 2005) than the Mons chalk (Pirson et al., 2008). Ravnås (2017) found that the Mons chalk has a carbonate content of 99.8% and a Biot coefficient of 0.95; while the Kansas chalk has a carbonate content of 96.9% and a Biot coefficient of 0.91, which are lower than those of Mons chalk, indicating a higher degree of contact cement. Both chalks are homogeneous on the plug scale (Fig. 2).

Cylinders of about 40 mm in diameter and 300 mm in length were drilled perpendicular to the bedding from larger-size rock
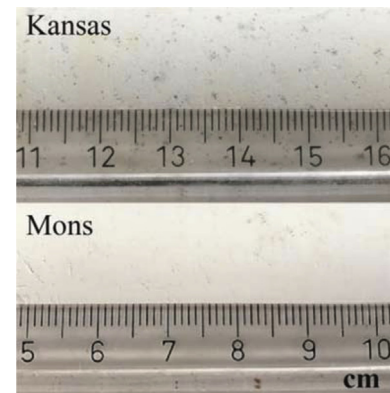
Fig. 2. Optical photography of Kansas and Mons chalks. The Kansas chalk has a higher content of microfossils seen as darker dots.

blocks (about 30 cm × 30 cm × 30 cm) from the two quarries. The long cylinders were then radially adjusted to 38.1 mm using a lathe, and cut into 156 disk-shaped samples with the length of 20−25 mm.

2.2. Petrographic and petrophysical characterizations

Characterization was performed on selected tested and untested samples. The untested samples were drilled from the same block as those for Brazilian test purposes.

For a visual assessment of the micro-structures of the chalk, polished samples were prepared, and backscatter electron micrographs were recorded using an FEI Inspect™ scanning electron microscope (SEM). The carbonate content was measured by dissolution of crushed samples using hydrochloric acid (HCl) and subsequent titration with NaOH. Based on the carbonate content measured by titration, a chalk sample large enough to yield 0.03 g of insoluble residue was dissolved in acetic acid. The non-carbonate minerals of the insoluble residue were identified by X-ray diffraction (XRD) using Cu K-α radiation and a PANalytical X'pert Pro X-ray Diffractometer.

P-wave velocity, v_p, of ultrasonic (200 kHz) elastic waves was recorded on dry cylindrical samples under uniaxial stress of 2 MPa (error: ±100 m/s). Based on the P-wave velocity and dry density ρ_d, the elastic P-wave modulus M was calculated as

$$M = \rho_d v_p^2 \tag{12}$$

The dry density ρ_d was measured using dry weight (error: ±0.01 g) and volume (error: ±0.044 cm^3) of a sample.

The grain density (ρ_g), nitrogen (N_2) porosity (ϕ), and permeability (k) were measured by using a PoroPerm Production 2 gas porosimeter from Vinci Technologies.

The specific surface area of crushed chalk samples (S_{BET}) was measured by a multipoint procedure using an Autosorb iQ gas sorption system from Quantachrome Instruments. This measured value was further used to derive the specific surface with respect to bulk volume (S_b) and that with respect to the porosity (S_ϕ):

$$S_b = S_{BET}\rho_g(1 - \phi) \tag{13}$$

$$S_\phi = S_b/\phi \tag{14}$$

The equivalent cylindrical pore radius r then becomes

$$r = 2\big/S_\phi \tag{15}$$

By assuming an irreducible water film thickness h, the irreducible water saturation S_{wir} can be estimated by

$$S_{wir} = hS_\phi \tag{16}$$

The actual pore size distribution was measured by low-field nuclear magnetic resonance (NMR) spectrometry using a GeoSpec 2/53 DRX-HF digital spectrometer from Oxford Instruments. The recycle delay was set to 3750 ms, the number of echoes was 22,727, and echo spacing was 0.11 ms. Measurements were recorded at signal to noise ratio (SNR) greater than 500. Using Lithometrix, acquired data were converted into a relaxation time (T_2) distribution:

$$1/T_2 = \rho S_\phi \tag{17}$$

where ρ is a relaxation constant.

The NMR method sends polarizing pulses that excite hydrogen protons in the pore fluid, and then measures the signal decay rate of each pulse, which is also called the relaxation time. Pore walls
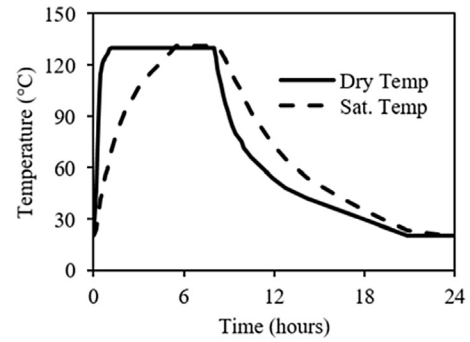
Fig. 3. A single temperature cycle for dry and saturated samples.

cause rapid dephasing, so in smaller pores, an excited proton has a shorter distance to the pore wall, thus decaying in less time, and inversely the relaxation time is longer for larger pores.

2.3. Brazilian tensile strength test

The disk-shaped samples from each location were randomly divided into two groups where half of the samples remained dry, and the others were saturated with calcite-equilibrated water of the ionic strength of 0.652 mmol/L (measured using ion chromatography). For each group, one third of samples were kept at room temperature (25 °C), while the remaining samples were repeatedly heated to 130 °C (8 h) and then cooled to room temperature (16 h). However, it took some time to reach the desired temperatures (Fig. 3). The target temperature was always reached within each cycle, and the samples were kept at the stable temperature for at least 1−2 h. During heating and cooling, the water-saturated samples were submerged in calcite-equilibrated water in a large steel container, which was kept at 3−5 bar (1 bar = 0.1 MPa) pressure to avoid evaporation and boiling.

The test matrix consists of chalks from two locations (Kansas and Mons), two saturation states (dry and water-saturated) and three kinds of cycles (0, 15 and 30). From each group, at 0, 15 and 30 temperature cycles, samples were randomly selected and their tensile strengths were measured by a Brazilian setup (Fig. 4). A total of 156 tensile tests were performed to obtain statistical confidence for the estimation of tensile strength.

Brazilian tests can measure the splitting tensile strength of brittle material. They were performed by subjecting each
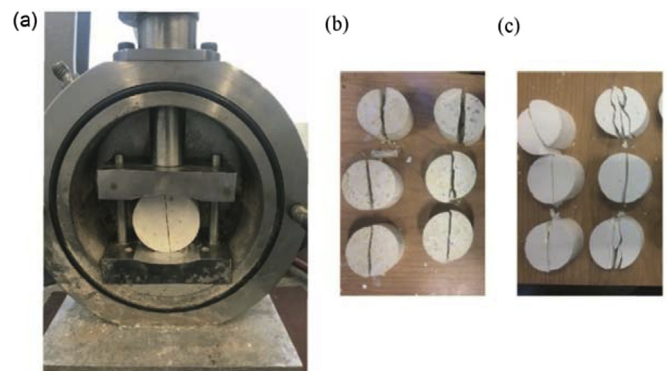
Fig. 4. (a) Brazilian test setup with a cylindrical chalk samples placed on the side between two parallelly loaded plates. Tensile fracture at failure is observed. (b) Optical photography of fractured Kansas chalk samples (15 cycles, dry). (c) Optical photography of fractured Mons chalk samples (15 cycles, dry).

cylindrical sample to load applied by two curved loading plates until the sample was split in half. Movement of the plates was controlled by injecting hydraulic oil with a Gilson 307 pump at a flow rate of 0.5 mL/min. Consequently, depending on the stiffness of the sample, the resulting loading rate will vary.

The normal force applied was measured by a transducer of type C2S and logged in a LabView routine. From the peak force (F) at which the sample fails, tensile strength (T_0) was calculated from the following equation:

$$T_0 = \frac{2F}{\pi Dt} \tag{18}$$

where D and t are the diameter and thickness of the disk, respectively.

3. Results

3.1. Petrographic and petrophysical characterizations

Using backscatter electron micrographs, we can observe the texture of the two chalk types (Figs. 5 and 6). The Kansas chalk has larger and more angular particles, as well as a larger contact area between the particles (Fig. 5). This is reflected in its higher induration of H3 (Henriksen et al., 1999). The Mons chalk has smaller particles and smaller contact areas between particles, as well as lower induration of H2 (Fig. 6). From Figs. 5 and 6, one can see that the frame of the rock is largely composed of calcite, whereas silicates and clays are rare, and do not contribute significantly to the frame. Hence, the analysis of the experimental results focuses on the temperature dependence on the contact between calcite particles.
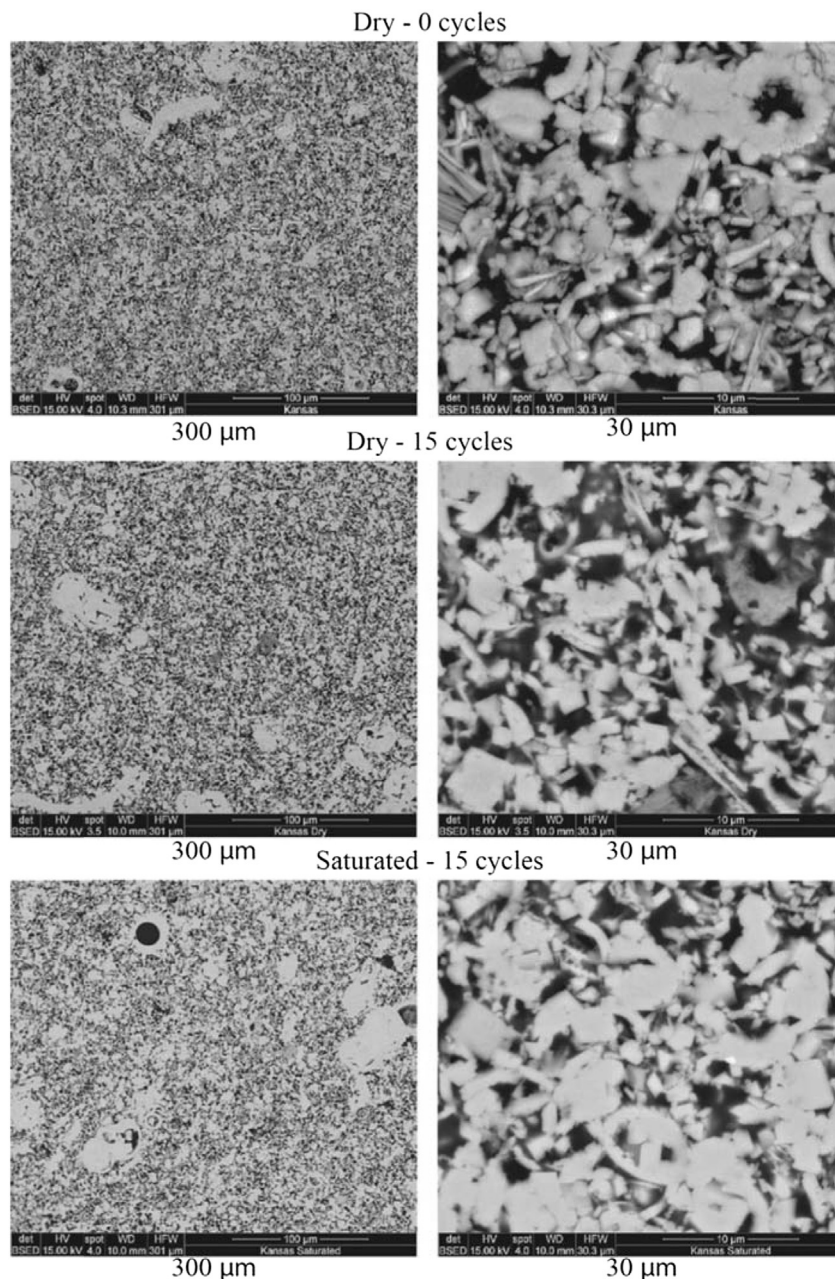
Fig. 5. Backscatter electron micrographs of Kansas chalk subjected to different numbers of temperature cycles in dry and saturated conditions.
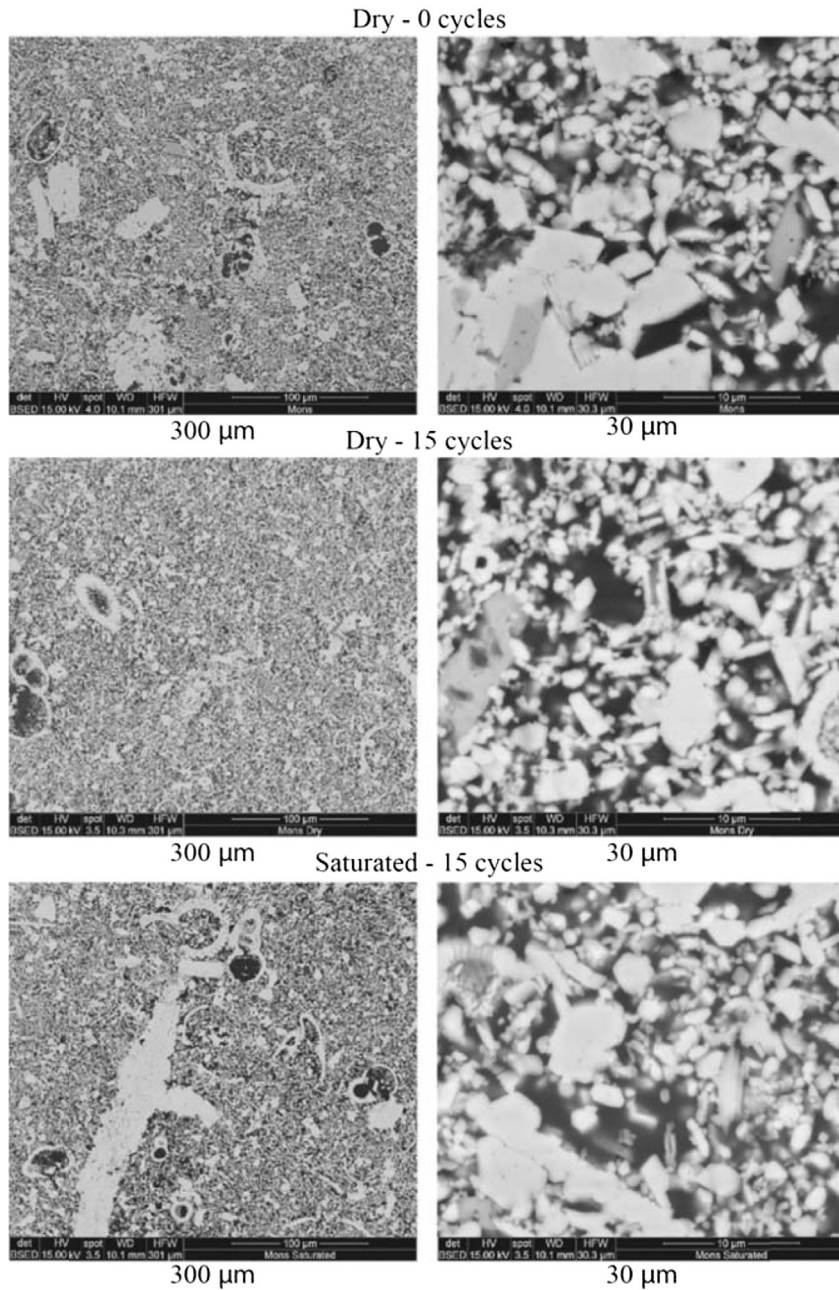
Fig. 6. Backscatter electron micrographs of Mons chalk subjected to different numbers of temperature cycles in dry and saturated conditions.

XRD analysis of the insoluble residue revealed that Kansas chalk also contains quartz, kaolinite and illite, as well as traces of feldspar, whereas Mons chalk contains smectite–illite and traces of apatite. It is evident that dry Kansas chalk has a higher P-wave modulus (M) than dry Mons chalk, indicating higher stiffness (Table 2).

Table 2
Carbonate content, mineral content and P-wave modulus (M) of dry Kansas and Mons chalk samples.

Chalk type	CaCO$_3$ content (%)	Error (%)	Other minerals	M (GPa)
Kansas	93.9–99.9	±0.1	Quartz, illite, kaolinite, and feldspar	14.4
Mons	99.6–99.9	±0.1	Smectite–illite, clinoptilolite, and apatite	9.5

In addition to the difference in mineralogy, Mons chalk has higher porosity and permeability than Kansas chalk. However, neither of these properties was significantly influenced by the temperature cycles (Table 3). Furthermore, as derived from S_{BET}, Mons chalk has a larger equivalent pore radius in comparison to Kansas chalk and therefore lower irreducible water saturation estimated. Only for Mons chalk did we find a significant increase in pore size due to temperature cycling (Table 3).

The increased pore size due to temperature cycling was further confirmed by the NMR data. Samples exposed to temperature cycling in the dry state indicated no change in the relaxation time (T_2) for Kansas chalk, whereas a shift to longer relaxation time was noticeable in all Mons chalk samples tested (Fig. 7). NMR measurements were performed on 4 samples from each location, all displaying the same trend, as shown in Fig. 7.

Table 3
Physical properties of Kansas and Mons chalks after 0 and 15 temperature cycles (dry samples).

Chalk type	Number of cycle	Porosity (%)	Permeability (mD)	S_{BET} (m²/g)	Equivalent pore radius (nm)	Equivalent irreducible water saturation (%)
Kansas	0	34.2 ± 1.3	1.5 ± 0.3	2.8 ± 0.1	135 ± 7	7.3 ± 0.4
	15	34.5 ± 1.2	1.6 ± 0.3	2.6 ± 0.1	147 ± 6	6.7 ± 0.4
Mons	0	43.0 ± 1.0	2.7 ± 0.6	2.1 ± 0.1	260 ± 5	3.8 ± 0.3
	15	43.3 ± 0.9	2.7 ± 0.4	1.9 ± 0.1	299 ± 5	3.3 ± 0.3

Note: S_{BET} was measured for this study. The errors are estimated at a 95% confidence interval (Kaiser and Watters, 2012).

3.2. Brazilian tensile strength tests

A typical loading curve obtained in the LabView routine is shown in Fig. 8, in which the normal force acting on the two parallel planes is plotted as a function of time. The slope of the curve (red line) indicates the loading rate of that particular sample. The red dot indicates the maximum force that a sample could sustain before a fracture was formed (Fig. 4), leading to an abrupt drop in the measured normal force.

The tensile strengths of samples in each test series, which consisted of 10–15 samples for each given chalk type (Kansas and Mons), saturation state (dry and wet) and number of temperature cycles (0, 15 and 30 cycles), are shown in Table 4. In Fig. 9a and b, the tensile strength is arranged in ascending order, starting from the weakest samples on the left to the strongest ones on the right. Each line represents the results from the 10–15 samples in each series. Based on the distribution of strengths for each test series, the average value and standard deviation were determined and the Gaussian distribution was calculated (Fig. 9c and d). The tensile strengths of dry Kansas and Mons chalks showed no significant dependence on the number of temperature cycles. The increase in strength of dry Kansas chalk due to temperature cycling was considered insignificant when compared to the standard deviation. By contrast, the tensile strength of water-saturated samples for both chalks was reduced with an increasing number of temperature cycles (Fig. 9 and Table 4). Even though the standard deviation makes data overlap, there was a clear descending trend for the average values of saturated samples with increasing number of temperatures cycles, while this cannot be observed for the average values of dry samples. In addition, a distinct difference exists between 0 and 30 cycles for both chalks even when the standard deviation is taken into account for saturated samples; while again, there was no clear trend for dry samples. A positive correlation

between the tensile strength and its standard deviation (σ) was observed, but all the standard deviations are found to be within 15%–30% of the average tensile strength T_0.

When comparing the impact of water saturation, before any temperature cycling was performed, the water weakening can be estimated for both chalk types. It was found that the initially stronger Kansas chalk was similarly susceptible to water weakening as Mons chalk (at zero cycle). The tensile strength of water-saturated Kansas and Mons chalks were 53% and 44% of the strength of dry samples, respectively. Since the Kansas chalk was initially stronger than Mons chalk, this implies that weakening by water saturation (in absolute terms) was 1.6 MPa for Kansas and 0.7 MPa for Mons chalk. The water-saturated Kansas chalk even had a lower tensile strength than the dry Mons chalk (Fig. 10a).

When increasing the number of temperature cycles in water-saturated conditions, the two chalks were weakened by the same absolute value (0.3 MPa) from 0 to 15 cycles (0.02 MPa/cycle). The strength reduction rate from 15 to 30 temperature cycles remained constant for Kansas chalk (0.3 MPa/15 cycles, or 0.02 MPa/cycle), but it was lower for Mons chalk (0.2 MPa/15 cycles, or 0.013 MPa/cycle). By the end of the 30th cycle, the proportion of strength reduction for saturated samples was almost equal for the two chalk types (Fig. 10b). However, if the temperature cycling effect is combined with the presence of pore fluid, comparing the dry and saturated samples subjected to 15/30 cycles, it is found that the Kansas chalk was more affected in terms of the absolute tensile strength loss (Fig. 11).

The significant change in tensile strength associated with water saturation was not caused by variations in porosity (Fig. 12), where no correlation was observed between the porosity and the tensile strength. However, due to the way in which the setup was designed and the flow rate of the hydraulic oil was controlled to supply the piston, the loading rate was affected by the stiffness of the sample,
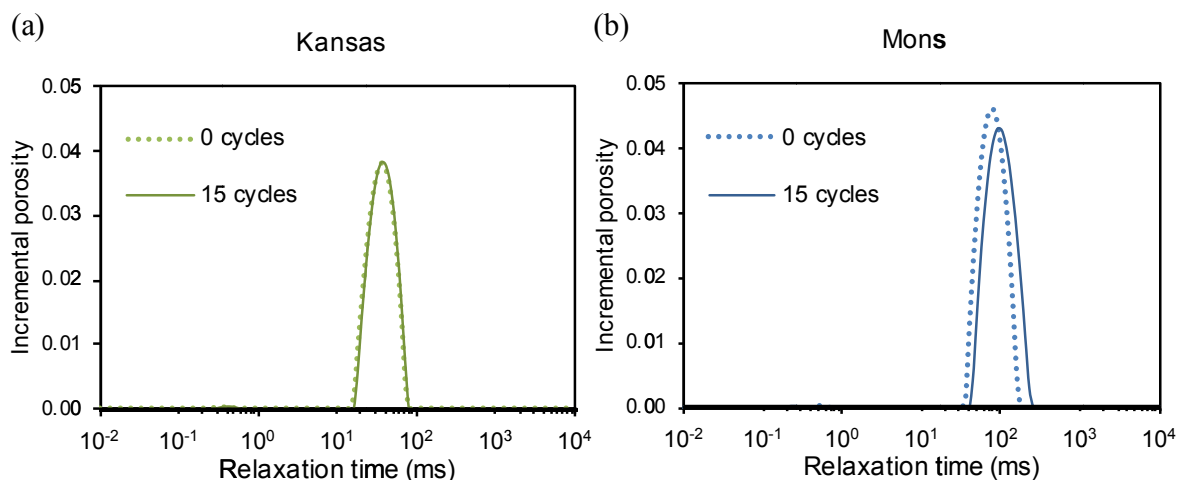

Fig. 7. Nuclear magnetic resonance (NMR) relaxation time after 0 and 15 temperature cycles in dry state. The NMR measurements were done after saturating these samples with water.
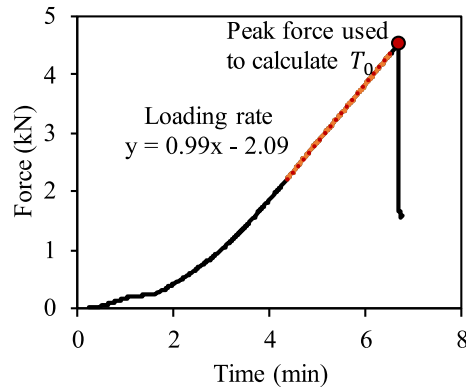
Fig. 8. Loading curve of a typical Brazilian test (dry Kansas sample). The curve was used to estimate the loading rate (red line) which correlates the stiffness of sample. The peak force is marked with the red dot and was used to estimate the tensile strength.

Table 4
Average values and standard deviations of the tensile strength measurements for each group of chalk samples. Even though the precision of the normal force measurement is high, the tensile strength for equally treated samples from the same block varies. As such, the tensile strength is presented only with one significant digit.

Chalk	State	Number of cycles	Number of samples	T_0 (MPa)	σ (MPa)	$T_{0dry} - T_{0sat}$ (MPa)
Kansas	Dry	0	10	3	0.4	—
		15	13	3.3	0.6	—
		30	10	3.3	0.6	—
	Saturated	0	14	1.4	0.2	1.6
		15	12	1.1	0.2	2.2
		30	12	0.8	0.2	2.5
Mons	Dry	0	13	1.6	0.3	—
		15	15	1.3	0.4	—
		30	15	1.4	0.4	—
	Saturated	0	13	0.9	0.2	0.7
		15	14	0.6	0.2	0.7
		30	15	0.4	0.1	1

and a strong correlation between the loading rate and tensile strength can be observed (Fig. 13). The stronger samples tend to have a higher loading rate, and the higher the loading rate, the stiffer the sample. From this relationship, it could be possible to predict the tensile strength from the loading rate without breaking the sample.

4. Discussion

In the dry state, we found no significant reduction in tensile strength with increasing number of temperature cycles for either Kansas or Mons chalk. Therefore, it seems that the contact cement is not influenced by the anisotropic thermal expansion of calcite particles in dry state. One significant change in the dry state was an increase in pore size of dry Mons chalk samples, although this difference was not observed for the dry Kansas chalk (Fig. 7). The change in pore size distribution agrees with the observed pore size increase calculated from S_{BET} data (Table 3), probably due to the clay alternation (smectite illitization) when heated at dry conditions. However, the process of dehydration of smectite does not seem to influence the tensile strength of the samples.

Our data show how water saturation immediately reduces the tensile strength of chalk before any temperature variation takes place (0 cycle). This is in line with other works (Madland et al., 2002; Risnes et al., 2005).

The 0.3 MPa reduction in tensile strength from 0 to 15 cycles implies that the saturated Mons chalk, by percentage, is more susceptible to weakening by the temperature cycling than Kansas chalk (33% and 21%, respectively), as it initially had lower tensile

It is observed that the water-saturated Kansas samples lost more initial tensile strength than Mons chalks, and even more so for 15 and 30 cycles (Fig. 11). Nevertheless, no significant difference was found in the relative behavior of Kansas and Mons chalks.

The tensile strength was constant for dry samples, but it decreased systematically for the water-saturated ones, suggesting that the contact cement bonds do not break in dry state but do in the water-saturated state. If we assume that weakening is caused by the breakage of bonds between neighboring particles, then the fact that the samples continued to weaken after the first 15 cycles implies that bond breakages are rare events compared to the number of bonds found in a sample. If this was not the case, all the bonds would break within the first initial temperature cycles and weakening of tensile strength would only be observed between 0 and 15 cycles, with no further reduction in tensile strength after 30 cycles. Since the Kansas samples had a constant weakening rate up to 30 cycles, whereas for Mons sample, the rate was reduced in 15–30 cycles, it could indicate that the overall number of bonds holding the sample together is less for Mons chalk than that for the Kansas chalk.

If it is assumed that the two scenarios shown in Fig. 1 hold, we can calculate the elastic strain energy of the bonds holding two neighboring chalk particles together, and then compare it to the energy needed to create a dry and water wet calcite surface between the particles as generated by breaking contact cement. By breaking the contact cement, two surfaces are created, one on each particle. If heating at 100 °C and a particle dimension of 10 μm are assumed, then the energies required to create either two dry or two wet surfaces are (using Eq. (2)):

$$U_{sur,dry} = 2 \times 0.32 \, J/m^2 \times (10 \, \mu m)^2 \times 10^{-12} \, m^2/(\mu m)^2 = 6.4 \times 10^{-11} \, J$$
$$U_{sur,sat} = 2 \times 0.15 \, J/m^2 \times (10 \, \mu m)^2 \times 10^{-12} \, m^2/(\mu m)^2 = 3 \times 10^{-11} \, J$$

strength (Fig. 10b). Additionally, the tensile strength difference of the two samples was noticed when considering both the temperature cycling in combination with the saturation state, and a greater total difference in tensile strength was observed for the same number of temperature cycles, due to a constant dry tensile strength and a decrease in saturated tensile strength (Table 4).

It can be seen that the energy necessary to form a dry fracture is twice the energy required for the water-saturated fracture. Thus, the fracture growth in dry state is half of that in a saturated state.

In scenario 1 (Fig. 1), properties of contracting a-axis (perpendicular to c-axis) apply (E_{11}), and using Eq. (3), we can calculate the tensile elastic energy between two neighboring particles:
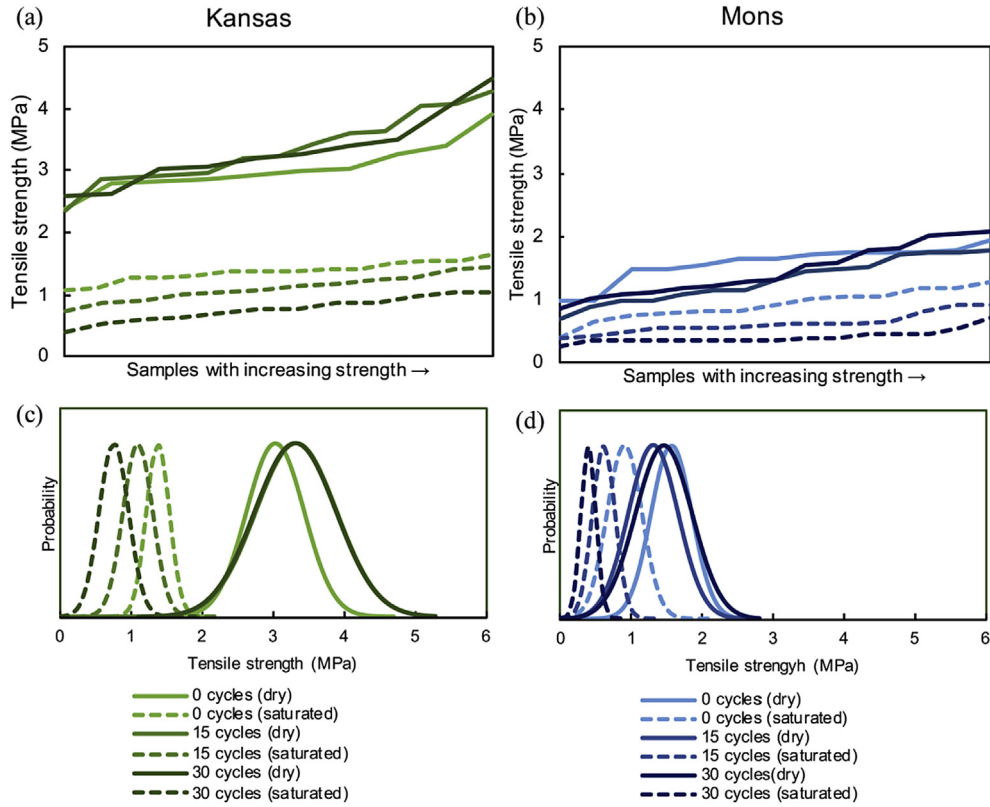
Fig. 9. Tensile strength from Brazilian tests on Kansas and Mons chalk samples in dry and saturated states subjected to varying number of temperature cycles. (a) and (b) represent individual samples for each group in increasing order from low (left) to high (right) tensile strength. (c) and (d) display the Gaussian distributions of each data set.

$$U_{el} = 2 \times \frac{1}{2} \times 110.9 \times 10^9 \, Pa \times 5.2 \times 10^{-6} \times 100 \, K \times (10 \, \mu m)^2$$
$$\times 10^{-18} \, m^3 / (\mu m)^3 = 2.3 \times 10^{-11} \, J$$

This value is lower than the results of the energy required to create either two dry or two wet surfaces (6.4×10^{-11} J and 3×10^{-11} J, respectively), thus the tensile energy caused by the thermal contraction of a-axis between two particles is not enough to generate a fracture.

In scenario 2, where one side of a particle contracts and the other expands, the strain energy created by shearing is calculated by Eq. (7). If we again assume a particle of 10 μm in dimension, and

that the shear zone thickness corresponds to a unit cell (c-axis = 17 Å) (Fig. 14), we can calculate the shear angle β from a ratio between the elongation and cemented area thickness:

$$\beta = \arctan \frac{\Delta x}{c\text{-axis}} = \arctan \frac{0.014 \, \mu m}{0.0017 \, \mu m} = 1.45°$$

The relative displacement between particles is calculated by assuming a heating of 100 °C in which one side of the contact expands along c-axis while the other side contracts along the a-axis. We calculate the shear stress as the sum of shear stress along the top contacting contact (τ_{11}) and that along the bottom elongating contact (τ_{33}):

Fig. 10. (a) Average tensile strength and standard deviation as a function of number of temperature cycles. Dry and water-saturated samples are shown as solid and dashed lines, respectively. (b) Tensile strength difference (in %) as a function of temperature cycling, with the dry and 0 cycle for each chalk type as reference.
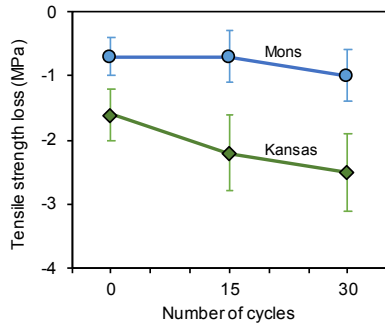
Fig. 11. Difference in tensile strength between dry and water-saturated samples for 0, 15 and 30 temperature cycles. The tensile strength of Kansas chalk was more reduced with an increasing number of temperature cycles than that of Mons chalk.

$$\tau_{11} = \frac{G_{11}}{\Delta x_{\text{top}}/c\text{-axis}} = \frac{45.8\ \text{GPa}}{2.94} = 15.6\ \text{GPa}$$

$$\tau_{33} = \frac{G_{33}}{\Delta x_{\text{bottom}}/c\text{-axis}} = \frac{34.1\ \text{GPa}}{13.53} = 2.5\ \text{GPa}$$

$$\tau = \tau_{11} + \tau_{33} = 18.1\ \text{GPa}$$

The elastic shear energy can thereby be calculated using Eq. (7):

$$U_{\text{shear}} = \frac{1}{2} \times 1.45 \times 1.81 \times 10^{10} \times (10 \times 10 \times 0.0017)$$
$$\times 10^{-18}\ \text{m}^3 / (\mu\text{m})^3 = 2.2 \times 10^{-9}\ \text{J}$$

As seen from the above results, the shear energy is greater than the energy needed to generate either dry or saturated calcite surfaces (6.4×10^{-11} J and 3×10^{-11} J, respectively). This is, however, an absolute upper limit. The two particles with orientations of c-axis perpendicular to each other are probably rare, and no weakening is found in dry samples. Scenarios 1 and 2 represent two extreme cases, and most neighboring particles are oriented with c-axis relative to each other in between those cases. The fact that we do not observe any weakening in dry samples indicates that the tensile and shear energies due to anisotropic thermal expansion are not sufficient to generate dry surfaces. However, the weakening by temperature cycling observed in water-saturated samples means that the energies are sufficient to generate water-saturated surfaces.
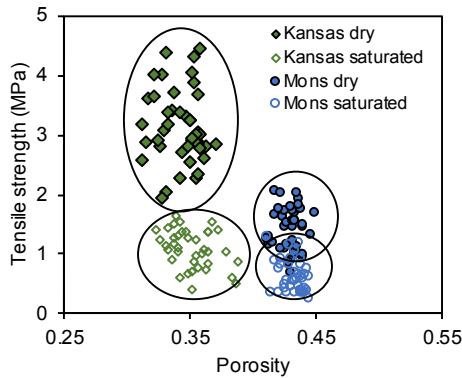
Fig. 12. Tensile strength plotted against the porosity of each sample. Mons chalk has a higher porosity than Kansas chalk and typically displays a lower strength. Water-saturated samples are weaker than dry samples. However, the porosity and the tensile strength do not correlate within individual chalk and saturated state.
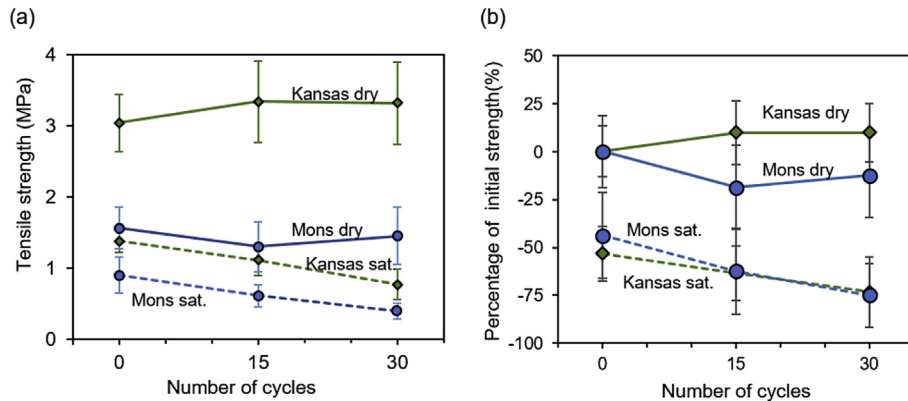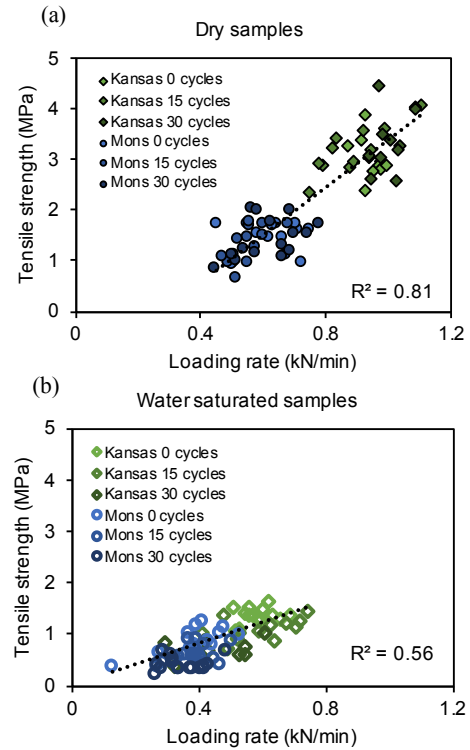

Fig. 13. Tensile strength plotted as a function of loading rate. Kansas chalk (green) is stronger than Mons chalk (blue). The strength of the dry samples (a) correlates better with loading rate than that of the saturated samples (b) with R^2 values of 0.81 and 0.56, respectively. No clear difference in strength is observed within the dry samples for an increasing number of temperature cycles (a), however, for the water-saturated samples, the loading rate is lowered by increasing the number of temperature cycles (b).

When the temperature is changed, fractures between particles may open gradually, and then water enters the fracture, inhibiting its closure when the temperature is reduced. This effect may be promoted by subcritical fracture processes which previously have shown to be driven by water. Even though the thermal cycling induces anisotropic thermal expansion of the calcite particles, irrespective of the pore fluid content, the tensile strength remains unchanged for the dry samples. However, for the water-saturated samples, the tensile strength is systematically reduced with increasing number of cycles for both chalks. This is in line with the behavior obtained in marble (Hansen et al., 2003). In our cases, the strength reduction induced by temperature cycling was more pronounced for the saturated Kansas chalk, which is more indurated than Mons chalk (Fig. 11). This indicates that water weakening phenomena play a role in the accumulated damage induced by the thermal cycles and can be linked to the understanding of how neighboring particles are held together. Royne et al. (2015) discussed how changes in nano-scale surface forces between two calcite particles developed using an atomic force microscope. They found that the forces between two calcite particles depend on the distance between the particles, which further depends on the water
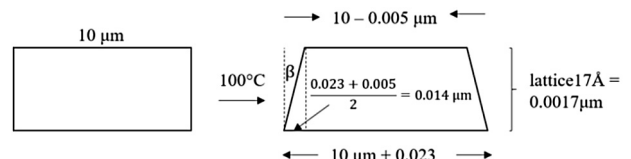
Fig. 14. Shear strain of contact between two 10 μm particles, caused by 100 °C heating.
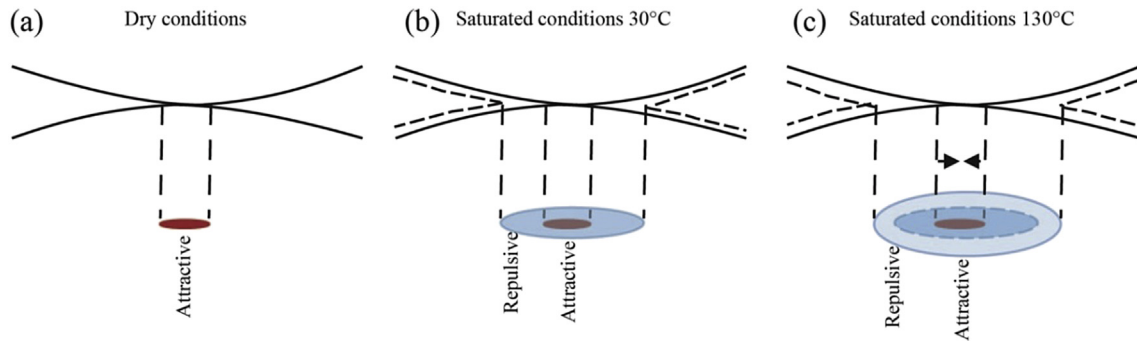
Fig. 15. Forces present between two calcite particles in (a) dry conditions, (b) water-saturated conditions at 30 °C, and (c) water-saturated conditions at 130 °C. An extra area of repulsive forces occurs at higher temperature associated with the increasing Debye length.

content. When there is no water present, only attractive forces pulling the particles together are observed. On the contrary, when water is present, a repulsive force is detected at intermediate practical distances, leading to a reduced cohesion between particles. The increased repulsion could facilitate the propagation of fractures that would not develop in the dry state, thereby creating greater repulsion and fracturing the contact cement. This thus weakens the samples as the number of temperature cycles is increased (Fig. 15). If we assume that the thickness of the charged layer is directly proportional to the Debye length, then the thickness of the layer depends on the temperature and increases with increasing temperature (Fig. 16). A thicker Debye length leads to an increase of repulsive area between the particles at higher temperatures, which causes further weakening of the water-saturated samples. As illustrated in Fig. 15c, not only the repulsive area increases, but also this increase may be sufficient to pull particles further apart, and water can then invade the fracture, reducing the attractive area.

To prevent dissolution/precipitation, we used calcite-equilibrated water as a saturating fluid. The equilibrated water was prepared at ambient temperature. Since the solubility is inversely correlated to temperature, the solution is over-saturated at higher temperatures. The solubility of calcite is 0.013 g/L, within one pore volume of each sample (approximately 10 mL). This amount reaches 0.00013 g of calcite that could precipitate, which would be less than 0.001% in weight compared to each sample (30 g). In addition, the solubility effect should only be observed by comparing the tensile strength in 0–15 cycles, and as such, increasing the number of cycles from 15 to 30 should not play a decisive role in tensile strength. This is because the maximum saturation has been achieved after the initial heating cycles. Therefore, it is conclusive that the effect observed in saturated samples is induced by temperature cycling, but not by dissolution/precipitation.

5. Conclusions

Brazilian tests were performed to evaluate the influence of temperature cycling on the tensile strength of chalk in dry and water-saturated conditions. In dry conditions, neither Kansas chalk nor Mons chalk samples demonstrate weakening effects caused by temperature cycles. However, for both chalks, the initial tensile strength was halved by water saturation, and then further reduced with an increasing number of temperature cycles. For both chalks, the tensile strength of water-saturated samples after 30 temperature cycles was reduced to only 25% of the initial strength of dry samples that were not exposed to temperature cycling. The estimates showed that the energy needed to create new surfaces between neighboring particles held together by contact cement is higher than the thermoelastic energy induced by the heating of two adjacent particles with c-axes parallel to each other, but lower than the shear energy with c-axes perpendicular to each other. However, the probability of thermally induced cement bond fracture is higher in the water-saturated state because the surface energy is lower than that of dry calcite crystals. Presences of water and anisotropic thermal expansion of calcite are the driving weakening mechanisms when chalk is exposed to thermal cycling, while tensile strength experiments on dry samples detect no weakening by anisotropic thermal expansion alone.

Fig. 16. Debye length increases with increasing temperature based on κ^{-1} equation (Eq. (1)).

References

Andreassen KA, Fabricius IL. Biot critical frequency applied to description of failure and yield of highly porous chalk with different pore fluids. Geophysics 2010;75(6):E205—13.

Atkinson BK, Meredith PG. Stress corrosion cracking of quartz: a note on the influence of chemical environment. Tectonophysics 1981;77(1—2):T1—11.

Atkinson BK. Subcritical crack growth in geological materials. Journal of Geophysical Research: Solid Earth 1984;89(B6):4077—114.

Burchette TP. Carbonate rocks and petroleum reservoirs: a geological perspective from the industry. Geological Society, London, Special Publications 2012;370(1):17—37.

Chen CC, Lin CC, Liu LG, Sinogeikin SV, Bass JD. Elasticity of single-crystal calcite and rhodochrosite by Brillouin spectroscopy. American Mineralogist 2001;86(11—12):1525—9.
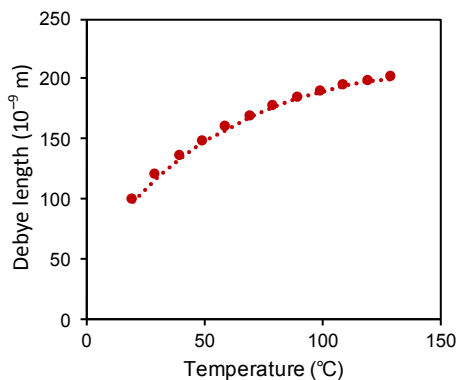
dos Reis JML. Effect of temperature on the mechanical properties of polymer mortars. Materials Research 2012;15(4):645—9.

Fabricius IL. Burial stress and elastic strain of carbonate rocks. Geophysical Prospecting 2014;62(6):1327—36.

Finn TM, Johnson RC. Niobrara total petroleum system in the Southwestern Wyoming Province. In: Petroleum systems and geologic assessment of oil and gas in the Southwestern Wyoming Province, Wyoming, Colorado, and Utah. US Geological Survey (USGS) Southwestern Wyoming Province Assessment Team; 2005.

Hansen KK, Leksø H, Grelk B. Assessment of the durability of marble cladding by laboratory exposure compared to natural exposure. In: Carmeliet J, Hens H, Vermeir G, editors. Research in building physics: proceedings of the 2nd international conference on building physics. CRC Press; 2003. p. 267—71.

Henriksen AD, Fabricius IL, Borre MK, Korsbech U, Theilgaard AT, Zandbergen JB. Core density scanning, degree of induration and dynamic elastic moduli of Palaeogene limestone in the Copenhagen area. Quarterly Journal of Engineering Geology 1999;32(2):107—17.

Hermansen H, Thomas LK, Sylte JE, Aasboe BT. Twenty five years of Ekofisk reservoir management. In: SPE annual technical conference and exhibition. Society of Petroleum Engineers (SPE); 1997. https://doi.org/10.2118/38927-MS.

Hua W, Dong SM, Li YF, Xu JG, Wang QY. The influence of cyclic wetting and drying on the fracture toughness of sandstone. International Journal of Rock Mechanics and Mining Sciences 2015;78:331—5.

Huang S, Xia KW. Effect of heat-treatment on the dynamic compressive strength of Longyou sandstone. Engineering Geology 2015;191:1—7.

Jay AH. The thermal expansion of bismuth by X-ray measurements. Proceedings of the Royal Society of London, Series A 1934;143(849):465—72.

Kaiser DL, Watters RL. Certificate of analysis. National Institute of Standards & Technology; 2012. https://www-s.nist.gov/srmors/certificates/1898.pdf.

Lee H, Lee H, Park Y, Kwon K. The mechanical and hydraulic characteristics of granite and gneiss under temperature variation. In: ISRM international symposium — EUROCK 96. Rotterdam: A.A. Balkema; 1996. p. 1371—7.

Lisabeth HP, Zhu WL. Effect of temperature and pore fluid on the strength of porous limestone. Journal of Geophysical Research: Solid Earth 2015;120(9):6191—208.

Lyklema J. Fundamentals of interface and colloid science. San Diego, USA: Academic Press; 2000.

Madland MV, Korsnes RI, Risnes R. Temperature effects in Brazilian, uniaxial and triaxial compressive tests with high porosity chalk. In: SPE annual technical conference and exhibition. SPE; 2002. https://doi.org/10.2118/77761-MS.

Markgraf SA, Reeder RJ. High-temperature structure refinements of calcite and magnesite. American Mineralogist 1985;70(5—6):590—600.

Mavko G, Mukerji T, Dvorkin J. The rock physics handbook: tools for seismic analysis of porous media. 2nd ed. Cambridge: Cambridge University Press; 2009.

Megawati M, Hiorth A, Madland MV. The impact of surface charge on the mechanical behavior of high-porosity chalk. Rock Mechanics and Rock Engineering 2013;46(5):1073—90.

Nermoen A, Korsnes RI, Storm EV, Stødle T, Madland MV, Fabricius IL. Incorporating electrostatic effects into the effective stress relation — insight from chalk experiments. Geophysics 2018;83(3):MR123—35.

Pirson S, Spagna P, Baele JM, Damblon F, Gerrienne P, Vanbrabant Y, Yans J. An overview of the geology of Belgium. In: Memoirs of the geological survey of Belgium. The 4th international meeting of anthracology, vol. 55. The Geological Survey of Belgium; 2008. p. 5—25.

Rao KVK, Naidu SVN, Murthy KS. Precision lattice parameters and thermal expansion of calcite. Journal of Physics and Chemistry of Solids 1968;29(2):245—8.

Ravnås C. Petrophysical and rock mechanical properties of heat treated chalk. Kongens Lyngby, Denmark: Technical University of Denmark; 2017.

Risnes R, Madland MV, Hole M, Kwabiah NK. Water weakening of chalk — mechanical effects of water-glycol mixtures. Journal of Petroleum Science and Engineering 2005;48(1—2):21—36.

Rosenholtz JL, Smith DZ. Linear thermal expansion of calcite, var. Iceland spar and Yule marble. American Mineralogist 1949;34:846—54.

Royne A, Bisschop J, Dysthe DK. Experimental investigation of surface energy and subcritical crack growth in calcite. Journal of Geophysical Research: Solid Earth 2011;116(B4):B04204.

Royne A, Dalby KN, Hassenkam T. Repulsive hydration forces between calcite surfaces and their effect on the brittle strength of calcite-bearing rocks. Geophysical Research Letters 2015;42(12):4786—94.

Stipp SLS. Toward a conceptual model of the calcite surface: hydration, hydrolysis, and surface potential. Geochimica et Cosmochimica Acta 1999;63(19):3121—31.

Sulak AM, Danielsen J. Reservoir aspects of Ekofisk subsidence. Journal of Petroleum Technology 1988;41(7):709—16.

Weiss T, Siegesmund S, Fuller ER. Thermal degradation of marble: indications from finite-element modelling. Building and Environment 2003;38(9—10):1251—60.

Wu TC, Shen AH, Weathers RS, Bassett WA, Chou IM. Anisotropic thermal-expansion of calcite at high-pressures — an in-situ x-ray-diffraction study in a hydrothermal diamond-anvil cell. American Mineralogist 1995;80(9—10):941—6.

Yakaboylu O, Harinck J, Smit KGG, de Jong W. Supercritical water gasification of manure: a thermodynamic equilibrium modeling approach. Biomass & Bioenergy 2013;59:253—63.
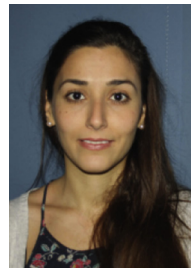
T. Voake is currently pursuing her PhD degree in Petroleum Technology at the University of Stavanger, Norway. She obtained her MSc degree in Geophysics from Memorial University of Newfoundland, and HBSc degree from the University of Toronto, Canada. She has worked on numerous field and laboratory projects classifying rock physical properties. She has previously worked in the petroleum industry for a software development company.

Paper II: Temperature cycling and its effect on mechanical behaviours of high-porosity chalks

Voake, T., Nermoen, A., Korsnes, R.I., Fabricius, I.L. (In review).

Full Length Article

Temperature cycling and its effect on mechanical behaviours of high-porosity chalks

T. Voake [a,b,*], A. Nermoen [b,c], R.I. Korsnes [a,b], I.L. Fabricius [a,d]

[a] *University of Stavanger, Stavanger, Norway*
[b] *The National IOR Centre of Norway, University of Stavanger, Stavanger, Norway*
[c] *International Research Institute of Stavanger (IRIS), Stavanger, Norway*
[d] *Technical University of Denmark (DTU), Copenhagen, Denmark*

ABSTRACT

Temperature history can have a significant effect on the strength of water-saturated chalk. In this study, hydrostatic stress cycles are applied to understand the mechanical response of chalk samples exposed to temperature cycling between each stress cycle, compared to the samples tested at a constant temperature. The total accumulated strain during a stress cycle and the irreversible strain are reported. Chalk samples from Kansas (USA) and Mons (Belgium), with different degrees of induration (i.e. amount of contact cementation), were used. The samples were saturated with equilibrated water (polar) and non-polar Isopar H oil to quantify water weakening. All samples tested during 10 stress cycles with varying temperature (i.e. temperature cycled in between each stress cycle) accumulated more strain than those tested at constant temperatures. All the stress cycles were performed at 30 °C. The two chalk types behaved similarly when saturated with Isopar H oil, but differently when saturated with water. When saturated with water, the stronger Kansas chalk accumulated more total strain and more irreversible strain within each stress cycle than the weaker Mons chalk.

© 2019 Institute of Rock and Soil Mechanics, Chinese Academy of Sciences. Production and hosting by Elsevier B.V. This is an open access article under the CC BY-NC-ND license (http://creativecommons.org/licenses/by-nc-nd/4.0/).

1. Introduction

Intermittent cold-water injection into a warm reservoir during oil production, or injection of supercritical CO_2 for carbon storage, would lead to cooling that could thermally degrade the formation surrounding an injection well. Thermal strain may potentially cause permanent damage, especially to a rock composed of anisotropic minerals, and eventually lead to well instability. This paper focuses on chalk reservoirs, where the proposed effect could be of high relevance, because chalk is primarily composed of calcite with a highly anisotropic thermal expansion coefficient. The calcite crystal has a trigonal axis of symmetry, with thermal expansion co-efficients of 23.8×10^{-6} K^{-1} and -5.2×10^{-6} K^{-1} in the directions parallel and perpendicular to the trigonal axis, respectively (Rosenholtz and Smith, 1949), thereby leading to thermal expansion and contraction when heated. For two calcite crystals in close

contact with each other, with unaligned trigonal axis, a temperature increase leads to strain differences in the two crystals, which localises stress at the cemented particle contact. The premise of this paper is to investigate to what extent thermal variation leads to measurable mechanical degradation for centimetre scale cylindrical core samples.

Chalk is a carbonate rock whose particles originate from skeletons of phytoplanktonic coccolithophores (algae), forming calcareous ooze composed of calcite. As the calcareous ooze is buried deeper, the stress at particle contacts builds up, resulting in pressure dissolution and thus the formation of contact cement. More cemented deeper chalks possess a lower Biot coefficient and higher initial strength and stiffness than less cemented chalks with higher Biot coefficients (Fabricius, 2014).

In materials composed of anisotropic particles held together by inter-granular contact cement, the contact zones can localise significant stresses because of local differences in the thermal strain, even though the temperature in the sample is uniform. For example, marble which is mineralogically similar to chalk with calcite as its main constituent is known to degrade when exposed to outdoor temperature variation, and some marble facades consequently tend to experience concave bowing (Weiss et al.,

2003). Hansen et al. (2003) found that marble cladding weakens with the number of years it has been exposed to seasonal climate, and that marble tested in the laboratory at 100% relative humidity accordingly weakens with increasing number of cooling and heating cycles; by contrast, dry samples tested did not demonstrate weakening upon temperature cycling. Similarly, no damage to a dry limestone was observed when it was heated up to 300 °C (Chen et al., 2009). Conversely, when tested for potential high-temperature thermal energy storage ($\geq$573 °C), mafic and felsic rocks performed much better than limestone and sandstone, as thermal cycling leads to increases in porosity and mineral dehydration (Becattini et al., 2017). Tests on well casing cement indicated that thermal cycling caused cracking failure mechanism due to a decrease in tensile strength (De Andrade et al., 2015). Weathering induced thermal cycling also had an effect on a granitic dome in California, USA, where accumulation of thermal stress between layers induced subcritical cracking and triggered exfoliation (Collins et al., 2018).

Further, the impact of water moisture has been shown to play an important role in rock mechanics. Studies performed on fibreglass that underwent 500 thermal cycles from −40 °C to 25 °C indicated that the damage development was minimal for samples tested in a dry state, but much more pronounced in water-saturated samples (Okeson et al., 2006). Also, the tensile strength of sandstone has been demonstrated to be weakened by cyclically submerging samples in water for 48 h and drying them at 105 °C for 24 h. Half of the strength was lost after just seven repeated wetting and drying cycles (Hua et al., 2015). These studies show that temperature cycling has a more pronounced weakening effect in the presence of moisture.

Saturation with a polar pore fluid generally reduces the strength of porous rocks, as observed in sandstone (Baud et al., 2000; Wasantha and Ranjith, 2014), limestone (Lebedev et al., 2014), and chalk (Risnes et al., 2005). Wasantha and Ranjith (2014) analysed water-weakening of Hawkesbury sandstone (Australia) in the brittle regime and found that water saturation led to a 13%−38% reduction of initial dry strength, with higher decreases at higher confining pressures. Baud et al. (2000) used four different sandstones (Gosford, Berea, Boise, and Darley Dale) in their study. Their testing results showed brittle strength reduction of 5%−17%, where Gosford sandstone with the lowest porosity had the highest reduction and Berea sandstone with higher porosity was the least influenced by water saturation. They also reported that samples with higher fractions of altered feldspar and clay had more pronounced weakening by water saturation. Water weakening effects were also observed in argillaceous siltstone by a reduction in compressive and shear strengths (Yang et al., 2016).

Water weakening of chalks has gained much attention and many studies have been conducted focusing on chalk weakening mechanisms (e.g. Hermansen et al., 1997). Madland et al. (2002) found reductions in tensile strength and hydrostatic yield stress due to water saturation. Risnes et al. (2005) experimentally reported chalk strength as a function of water activity by mixing water and glycol as pore fluid, and a positive correlation was proposed. It has also been observed that the weakening effect is sensitive to fluid composition (Katika et al., 2015). Lisabeth and Zhu (2015) concluded that greater weakening in carbonate rocks is observed when pore fluid is far from equilibrium with the host rock, and also at higher temperatures. Similarly, Megawati et al. (2013) suggested that the weakening is enhanced with increasing negative surface charge of chalk due to pore fluid composition, where pore walls with greater negative charge would lead to greater overlap of electrical double layers and hence a rise in disjoining pressure.

In this paper, we explored how the mechanical hydrostatic stress cycles combined with temperature cycles affected the accumulation of strain in chalk. The effect of pore fluid was tested using two saturating solvents of different reactivities: water equilibrated with calcite and Isopar H oil. Also two chalk types from two different localities were selected, due to their differences in induration, Biot coefficient and associated amount of contact cementation between particles.

2. Materials and method

2.1. Materials

Chalks sampled from two quarries were used in this study, i.e. Kansas chalk from the Niobrara Formation, Fort Hays Member, USA (Late Cretaceous), and Mons chalk from the Trivières Formation, Harmignies, Belgium (Late Cretaceous). The two chalk blocks were selected because of their different degrees of induration, and hence different degrees of contact cementation. Induration is used for classification of carbonate rocks, with a four-point scale, H1 being loose and soft, and H4 being very strong and weakly metamorphosed. Kansas chalk has a larger contact area between the grains, which is reflected in its higher induration of H3 (Henriksen et al., 1999). The Mons chalk has a smaller contact area between the grains, which gives a lower induration of H2 (see Fig. 1). The Mons chalk has a carbonate content of 99.8% and a Biot coefficient, α, of 0.95, while the Kansas chalk has a carbonate content of 96.9% and a Biot coefficient of 0.91 (Ravnås, 2017).

From each chalk block, cylindrical cores of approximately 40 mm in diameter and 200 mm in length were drilled. The core diameter was adjusted to 38.1 mm, and each core was cut into plugs of about 70 mm in length. Eight plug samples from each block were prepared for testing (Table 1). The porosity was measured by using two methods. In the first method, porosity from saturation was calculated using the difference between dry and wet weights obtained by saturating the samples with distilled water in a vacuum
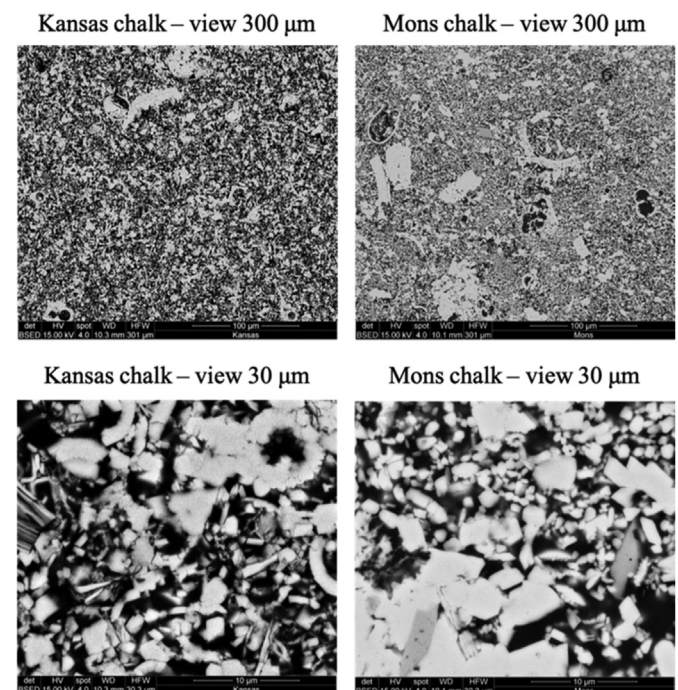
Fig. 1. Backscatter electron micrographs of Kansas and Mons chalks with two magnifications (30 μm and 300 μm images).

Table 1
Physical properties of samples used in this study. All samples had a diameter of 38.1 mm. Water is equilibrated with calcite.

Sample	Locality	Pore fluid	Temperature type	Length (mm)	ϕ_{sat} (%)	$\phi_{\rho_{gr}}$ (%)	V_p (m/s)
K19a	Kansas	Water	Cycled	72.1	35.4	35.5	
K40	Kansas	Water	Cycled	69.8	34.9	34.8	2860
K17a	Kansas	Water	Constant	73.5	35.1	35.3	
K18b	Kansas	Water	Constant	70.5	32.1	32	
K44a	Kansas	Isopar H oil	Cycled	70	34.6	34.8	2943
K22	Kansas	Isopar H oil	Cycled	73	33.9	34	3033
K25	Kansas	Isopar H oil	Constant	71.4	33	33.3	3043
K44b	Kansas	Isopar H oil	Constant	70	32.3	32.5	2942
M36b	Mons	Water	Cycled	70.4	43.8	44	2304
M31b	Mons	Water	Cycled	70	43.7	43.8	2288
M13	Mons	Water	Constant	68.8	44.4	42.9	2263
M24	Mons	Water	Constant	72.6	44.3	44.2	2298
M30	Mons	Isopar H oil	Cycled	70.2	42.6	42.6	2228
M36a	Mons	Isopar H oil	Cycled	67.8	41.5	41.7	2379
M18	Mons	Isopar H oil	Constant	71.8	43.1	43.4	2310
M32b	Mons	Isopar H oil	Constant	67	41.8	42.2	2335

Note: ϕ_{sat} and $\phi_{\rho_{gr}}$ are the porosity from saturation and porosity from grain density, respectively.

chamber. In the second method, porosity from grain density was derived from dry weight and volume of the samples, using the grain density of calcite (2.71 g/cm³). P-wave velocity, V_p, was measured in dry state prior to saturating the samples with the pore fluid, using CNS Farnell PUNDIT 7 (precision ± 0.1 μs). Based on these data and dry density, ρ_d, elastic P-wave modulus, M_p, was calculated as

$$M_p = \rho_d V_p^2 \tag{1}$$

Sixteen cylindrical core samples were tested, eight from each chalk type, of which four were saturated with calcite-equilibrated water of 0.652 mmol/L (polar fluid), and four with Isopar H oil (non-polar fluid). The equilibrated water was made by dissolving chalk powder in distilled water. Once the equilibrium was reached, the solution was filtered using a 0.65 μm filter. Both fluids were selected to minimise the impact of chemical reactions, thereby focussing this study on the rock−fluid interactions that are related to ion adsorption on mineral surfaces rather than dissolution and precipitation. Two of the four cores (with a given fluid and chalk type) were mechanically tested with constant temperature of 30 °C, and two were tested with a temperature cycle from 30 °C to 130 °C to 30 °C between each stress cycle. All stress cycles were performed at 30 °C. Each chalk type, fluid saturation, and temperature history

were tested twice to investigate the repeatability of the results (see Table 1).

2.2. Mechanical tests

Mechanical tests on the samples were performed in a triaxial cell (see Fig. 2). Two different pumps were connected to the cell. The flow of the pore fluid was delivered by a Gilson pump (model 307 HPLC) while the confining pressure was controlled by a hydraulic Quizix pump, model QX-20000 HC. The confining pressure pump was equipped with two cylinders, assuring constant pressure applied. The pumps were individually operated through a LabVIEW routine. A back-pressure regulator was connected on the outlet side of the sample to ensure constant pore pressure of 0.7 MPa. The cell was also equipped with a 1000 W heating jacket controlled by an Omron E5CN PID temperature controller. The precision of the temperature controller is ± 0.1 °C. The vertical displacement of the sample was measured by linear variable displacement transducer (LVDT, MHR 250 from Measurement Specialties™). The radial deformation was measured using an extensometer, where the circumference changes were detected by LVDT MHR 100 from Measurement Specialties™.

Volumetric strain was measured from the relative changes in length and diameter compared to the original dimensions of the
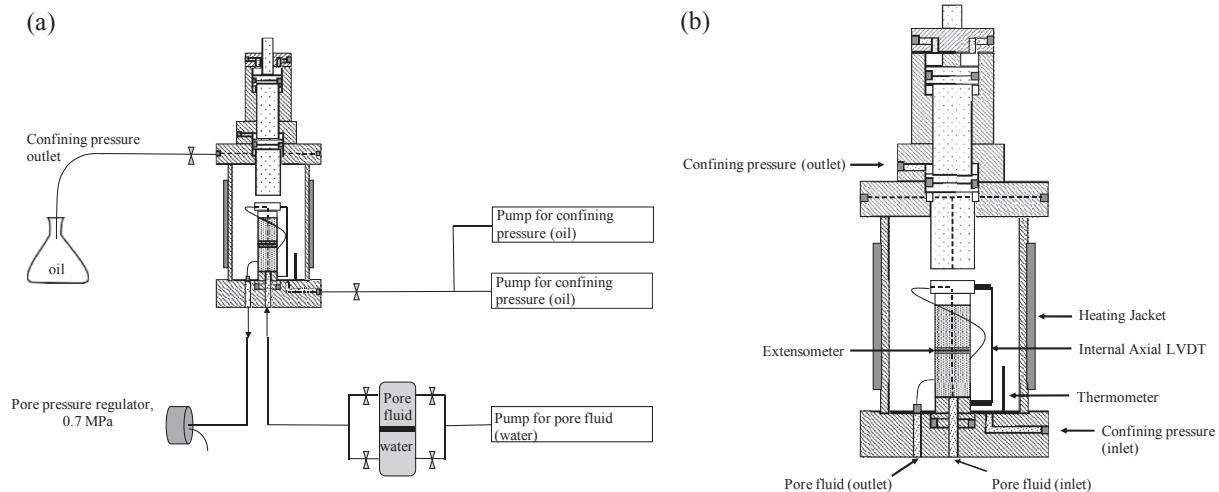
Fig. 2. (a) Experimental setup, and (b) triaxial cell with pressure regulating system.

cylindrical samples. Here, the volumetric strain of the cylindrical sample was estimated (omitting higher order terms) by

$$\varepsilon_{\text{vol}} = \varepsilon_z + 2\varepsilon_r \tag{2}$$

where ε_z is the axial strain from the change in length of the core, and ε_r is the radial strain measured by the change in the sample's diameter.

Hydrostatic stress cycles, i.e. the loading/unloading cycles, were performed by controlling the pressure in the hydraulic oil in the triaxial chamber, thus the applied pressure was equal at all sides, i.e. σ_{hyd}. The effective stress, σ_{eff}, experienced by the porous material was determined by

$$\sigma_{\text{eff}} = \sigma_{\text{hyd}} - \alpha P_{\text{pore}} \tag{3}$$

where P_{pore} is the pore pressure. The effective hydrostatic stress changed from 0.5 MPa to 4.5 MPa over 30 min, and decreased back to 0.5 MPa over 30 min when the volumetric strain was measured (Fig. 3a).

2.3. Material response to hydrostatic stress cycling

The peak volumetric strain (Fig. 3a) at the maximal stress was divided into reversible ε_{rev} (elastic) and irreversible ε_{irr} (plastic) components obtained at the end of the stress cycle (Fig. 3b). An additive division in the elastic and plastic behaviours was used:

$$\varepsilon_{\text{tot}} = \varepsilon_{\text{rev}} + \varepsilon_{\text{irr}} \tag{4}$$

It has been found that the bulk modulus K calculated from the unloading slope between the hydrostatic effective stress and volumetric strain provides a better match to the static modulus obtained from ultrasonic velocity measurements (Olsen et al., 2008). The lower K obtained from the loading curve is interpreted to be caused by the closure of unloading cracks formed when the sample was acquired from field, which causes additional artificial strain, especially during the first loading. This strain also causes unnecessary variability in the reported data and furthermore, it can be minimised by analysing the upper part of the unloading curve in which the nonlinear effects are less significant (Olsen et al., 2008). Therefore, we estimated the bulk modulus K from the stress–strain curves as follows when the effective stress varied from 4.5 MPa to 3.8 MPa:

$$K = \frac{\partial \sigma_{\text{eff}}}{\partial \varepsilon_{\text{vol}}} \tag{5}$$

For completeness purpose, the average slopes of the complete loading and unloading curves (between 0.5 MPa and 4.5 MPa) are also reported. Since the experiment was performed in drained conditions, the Biot coefficient using K can be estimated as

$$\alpha \approx 1 - K/K_{\text{min}} \tag{6}$$

where $K_{\text{min}} = 70.8$ GPa is the average bulk modulus of calcite (Mavko et al., 1998).

The experiments were performed according to the following procedures:

(1) Once a sample was mounted on the triaxial cell, the confining stress was increased to 0.5 MPa.
(2) Simultaneous increases in confining stress and pore pressure were performed up to 1.2 MPa and 0.7 MPa, respectively.
(3) Temperature was set to 30 °C and the setup was left to rest until stable diameter readings were obtained.
(4) The hydrostatic stress was increased from 1.2 MPa to 5.2 MPa over 30 min, immediately followed by unloading to 1.2 MPa at the same stress rate (0.133 MPa/min). At the same time, the volumetric strain was measured continuously so that the loading/unloading slope was estimated as an average value during both phases, along with the elastic modulus which was measured during the initial unloading phase. During the stress cycle, the reversible and irreversible strain components were measured.
(5) For the samples exposed to temperature cycling, the temperature was increased to 130 °C over approximately 90 min after the hydrostatic loading/unloading cycle was completed. Then the setup was left to stabilise at 130 °C for approximately 360 min, before the Omron E5CN PID temperature controller was set to 30 °C and the triaxial cell cooled during approximately 450 min and then stabilised overnight, until another cycle was performed. For the samples tested at a constant temperature, the temperature cycle was omitted (Fig. 4). The same time interval between each stress cycle was used in all tests, and all stress cycles were performed at 30 °C.
(6) Steps 4 and 5 were repeated 10 times continuously over 10 d.
(7) For the samples exposed to temperature cycling, an additional 11th hydrostatic stress cycle was performed, without a
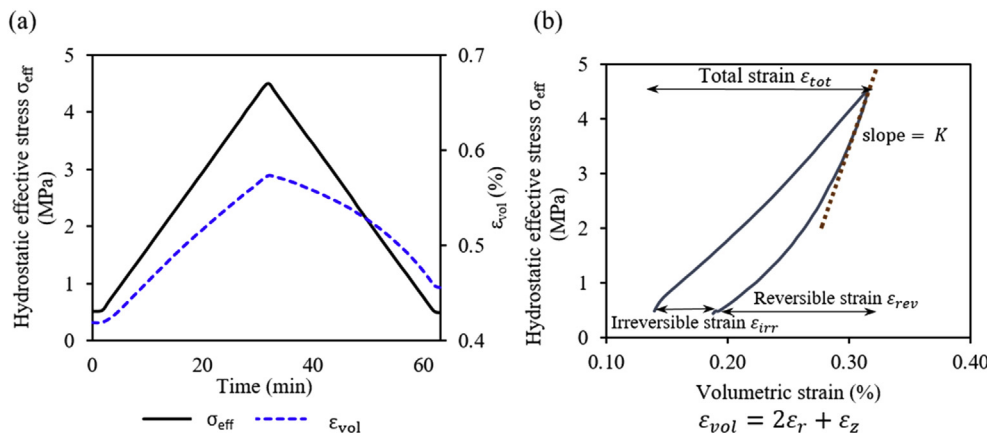

Fig. 3. Stress–strain relation during a stress cycle. (a) Strain response to stress changes. (b) After a complete stress cycle, strain is divided into elastic/reversible strain and plastic/irreversible strain. The elastic modulus K is measured as the slope of the steepest initial unloading phase.

Fig. 4. (a) Test history between two stress cycles for samples tested with temperature cycling (in which a heat pulse is included between each stress cycle); and (b) Test history at constant temperature. The time interval between stress cycles were 24 h.

Fig. 5. Yield stress was determined when the stress difference between the measured stress–strain curve and the linear-elastic line exceeded 0.25 MPa.

3. Results

A marked difference was found between samples tested at a constant temperature and those exposed to a temperature cycle between each stress cycle (see Fig. 6), and more strain was accumulated in the samples exposed to temperature variations. The greatest accumulation of irreversible strain was found in the water-saturated Kansas chalk, where the strain accumulated during only a single cycle is approximately equal to the strain accumulated after all ten cycles in a sample tested at constant temperature.

For both chalks and both pore fluids, the samples exposed to temperature cycling have a larger proportion of irreversible strain for each cycle than the samples tested at a constant temperature (Fig. 7). The effect of temperature was pronounced for the water-saturated Kansas chalk samples that had approximately twice the irreversible strain (for each cycle) when the samples were subjected to constant temperature tests. It should be noted that when an additional 11th stress cycle was performed without a prior temperature cycle, the irreversible strain dropped to the value observed in samples tested at constant temperature. This indicates that a temperature pulse of 30 °C–130 °C–30 °C causes the material to behave less elastically.

From the 2nd to the 10th and 11th cycles, the bulk modulus for individual samples did not change significantly, irrespective of constant or cycled temperature tests whereas the samples accumulated plastic strain (Fig. 8 and Table 2). The same behaviour could also be observed for the average loading and unloading slopes (Table 2), in which the stiffness did not change. On average, Kansas chalk had a higher K than Mons chalk, and Kansas chalks saturated with Isopar H oil had a higher stiffness than that saturated by water. For the experiments conducted on Mons chalk, this difference was not observed.

With respect to hydrostatic loading to failure, the Kansas chalk, with a higher degree of contact cementation, is stronger than the Mons chalk (Fig. 9 and Table 3). For hydrostatic failure, pore fluid also plays a role. The samples saturated with water, which is a polar fluid, are weaker than the samples saturated with Isopar H oil (non-polar fluid). We did not observe a significant influence of the temperature cycling on the failure stress.

4. Discussion

All samples tested with temperature cycling accumulated more strain than samples tested at constant temperature during 10 stress cycles (Figs. 6 and 7), even though all stress cycles were performed

temperature cycle. This was to assess whether the observed stress–strain behaviour during loading was affected by the heat pulse applied to the core.

(8) To complete the experiments, the samples were hydrostatically loaded to pore collapse failure. This was to determine the stress for onset of yield and check to what degree the stress cycles were performed within the elastic region. The loading rate was the same as that for the stress cycles, i.e. 0.133 MPa/min. The yield stress was defined as the one at which the stress–strain curve deviated from the linear-elastic path for a stress increase greater than 0.25 MPa (Fig. 5). The error was estimated when the deviation from the elastic path reached 1 MPa.

The experimental procedure allows us to compare the strain accumulated during the stress cycles when samples are tested at constant temperature to those subjected to temperature cycle (30 °C–130 °C–30 °C) in between each stress cycle. By using the two different indurated chalks, the mechanical effect of the contact cement is explored, as well as the role of the pore fluid (polar vs. non-polar). Because all the stress cycles were performed at 30 °C, and each cycle started after the previous cycle ended, the effects of temperature on the testing equipment could be excluded, and thus it was assumed that no strain was accumulated between stress cycles. The Biot coefficient was estimated as an average value from cycles 5 to 10 using Eq. (6).

Fig. 6. Stress−strain curves for Kansas (two upper row) and Mons (two lower rows) chalks tested at a constant temperature (10 cycles, the two columns on the left) and with a temperature cycle in between stress cycles (11 cycles, the right two columns).
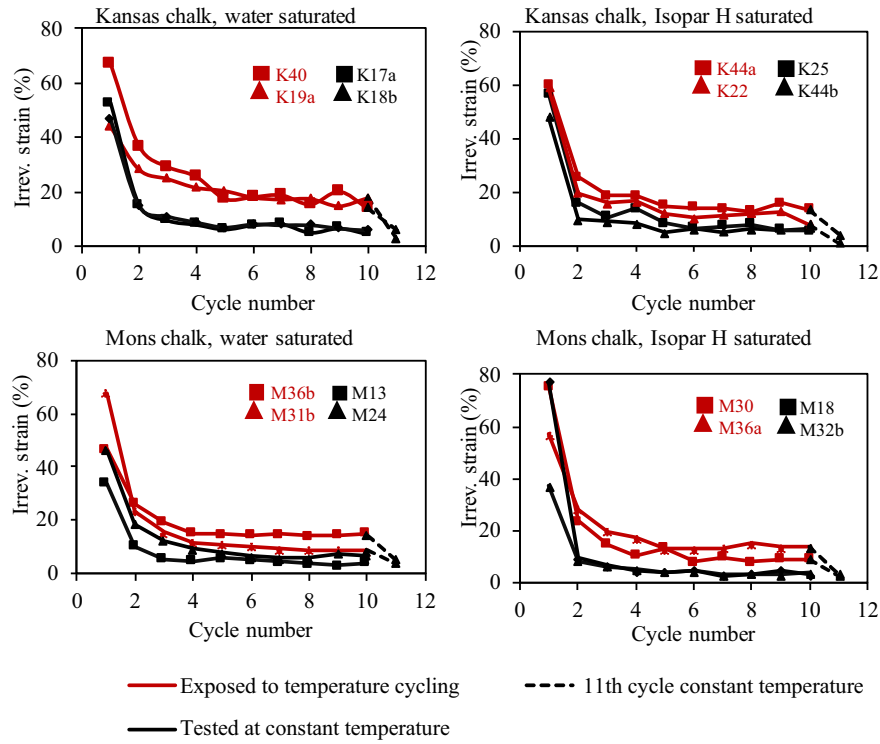
Fig. 7. Irreversible strain for individual stress cycles. The red lines display the test results for samples exposed to temperature cycles, and black lines the samples tested at constant temperature. The dashed line represents the 11th cycle before which the temperature was not varied, in contrast to the 10 cycles before.
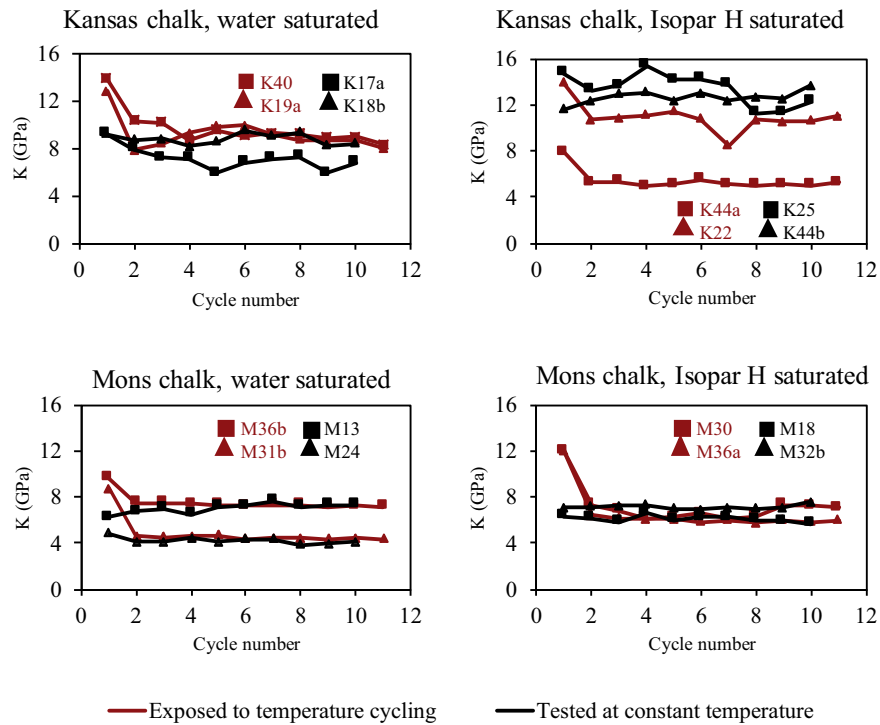
Fig. 8. Elastic bulk modulus K from hydrostatic stress cycles (at 30 °C). Red lines represent samples exposed to temperature variation in between each stress cycle, and black lines correspond to samples tested at constant temperature. The high K for the first stress cycle, were attributed to equipment alignment or/and closure of microcracks.

Table 2
Average loading and unloading slopes, as well as the elastic bulk modulus through hydrostatic stress cycles.

Sample	Fluid	Temperature cycle	Loading slope (GPa)				Unloading slope (GPa)				Elastic bulk modulus (GPa)			
			1 cycle	3 cycles	7 cycles	10 cycles	1 cycle	3 cycles	7 cycles	10 cycles	1 cycle	3 cycles	7 cycles	10 cycles
K19a	Water	Yes	1.6	2.5	2.7	2.8	2.9	3.5	3.4	3.3	12	8.4	9.2	8.6
K40			3.6	4.7	4.5	4.6	11	6.7	5.7	5.6	13	10.2	9.3	8.9
K17a		No	1.6	2.5	2.5	2.5	3.1	2.6	2.7	2.6	9.2	7.2	7.1	6.8
K18b			2.2	3.5	3.7	3.7	4.7	4.	4.2	4.2	9.2	8.8	9	8.4
K44a	Isopar H oil	Yes	1.4	2.7	2.8	2.7	3.7	3.2	3.1	3.2	7.9	5.3	5.1	5
K22			3	6.3	6.7	7	7.4	7.7	7.4	7.7	14	11	8.9	10.7
K25		No	3.7	6.8	7.1	7.1	6.7	6.9	7	7.1	11.7	13	12.4	13.8
K44b			2.1	3.9	4.1	4.9	3.9	4.1	4.2	5.1	14.8	13.7	13.8	12.3
M36b	Water	Yes	2.6	3.6	3.9	3.9	4.5	4.4	4.5	4.4	9.7	7.5	7.3	7.3
M31b			1.9	2.7	2.9	2.9	6.1	3.1	3.1	3.1	8.8	4.5	4.4	4.4
M13		No	2.5	3.5	3.7	3.6	3.6	3.6	3.7	3.7	6.2	7	7.6	7.3
M24			1.8	1.8	1.8	1.9	3.1	3.5	3.8	3.7	4.8	4.1	4.4	4.1
M30	Isopar H oil	Yes	2.2	3.8	4.1	4.1	8.7	4.5	4.3	4.4	12	6.8	6.1	7.3
M36a			2.4	3.6	4.1	4	7.7	4.5	4.6	4.6	12	6.2	6	5.8
M18		No	2.8	4	4	4	4.6	4.1	4	4	6.3	5.9	6.2	5.7
M32b			3.1	4.6	4.7	4.7	4.9	4.9	4.8	4.9	7.1	7.3	7.1	7.6
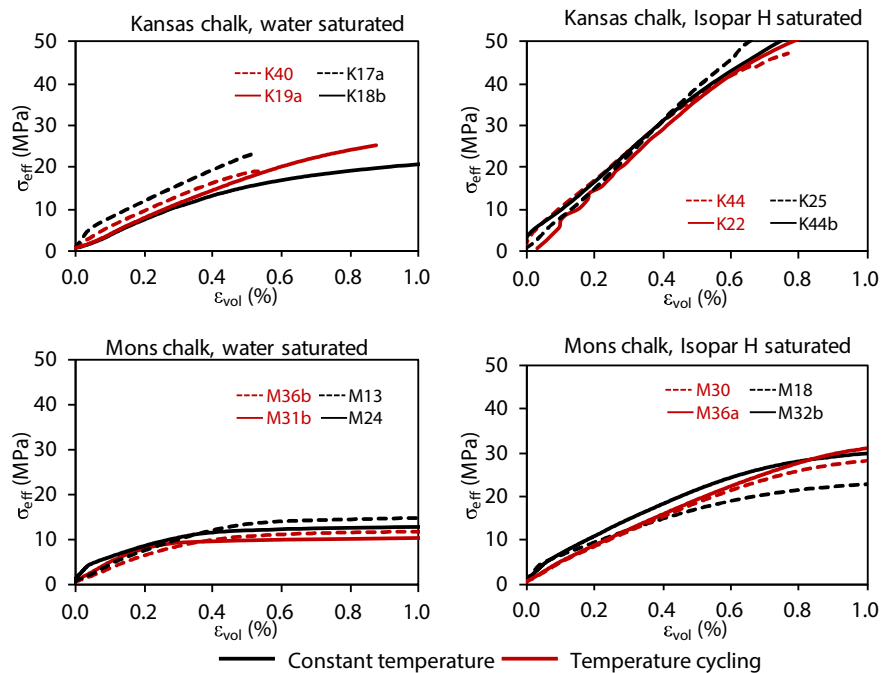
Fig. 9. Hydrostatic failure curves of all the samples tested. Red lines illustrate the test results for samples that have been exposed to temperature cycling, and black lines for the samples tested at a constant temperature.

at 30 °C. The irreversible plastic strain component of the additional 11th stress cycle, which was performed without the temperature cycle in between each stress cycle, dropped to the same value as that of the samples tested at a constant temperature during the whole experiment. This pattern was observed for all tests on both Mons and Kansas chalks saturated with both Isopar H oil and water (Fig. 7). The elastic bulk modulus K, however, did not vary significantly from the 2nd to the 10th cycle for either the temperature cycle or the constant temperature tests (Fig. 8), indicating that the elastic behaviour remains the same even though plastic permanent damage accumulates. In Fig. 6, the temperature cycle between each hydrostatic stress cycle leads to greater accumulated strain over the 10th and 11th cycles, and this behaviour is attributed to plasticity effects rather than the changes in elastic behaviour. Furthermore, temperature cycles did not significantly influence the yield strength, and no significant difference after testing could be

observed between the samples that had been or not exposed to temperature cycling (Fig. 9). The effect of water weakening, however, was significant, as the hydrostatic yield stress reduced from 13.2–16.3 MPa for Isopar H oil-saturated to 7.9–10.3 MPa for water-saturated Mons chalk, and from 32.2–36.8 MPa to 12.9–18.7 MPa for Kansas chalk (Table 3).

As shown in Fig. 7, the irreversible strain was consistent for the duplicated experiments. However, the total strain accumulated varied for some of the duplicates (Fig. 6). A significant difference between duplicates was found for the Kansas chalk samples saturated with Isopar H oil that had been exposed to temperature cycles between stress cycles. One sample accumulated 0.2% and the other accumulated 0.5% volumetric strain during the tests (Fig. 6). This could be due to the difference in elastic modulus of the two samples. Even though the Kansas chalk samples were cycled at a smaller proportion of yield stress (33% and 40% for water-saturated

Table 3
Yield failure of all samples and comparison to the maximum stress during a hydrostatic cycle. The maximum stress of 5.2 MPa during a hydrostatic cycle is well below the yield failure in all cases.

Sample	Saturating fluid and constant/cycled temperature	Yield failure (MPa)	Percentage of maximum stress (5.2 MPa) to yield stress (%)
K19a	Water/cycle	12.9 ± 2.8	40
K40	Water/cycle	15.9 ± 3.2	33
K17a	Water/constant	18.7 ± 4.4	28
K18b	Water/constant	16.7 ± 4.5	31
K44a	Isopar H oil/cycle	35.2 ± 6.8	15
K22	Isopar H oil/cycle	34.4 ± 4.6	14
K25	Isopar H oil/constant	36.8 ± 6.4	16
K44b	Isopar H oil/constant	32.2 ± 4.7	15
M36b	Water/cycle	8.5 ± 1.9	62
M31b	Water/cycle	7.9 ± 2.2	66
M13	Water/constant	10.3 ± 2.6	51
M24	Water/constant	9.7 ± 2	53
M30	Isopar H oil/cycle	15.2 ± 5.7	34
M36a	Isopar H oil/cycle	16.3 ± 5.4	32
M18	Isopar H oil/constant	13.2 ± 4	39
M32b	Isopar H oil/constant	15.5 ± 5.3	33

chalks, and 14% and 16% for oil-saturated chalks, see Table 3 and Fig. 6), it showed that the temperature cycling led to more or equal amounts of volumetric strain after 11 cycles than the cycling performed on Mons chalk where the peak cycle stress was 62% and 66% of yield stress for the water-saturated samples and 32% and 34% for oil-saturated samples. It would be expected that when approaching the failure envelope, more plastic damage would accumulate, but this was not observed.

In order to find how the accumulated strain is linked to other measurable parameters, the total accumulated strain from the 2nd to the 10th cycle (ε_{tot}) was plotted against the initial porosity (ϕ) and the Biot coefficient (α) (Fig. 10). The first cycle was omitted from these correlations to avoid inherent large variability observed in the first load cycle (Fig. 6) as seen for all the tests. Even though the statistical significance is limited, it may be seen that the Kansas-Isopar H experiments accumulate more strain (open green circles) when both the porosity and Biot coefficient increase (Fig. 10a and c). Furthermore, the experiments on water-saturated Kansas chalk displayed a positive correlation between ε_{tot} and ϕ (closed green circles), while ε_{tot} was not correlated to the Biot coefficient (Fig. 10a and c). For Mons chalk samples, the same correlations were not observed, neither between ε_{tot} and ϕ, nor between ε_{tot} and α. As such, a univocal statistical pattern relating the porosity and Biot coefficient to the total accumulated strain for both Kansas and Mons chalks cannot be observed. It is interesting to note that, however, the highly indurated chalk displays such a correlation, whilst the less indurated Mons chalk does not.

Fig. 10b and d displays the correlations of ε_{tot} vs. ϕ and ε_{tot} vs. α, respectively, discriminated by testing methods. Here the samples are split into four groups in combination with Kansas chalk (circles) and Mons chalk (triangles), and constant temperature (black) and temperature cycles (red). For all four groups, positive correlations between volumetric strain and porosity (Fig. 10b), and between ε_{tot} and α can be seen. This observation is interesting because more.

For each individual stress cycle, approximately double irreversible strain was accumulated if the temperature cycling was performed, as opposed to the experiments at a constant temperature. This plastic component was most pronounced for the water-

Chalk type and pore fluid

Testing method
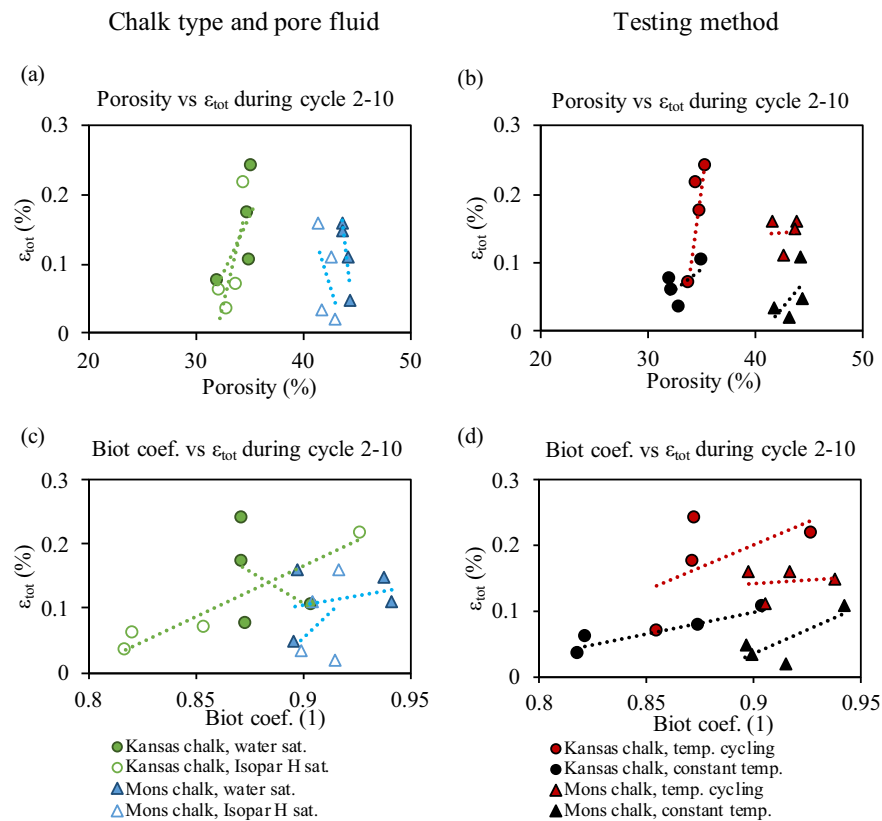
Fig. 10. Correlation between the total strain accumulated between cycles 2−10 and saturation porosity (top) and Biot coefficient (bottom). On the left, the correlation is made for different chalk types and their saturating fluids. No uniform trend was found. On the right, the correlation is made according to the testing method, whether the chalk samples were exposed to a constant temperature or to temperature cycling. These correlations all display a similar trend, indicating that the total strain accumulated increases with the increasing porosity and Biot coefficient.

saturated and highly indurated Kansas chalk samples (Fig. 7). The two chalk types behaved differently when saturated with water, but no significant behavioural difference was observed in Isopar H oil-saturated samples. The highly indurated Kansas chalk accumulated both more total strain and more irreversible strain within each stress cycle than Mons chalk when saturated with water. This indicates that the greater amount of contact cementation (lower Biot coefficient) is more susceptible to anisotropic thermal expansion and contraction of calcite particles when saturated with water, a polar fluid.

The saturating fluid thus plays an important role in mechanical testing. Our data show that water saturation reduces hydrostatic yield strength (Fig. 9). This is in line with the conclusions of other works (Madland et al., 2002; Risnes et al., 2005). Water is a polar fluid and it can be adsorbed to the calcite surfaces in chalk. Isopar H oil is no-polar fluid and cannot be adsorbed to the calcite surface.

Calcite crystals have surfaces populated by positively charged Ca^{2+} and negatively charged CO_3^{2-} surface sites (Stipp et al., 1999). At the basic equilibrium-pH of water and calcite, adsorption of divalent positive ions (Ca^{2+}) and monovalent negative ions (HCO_3^-) causes an overall positive surface charge. Røyne et al. (2011) used glycol-water mixtures to measure surface energy of calcite depending on water concentration, and they found that the surface energy decreased with increasing water concentration. The decline in hydrostatic yield strength by saturation could be related to the observations of fracture generation in dry calcite. The energy needed to create a calcite surface depends on the presence of water, where the energy needed for generating a dry surface is 0.32 J/m^2, whereas it is 0.15 J/m^2 for a fully hydrated calcite surface (Røyne et al., 2011). This means that it takes almost double the energy to create a dry calcite surface than that for a hydrated one, and hence in water-saturated samples, it would be easier to break contact cementation and make a new surface between two neighbouring particles. When employing these results to the fracture formation between calcite particles placed next to each other with a non-zero difference in c-axis angle, thermally induced strain would result in thermal stress concentrations within the contact cement, which would lead to bond breakage when the energy for generating a new surface is minimised.

When the saturating fluid has electrical charge exchange with the calcite surface, it creates an electrical double layer (Al Mahrouqi et al., 2017). If we assume that the thickness of the charged layer is directly proportional to the Debye length, then the thickness of the layer also depends on the temperature, and it increases with increasing temperature. Increasing this area of repulsion between particles would stress the areas of contact cementation extremely, and thus more indurated samples would be more influenced at higher temperatures. However, as it was not observed that yield stress depends on whether the sample has been exposed to temperature cycling or not, but a greater plastic strain accumulation was observed at cycled temperature, it is proposed that increasing the length of the electrical double layer enhances the number of contacts with broken cement (micro-fractures). This would not affect the overall strength, which depends on the strength of the weakest bond rather than the number of weak bonds.

Experimental results imply that contact cementation breakage affects neither yield strength nor bulk modulus, but rather directly the amount of irreversible strain. The temperature sensitivity occurs to a lower extent for the less cemented Mons chalk, because cementation is not contributing as much to Mons chalk stiffness and strength, as it does for Kansas chalk, which gains its higher stiffness and strength from higher degree of contact cementation.

Even for elastic-perfectly metallic electric alloys, such as the compound of lead and tin (Pb/Sn) used in microelectronic packaging, it demonstrates that inelastic strain accumulates during 100 temperature cycles between 0 °C and 75 °C. This accumulation was found to be caused by the component bonded to the alloy having a different thermal expansion coefficient from the alloy itself (Dishongh et al., 2002). As such, stress concentrations induced by the differences in thermal strain at given material contacts lead to failure — a microscopic effect that may propagate to the mesoscopic scale. As such, due to the anisotropic thermal expansion of calcite, chalk samples with higher area of contact cementation are expected to be more influenced by temperature variation.

5. Conclusions

This paper aimed to better understand the mechanical stability of chalk during water injection, which can cause temperature to fluctuate. In response to temperature fluctuation, the anisotropic thermal expansion of calcite crystals induces thermal stress that results in accumulation of irreversible strain. From the experiments performed in this study, all samples exposed to temperature cycling accumulated more strain than the samples tested at a constant temperature. This was specifically pronounced for water-saturated Kansas chalk, which has a relatively high induration and a high degree of contact cementation. Polarity of the saturating fluid plays a greater role in more indurated chalk exposed to temperature cycling. However, temperature cycling had an effect on irreversible strain accumulated, but no significant influence on elastic modulus or yield stress. Furthermore, it was also found that the peak in each stress cycle relative to the failure strength is not the deterministic parameter for the permanent damage accumulated during stress and temperature cycles. This is conclusive that temperature cycling resulted in an increase in the number of micro-fractures, which hence accumulated more strain during stress variation in the elastic domain, but did not influence the overall strength of the samples. Our results indicate that the risk of degrading the mechanical integrity of chalk by temperature variation is more relevant for deeper and thus more contact-cemented chalk reservoirs, with low Biot coefficient, than for shallower chalk reservoirs with high Biot coefficient.

Conflicts of interest

The authors wish to confirm that there are no known conflicts of interest associated with this publication and there has been no significant financial support for this work that could have influenced its outcome.

References

Al Mahrouqi D, Vinogradov J, Jackson MD. Zeta potential of artificial and natural calcite in aqueous solution. Advances in Colloid and Interface Science 2017;240:60–76.

Baud P, Zhu WL, Wong TF. Failure mode and weakening effect of water on sandstone. Journal of Geophysical Research: Solid Earth 2000;105(B7):16371–89.

Becattini V, Motmans T, Zappone A, Madonna C, Haselbacher A, Steinfeld A. Experimental investigation of the thermal and mechanical stability of rocks for high-temperature thermal-energy storage. Applied Energy 2017;203:373–89.

Chen LJ, He J, Chao JQ, Qin BD. Swelling and breaking characteristics of limestone under high temperatures. Mining Science and Technology (China) 2009;19(4):503–7.

Collins BD, Stock GM, Eppes MC, Lewis SW, Corbett SC, Smith JB. Thermal influences on spontaneous rock dome exfoliation. Nature Communications 2018;9:762. https://doi.org/10.1038/s41467-017-02728-1.

De Andrade J, Sangesland S, Todorovic J, Vrålstad T. Cement sheath integrity during thermal cycling: a novel approach for experimental tests of cement systems. In: SPE bergen one day seminar. Society of Petroleum Engineers (SPE); 2015. https://doi.org/10.2118/173871-MS.

Dishongh T, Basaran C, Cartwright AN, Zhao Y, Liu H. Impact of temperature cycle profile on fatigue life of solder joints. IEEE Transactions on Advanced Packaging 2002;25(3):433—8.

Fabricius IL. Burial stress and elastic strain of carbonate rocks. Geophysical Prospecting 2014;62(6):1327—36.

Hansen KK, Leksø H, Grelk B. Assessment of the durability of marble cladding by laboratory exposure compared to natural exposure. In: Carmeliet J, Hens H, Vermeir G, editors. Research in building physics: proceedings of the 2nd international conference on building physics. CRC Press; 2003. p. 267—71.

Henriksen AD, Fabricius IL, Borre MK, Korsbech U, Theilgaard AT, Zandbergen JB. Core density scanning, degree of induration and dynamic elastic moduli of Palaeogene limestone in the Copenhagen area. Quarterly Journal of Engineering Geology and Hydrogeology 1999;32(2):107—17.

Hermansen H, Thomas LK, Sylte JE, Aasboe BT. Twenty five years of Ekofisk reservoir management. In: SPE annual technical conference and exhibition. Society of Petroleum Engineers (SPE); 1997. https://doi.org/10.2118/38927-MS.

Hua W, Dong SM, Li YF, Xu JG, Wang QY. The influence of cyclic wetting and drying on the fracture toughness of sandstone. International Journal of Rock Mechanics and Mining Sciences 2015;78:331—5.

Katika K, Addassi M, Alam MM, Fabricius IL. The effect of divalent ions on the elasticity and pore collapse of chalk evaluated from compressional wave velocity and low-field nuclear magnetic resonance (NMR). Journal of Petroleum Science and Engineering 2015;136:88—99.

Lebedev M, Wilson MEJ, Mikhaltsevitch V. An experimental study of solid matrix weakening in water-saturated Savonnieres limestone. Geophysical Prospecting 2014;62(6):1253—65.

Lisabeth HP, Zhu WL. Effect of temperature and pore fluid on the strength of porous limestone. Journal of Geophysical Research: Solid Earth 2015;120(9):6191—208.

Madland MV, Korsnes RI, Risnes R. Temperature effects in Brazilian, uniaxial and triaxial compressive tests with high porosity chalk. In: SPE annual technical conference and exhibition. SPE; 2002. https://doi.org/10.2118/77761-MS.

Mavko G, Mukerji T, Dvorkin J. The rock physics handbook: tools for seismic analysis in porous media. Cambridge, UK: Cambridge University Press; 1998.

Megawati M, Hiorth A, Madland MV. The impact of surface charge on the mechanical behavior of high-porosity chalk. Rock Mechanics and Rock Engineering 2013;46(5):1073—90.

Okeson MA, Kellogg KG, Kallmeyer AR. Impact damage growth in fiberglass/epoxy laminates subjected to moisture and low temperature thermal cycling. In: Ayer R, Chung JS, Ames N, Wheat HG, editors. Proceedings of the 16th international offshore and polar engineering conference. International Society of Offshore and Polar Engineers (ISOPE); 2006. p. 279—86.

Olsen C, Christensen HF, Fabricius IL. Static and dynamic Young's moduli of chalk from the North Sea. Geophysics 2008;73(2):E41—50.

Ravnås C. Petrophysical and rock mechanical properties of heat treated chalk. Kongens Lyngby: Technical University of Denmark; 2017.

Risnes R, Madland MV, Hole M, Kwabiah NK. Water weakening of chalk — mechanical effects of water-glycol mixtures. Journal of Petroleum Science and Engineering 2005;48(1—2):21—36.

Rosenholtz JL, Smith DZ. Linear thermal expansion of calcite, var. Iceland spar, and Yule marble. American Mineralogist 1949;34(11—12):846—54.

Røyne A, Bisschop J, Dysthe DK. Experimental investigation of surface energy and subcritical crack growth in calcite. Journal of Geophysical Research: Solid Earth 2011;116(B4). https://doi.org/10.1029/2010JB008033.

Stipp S, Brady PV, Ragnarsdottir KV, Charlet L. Geochemistry in aqueous systems — a special issue in honor of Werner Stumm — preface. Geochimica et Cosmochimica Acta 1999;63(7):3121—31.

Wasantha PLP, Ranjith PG. Water-weakening behavior of Hawkesbury sandstone in brittle regime. Engineering Geology 2014;178:91—101.

Weiss T, Siegesmund S, Fuller ER. Thermal degradation of marble: indications from finite-element modelling. Building and Environment 2003;38(9—10):1251—60.

Yang YC, Zhou JW, Xu FG, Xing HG. An experimental study on the water-induced strength reduction in Zigong argillaceous siltstone with different degree of weathering. Advances in Materials Science and Engineering 2016. https://doi.org/10.1155/2016/4956986.
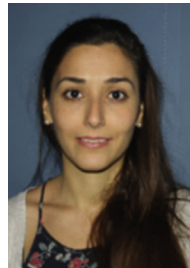
T. Voake is currently pursuing her PhD degree in Petroleum Technology at the University of Stavanger, Norway. She obtained her MSc degree in Geophysics from Memorial University of Newfoundland, and Honours Bachelor of Science (HBSc) degree from the University of Toronto, Canada. She has worked on numerous field and laboratory projects classifying rock physical properties. She has previously worked in the petroleum industry for a software development company.

Paper III: Elastic moduli dependence on temperature cycling in high porosity chalks

Voake, T., Nermoen, A., Korsnes, R.I., Fabricius, I.L. (In review).

Elastic moduli dependence on temperature cycling in high porosity chalks

1 **Elastic moduli dependence on temperature cycling in high porosity chalks**

2

3 **T. Voake[1, 2*], A. Nermoen[2, 3], R. I. Korsnes [1, 2], and I. L. Fabricius [1, 4]**

4 [1]University of Stavanger, Stavanger, Norway

5 [2]The National IOR Centre of Norway

6 [3]NORCE – Norwegian Research Centre AS

7 [4]Technical University of Denmark (DTU), Copenhagen, Denmark

8 Corresponding author: Tijana Voake (tijana.voake@uis.no)

9 Postal Address: University of Stavanger

10   Kjell Arholmsgate 41, 4036 Stavanger

11   Norway

12 Telephone: +47 94 868186

13

14 **Abstract:**

15 Chalk petroleum reservoirs can be prosperous, but influence from the production on their
16 stability is not well understood. Temperature cycling has been proven to have a degrading effect
17 on other carbonates such as marble. This study aims to gain a better understanding of
18 temperature cycling effects on the elastic properties of chalk. Two types of chalk are studied,
19 Kansas and Mons chalk, with p-q diagrams provided for both. Elastic bulk moduli tested under
20 hydrostatic conditions demonstrates a decrease for Mons chalk, while Kansas chalk modulus
21 was not significantly influenced by temperature cycling. Young´s modulus and compressional
22 modulus measured under confined constant overburden stress showed no effect of temperature
23 cycling. Linear thermal expansion coefficients had a similar value for the two chalks tested, but
24 had a negative correlation with increasing number of temperature cycles.

25 **1. Introduction**

26 It is estimated that more than 60% of the world's oil is held in carbonate reservoirs, and in the
27 central North Sea chalk, chalk formations such as Ekofisk, Tor and Hod dominate oil
28 production. The chalk reservoirs in this region are ageing and declining in production. In order
29 to maintain recovery, focus for the last 30 years has been on developing new technologies,
30 mainly focusing on the interaction between flooding fluid and the reservoir (Austad, et al., 2008,
31 Puntervold and Austad, 2008, Fathi, et al., 2011). Varying reservoir temperature and the effect
32 this may have on reservoir stiffness has not received as much attention.

33 During oil recovery, cold fluid is injected into hot reservoirs on a periodic basis over the lifetime
34 of a field, locally cooling the surrounding reservoir rock. This rock will then warm when
35 injection stops. These temperature fluctuations can potentially cause considerable deformation
36 to the reservoir because thermoelastic expansion and contraction strains the contact of
37 neighbouring particles. That temperature fluctuations can have significant effect is documented
38 by observations made of carbonate rocks used for construction that are exposed to moisture and
39 temperature variations. Examples include the cladding on the Finlandia Hall in Helsinki, which
40 consists of Carrara marble (Weiss, et al., 2003), and two types of cladding marble, one from
41 Greenland and the other from Norway, exposed to weathering in Copenhagen (Hansen, et al.,
42 2003).

43 This paper aims to describe how temperature variation impacts the elastic behaviour of chalk.
44 Even though the calcite mineral itself is highly anisotropic, bulk limestone and chalk samples
45 are found to have isotropic volumetric thermal expansion coefficients (**Table 1**). At particle
46 level, heating leads to thermal expansion along the c-axis and contraction in the perpendicular
47 plane. For two adjacent particles held together by contact cement, the difference in thermal
48 strain could result in stress localization at particle contacts. We aim to quantify the mechanical
49 impact of these internally induced stress concentrations, and how they lead to degradation.

50 **Table 1**. Thermal expansion coefficient (α) data for limestone and calcite

Reference – limestone	Limestone region	α (10^{-6} K^{-1})
Harvey (1967)	Illinois	5.2 - 5.7
Johnson and Parsons (1944)	Mille Roche, Canada	3.8 - 4.1
	St Louis Cp., MO	3.8 - 4.4
	Bethany Falls, MO	3.0 - 4.3
	Jordanville, NY	4.0 - 4.4

Goncalves and Brito (2017)	North le Roy, NY	5.6 - 5.8
	Paso Pobles, CA	8.6 - 9.4
	Anca, Portugal	4.6
Reference – calcite	$\alpha \parallel c \ (10^{-6} \ \text{K}^{-1})$	$\alpha \perp c \ (10^{-6} \ \text{K}^{-1})$
Rosenholtz and Smith (1949)	23.8	-5.2
Markgraf and Reeder (1985)	32.3	-2.8
Wu, et al. (1995)	28.798	-5.371
Rao, et al. (1968)	25.10	-3.68

51

52 Numerous studies cover the differences in mechanical properties of material tested at different
53 temperatures (Madland, et al., 2002, dos Reis, 2012), but few describe how temperature cycling
54 leads to mechanical degradation. Hua et al. (2015) demonstrated how the tensile strength of
55 sandstone from Sichuan region weakened by 50% after just seven repeated cycles of
56 submerging specimens in water and drying them at 105°C. Furthermore, when Alpine rocks
57 were tested for potential high temperature thermal energy storage (573°C and over), igneous
58 rocks demonstrated much less fracturing, increase in porosity and mineral dehydration than
59 sedimentary rocks (Becattini, et al., 2017).

60 This paper focuses on how the thermal expansion coefficient and the mechanical parameters
61 describing elastic behaviour are affected by temperature cycling of water saturated chalks. We
62 compared two chalks with different degrees of contact cementation, to identify how differences
63 in particle contacts play a role in the mechanical degradation. In previous studies, it has been
64 observed that tensile strength is weakened by temperature cycling in water saturated chalks, as
65 well as that chalk with a higher degree of contact cement accumulates more irreversible strain
66 when exposed to temperature cycling (Voake, et al., 2019a, Voake, et al., 2019b).

67 We assume that the studied chalks are isotropic on a sample scale, so that elastic properties can
68 be discussed from two perspectives: Bulk modulus was found from unloading experiments
69 under hydrostatic conditions, whereas Young's modulus and uniaxial compaction modulus
70 were measured from constant overburden tests with varying lateral stress. In experiments
71 performed under hydrostatic stress we are able to determine both bulk modulus and the
72 coefficient of thermal expansion. In the constant overburden test, we mimic a reservoir where
73 the magnitude of the vertical stress is constant, but the radial stress along with axial and radial
74 strain, is free to change.

75 **2. Theory**

76 The vertical applied stress was chosen to be constant and equal 70% of the stress required to
77 induce shear failure. In this stress geometry, Poisson's ratio was estimated, and if higher that
78 0.1, a significant lateral strain is indicated and the elastic Young's modulus was calculated,
79 whereas if apparent "Poisson's ratio" seemed to be lower than 0.1, no significant lateral strain
80 is indicated and uniaxial compaction modulus was derived.

81 2.1 Strain measurements in cylindrical geometries

82 In rock mechanical tests, the strain (ε) of a cylindrical rock sample exposed to effective stress
83 changes, is calculated form the differences between the measured length (L) and diameter (D)
84 and the original length (L_0) and diameter (D_0) of the sample, according to,

$$\varepsilon_z = \frac{L_0 - L}{L_0}, \text{ and } \varepsilon_r = \frac{D_0 - D}{D_0}. \tag{1}$$

85

86

2.2 Coefficient of thermal expansion

The coefficient of thermal expansion (α) is determined from the sample's strain during temperature change (ΔT),

$$\varepsilon = -\alpha\Delta T \tag{3}$$

This parameter was measured during hydrostatic stress geometry, in which the sample was not constrained in any direction.

2.3 Bulk modulus determination from hydrostatic test

Using Hooke's law on a sample tested under hydrostatic stress (σ'_{hyd}) the bulk modulus (K) can be calculated according to,

$$K = \frac{\Delta\sigma'_{hyd}}{\Delta\varepsilon_{vol}}, \tag{2}$$

where the volumetric strain of an isotropic samples is estimated from $\varepsilon_{vol} \simeq 3\varepsilon_r$, and higher order terms are omitted. The bulk modulus describes the stiffness of a sample and its resistance towards hydrostatic stress.

2.3 Determination of Poisson's ratio and elastic moduli from constant overburden tests

If a sample is tested at constant overburden conditions, where the axial and radial stresses differ, $\sigma_z \neq \sigma_r$, and if an assumption is made that a sample is linearly elastic, homogeneous and isotropic, then Young's modulus (E) and Poisson ratio (ν) can be estimated. The effective stress (σ_i') in the radial and axial direction is calculated using Biot coefficient (β) and the pore pressure (P_{pore}), $\sigma_i' = \sigma_i - \beta P_{pore}$, where $i = r, z$. For cylindrical samples, Hooke's law becomes,

$$E\varepsilon_r = (1 - \nu)\sigma'_r - \nu\sigma'_z, \text{ and} \tag{4}$$

$$E\varepsilon_z = \sigma'_z - 2\nu\sigma'_r. \tag{5}$$

As it can be seen from these expressions, a change in the radial effective stress leads to axial strain, and *vice versa*. Elastic coefficients can be estimated from incremental changes in the effective stresses and measured changes in strains. For incremental changes Δ, assuming that the rock remains the same such that E and ν are constant, equation (4) and (5) can be rewritten as,

$$E\Delta\varepsilon_r = (1 - \nu)\Delta\sigma'_r - \nu\Delta\sigma'_z, \text{ and} \tag{6}$$

$$E\Delta\varepsilon_z = \Delta\sigma'_z - 2\nu\Delta\sigma'_r. \tag{7}$$

For the experiments conducted in this study, the pore pressure and axial vertical stress is constant, so $\Delta\sigma'_z = 0$, while the radial stress is changed $(\Delta\sigma'_r \neq 0)$, and the equations simplify,

$$\Delta\sigma'_r = \frac{E\Delta\varepsilon_r}{(1-v)}, \text{and} \tag{8}$$

$$\Delta\sigma'_r = -\frac{E\Delta\varepsilon_z}{2v}. \tag{9}$$

113 In order to express E and v in terms of stress and strain that are measured in the experiment,
114 both Eq. 8 and 9 are rearranged,

$$E = \frac{\Delta\sigma'_r(1-v)}{\Delta\varepsilon_r} \tag{10}$$

$$E = -\frac{2\Delta\sigma'_r v}{\Delta\varepsilon_z} \tag{11}$$

115 By observing that Eq. 10 and 11 are equal, v can be expressed in terms of stress and strain as,

$$\frac{\Delta\sigma'_r(1-v)}{\Delta\varepsilon_r} = -\frac{2\Delta\sigma'_r v}{\Delta\varepsilon_z} \tag{12}$$

$$v = \frac{-\Delta\varepsilon_z}{2\Delta\varepsilon_r - \Delta\varepsilon_z} \tag{13}$$

116

117 In order to express Young's modulus E in only stress and strain terms, Eq. 13 is substituted into
118 either Eq. 10 or 11,

$$E = \frac{2\Delta\sigma'_r}{2\Delta\varepsilon_r - \Delta\varepsilon_z} \tag{14}$$

119 However, when testing elasticity near failure conditions, permanent deformation may occur and
120 a large difference between high vertical (overburden) stress and low lateral stress may result in
121 very low lateral strain, and hence an apparent very low Poisson's ratio. We selected a cut off
122 value of apparent Poisson's ratio of 0.1 In this case, the uniaxial compressibility modulus H is
123 calculated,

$$H = \frac{\Delta\sigma'_r}{\Delta\varepsilon_r} \tag{15}$$

124 **3. Material and Equipment:**

125 3.1 Material:

126 The mechanical behaviour of chalk from two quarries were described in this paper, Kansas
127 chalk from Niobrara Formation, Fort Hays Member, USA (Late Cretaceous), and Mons chalk
128 from Trivières Formation, Harmignies, Belgium (Late Cretaceous). The two chalks differ in
129 their degree of contact cementation between particles, where Kansas chalk has a larger contact
130 area between the calcite particles than Mons chalk. This is reflected in the induration, H3 for
131 more indurated Kansas chalk, and H2 for less indurated Mons chalk (Henriksen et al., 1999).
132 The Biot coefficient β for Mons chalk is 0.95 and for Kansas chalk 0.91, while the carbonate
133 content of Mons and Kansas samples were determined to be 99.8% and 96.9% respectively
134 (Ravnaas, 2017).

135 Cylindrical samples were drilled (approx. 40 mm diameter and 30 cm length) from blocks from
136 each locality. The sample diameter was adjusted to 38.1 mm, and the length of the samples

137 were cut to approximately 70 mm. The initial porosity of the samples (ϕ-*sat*) was determined
138 by saturating the samples with distilled water in a vacuum chamber and using the difference
139 between dry and saturated weight to obtain pore volume. Porosity from grain density (ϕ-ρ_{grain})
140 was calculated using volume of the sample, its dry weight, and grain density of calcite
141 ($\rho_{calcite} = 2.71$ g/cm^3). The P-wave velocity (v_p) was measured in the dry state prior to the
142 saturation of the samples with pore fluids, using CNS Farnell PUNDIT 7 (precision ±0.1 μs).
143 Based on these data and dry bulk density (ρ_d), elastic P-wave modulus (M_{dry}) was calculated
144 as:

$$M_{dry} = \rho_d v_p^2 \tag{16}$$

145 The physical properties of the samples used in this study are reported in **Table 2** and **Table 3**.

146 **Table 2**. Physical properties of samples tested for elastic moduli in hydrostatic conditions

Chalk type	Sample	Diameter (mm)	Length (mm)	ϕ-*sat.* (%)	ϕ-ρ_{grain} (%)	v_p (m/s)	M_{dry} (GPa)
Kansas	K40b	38.1	74.9	32.6	32.4	3056	17.1
	K41b	38.1	77.2	32.8	32.8	3178	18.4
Mons	M31a	38.1	70.3	41.3	41.7	2280	8.7
	M32a	38.1	70.0	43.2	42.5	2343	8.1

147

148 **Table 3**. Physical properties of the samples tested for elastic moduli under constant overburden

Chalk type	Sample	Diameter (mm)	Length (mm)	ϕ-*sat.* (%)	ϕ-ρ_{grain} (%)	$v_{p\ dry}$ (m/s)	M_{dry} (GPa)
Kansas	K30b	38.1	77.2	32.8	32.8	3178	18.4
Mons	M12	38.1	69.2	43.1	43.8	2262	7.8

149

150 Upon mounting in triaxial cells, the samples were saturated with calcite-equilibrated water of
151 0.652 mmol/L ionic strength.

152

153   3.2 Mechanical tests using triaxial cells
154 The experiments were performed using a triaxial cell (**Figure 1**). The independent applied radial
155 and axial stresses were controlled by two different pumps connected to the cell. A Hydraulic
156 Quizix pump, model QX-20000 HC equipped with two cylinders was used for radial confining
157 pressure control, and the other pump, Teledyne Isco Syringe Pump model 260D, controlled the
158 piston pressure that acted as the axial stress. The radial deformation was measured using an
159 extensometer, where the circumference changes were detected by LVDT MHR 100 from
160 Measurements Specialties™. The axial deformation was measured internally by LVDT MHR
161 250 from Measurements Specialties™. Both LVDTs have a precision of 0.15% of the
162 measurement. A Gilson Pump (model 307 HPLC) controlled the flowrate of the injected pore
163 fluid and the back pressure regulator was connected on the outlet side of the sample to ensure
164 constant pore pressure of 0.7 MPa. All pumps were individually operated through a LabVIEW
165 routine. The exterior of the cell was equipped with a 1000 W heating jacket, which was
166 controlled by an Omron E5CN PID for temperature control (±0.1°C precision).
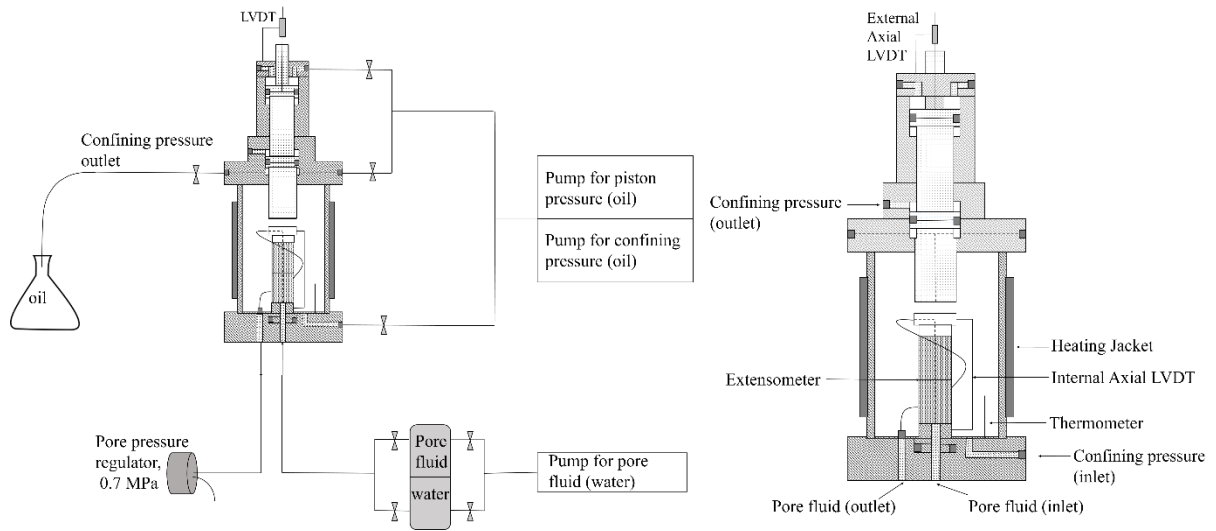
167

168 **Figure 1**. Triaxial testing set up

169 The effective radial stress is calculated directly,
170

$$\sigma_r' = \sigma_r - \beta P_{pore}$$

171 whereas a correction must be applied to the effective axial stress,

$$\sigma_z' = \sigma_r + f(P_{pist} - P_{fric}) - \beta P_{pore}$$

172 (P_{fric}) is the friction of the piston measured during initial movement (around 0.25 MPa).

173 The first and third stress invariants, p and q respectively, are particularly useful for displaying
174 failure data, because the values obtained from the cylindrical geometry apply to any coordinate
175 system. The pq-diagram in cylindrical geometries are expressed as,

$$q = \sigma_z - \sigma_r$$

$$p' = \frac{1}{3}(2\sigma_r' + \sigma_z')$$

176 The different failure modes are illustrated in **Figure 2.** A series of shear failure tests at different
177 confining stresses were performed to plot the shear failure line. Tensile strength and hydrostatic
178 yield stress were determined by Voake, et al. (2019a), Voake, et al. (2019b). The stress path
179 upon variation in side and axial stress, can be traced as a line in the pq-diagram, and failure
180 occurs once a failure line is crossed.
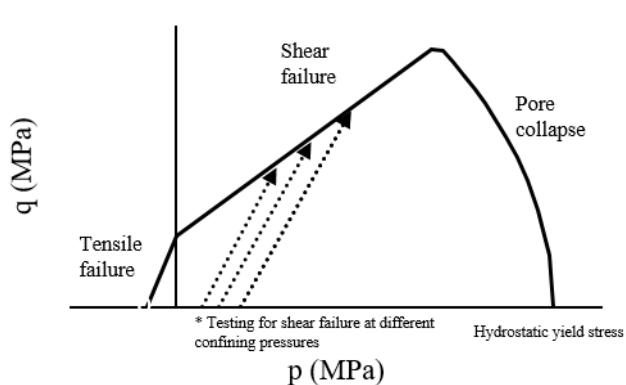
Figure 2. *p-q* diagram indicating different modes of failure. The arrows represent the direction of deviatoric loading at different confining pressure until shear failure line is reached and the sample fails.

3.2.1 Determination of shear failure line

Shear failure tests were performed on samples from the Kansas and Mons chalk blocks, in which the axial stress was increased until failure at four confining stresses (0.8, 1.2, 2, and 3 MPa). Two samples for each confining stress were tested to check repeatability of the results, so a total of eight samples were used to obtain the shear failure line for each chalk type. All tests were performed at 30°C, and samples were saturated with calcite equilibrated water.

Each experiment was performed according to following procedure:

- The confining pressure was increased to 0.5 MPa (apart from the tests at 0.8 MPa confining pressure, where the initial loading was set to 0.1 MPa).
- This was followed by simultaneously increasing confining and pore pressure to 1.2 MPa and 0.7 MPa respectively (apart from the tests at σ_r= 0.8 MPa, where confining and pore pressure were increased to 0.8 and 0.3 MPa).
- The temperature was set to 30°C and the samples were left until the extensometer obtained a stable reading (around 3000 min).
- The piston was lowered to touch the sample to measure the piston friction (P_{fric}) at the given corresponding confining stress.
- Tests at 0.8 MPa and 1.2 MPa were already at the desired confining pressures. For the tests at 2 MPa and 3 MPa, the confining pressure was increased at the rate of 0.03 MPa/min.
- Deviatoric loading was performed by increasing the piston pressure at a rate of 0.03 MPa/min until failure. The *p* and *q* values were calculated using the confining pressure at which the loading was performed and the axial pressure at which the sample failed.

3.2.2 Temperature effects on Bulk modulus

Bulk modulus, *K* was measured at 30°C during reduction of the hydrostatic stress from 4 MPa to 0.8 MPa, such that an unloading modulus was obtained. For each sample, three temperature cycles of 30°C to 90°C and back to 30°C were performed. After each temperature cycle once the samples' dimensions was stabilized, *K* was measured. Two Kansas chalk samples and two Mons chalk samples were tested (**Table 2**). The experimental steps were as follows:

- Confining pressure increased to 0.5 MPa.
- Simultaneous increase of confining and pore pressure to 1.2 MPa and 0.7 MPa, respectively.

- Hydrostatic loading was performed from 1.2 to 4 MPa with confining pressure increased at a rate of 0.03 MPa/min. At this stage initial elastic bulk modulus K_{int} was measured prior to any heating cycles
- The temperature was set to 90˚C and the experiments were left until the diameter stabilised (1-2 days).
- Temperature was reduced from 90°C to 30°C, at which stage the linear thermal expansion coefficient was measured.
- Confining pressure was lowered from 4 MPa to 0.8 MPa in 96 minutes for both chalk types. During this stage bulk modulus K was measured.
- Confining pressure was raised from 0.8 MPa to 4 MPa in 96 minutes and temperature increased back to 90°C. The loading elastic bulk modulus (K_{load}) was measured during this step.
- Last three steps were repeated two more times to investigate the impact of how the mechanical properties of the core reacted to the temperature and stress cycling.

The dynamic elastic modulus measured from ultrasonic velocity have a much better match with the static modulus when the static modulus is measured during the unloading part of a stress cycle (Olsen, et al., 2008). Therefore, the bulk modulus reported and presented in graphs are determined during the hydrostatic stress reduction.

3.2.3 Temperature effects on E modulus and ν

In order to estimate the shear modulus from Young's modulus and Poisson's ratio, the variation in the axial and radial stresses and corresponding radial and axial strains were used (Eq. 13, Eq. 14 and Eq. 15). All stress variation tests were performed at 30°C and the shear modulus was determined during side stress unloading. The axial stress was kept constant at 70% of the value required to induce shear failure at 2 MPa corresponding to $\sigma_z' = 11.8$ MPa for Kansas chalk and $\sigma_z' = 5.3$ MPa for Mons chalk. One Mons chalk sample and one Kansas chalk sample were used (**Table 3**). The deviatoric unloading was performed three times for each sample following a temperature cycle (30˚C to 90˚C and back to 30˚C). The experimental steps were:

- Confining pressure was loaded to 0.5 MPa.
- A simultaneous increase of confining and pore pressure to 1.2 MPa and 0.7 MPa, respectively.
- The piston was lowered to touch the sample. During lowering of the piston friction (P_{fric}) was measured.
- Hydrostatic loading was performed from 1.2 to 2 MPa confining pressure at a rate of 0.03 MPa/min.
- The axial stress was increased to 70% of the shear strength.
- The temperature was set to 90˚C, and the experiments were left until the diameter stabilised (1-2 days).
- A Labview program was set up to constant overburden mode such that the piston pressure varied according to σ_r.
- The temperature was reduced from 90°C to 30°C.
- Confining pressure was lowered from 2 MPa to 0.8 MPa in 36 minutes for Mons chalk and 72 minutes for Kansas chalk (since Kansas chalk was stiffer and reacted slower to changes), during which apparent Poisson's ratio was measured. If the value is higher

260   than 0.1, then Young's modulus E was estimated from Eq 14, and if v lower than 0.1,
261   then uniaxial compression modulus H was estimated using Eq 15.
262   – Confining pressure was raised from 0.8 MPa to 2 MPa in 36 minutes for Mons chalk
263   and 72 minutes for Kansas chalk and temperature increased back to 90°C. The v_{load}
264   and loading elastic modulus were measured at this stage, E_{load} and H_{load}.
265   – The last three steps were repeated two times to investigate the impact of how the
266   mechanical properties of the samples reacted to the temperature and stress cyclic
267   behaviour, after the third stress cycle the experiment was ended with unloading and
268   the stress loading was not performed.

269 **4. Results**

270 The results of the shear failure test are reported in terms of $p - q$ values, followed by the
271 analysis of the hydrostatic tests, and then by the analysis of the tests performed with constant
272 overburden.

273

274   4.1 Shear failure line and $p - q$ diagram
275 The shear failure line was obtained from eight tests for each chalk type at four different
276 confining pressures. Samples used were from the same blocks as the samples used for elastic
277 modulus measurements. The results are presented in **Table 4,** with p and q values representative
278 of the peak stress points the samples were able to sustain.

279

280 **Table 4**. Mechanical test results for samples used to plot shear failure lines for Mons and
281 Kansas chalk.

σ_r	Kansas chalk			Mons chalk		
	Sample	***p***	***q***	**Sample**	***p***	***q***
0.8	K20a	4.4	12.5	M10a	1.8	5.1
0.8	K21b	4.1	11.6	M8	1.9	5.1
1.2	K30a	4.7	12.3	M4b	2.7	6.2
1.2	K29b	5.7	15.2	M9b	2.6	5.9
2.0	K19b	6.8	16.2	M5a	3.5	6.3
2.0	K25a	6.3	14.6	M5b	3.2	5.2
3.0	K25b	8.2	17.4	M3	4.7	6.8
3.0	K29a	8.2	17.4	M7	4.6	6.7
			Stan. dev			Stan. dev
	Slope	1.375	0.128	Slope	0.534	0.144
	Cohesion	6.344	0.796	Cohesion	4.236	0.471

282

283 Combining the shear failure information with data from previously published data, tensile
284 failure and hydrostatic failure, a $p - q$ failure envelop for Kansas and Mons chalks saturated
285 with calcite equilibrated water at 30°C is produced (**Figure 3**), indicating the higher strength of
286 the more indurated Kansas chalk.

287
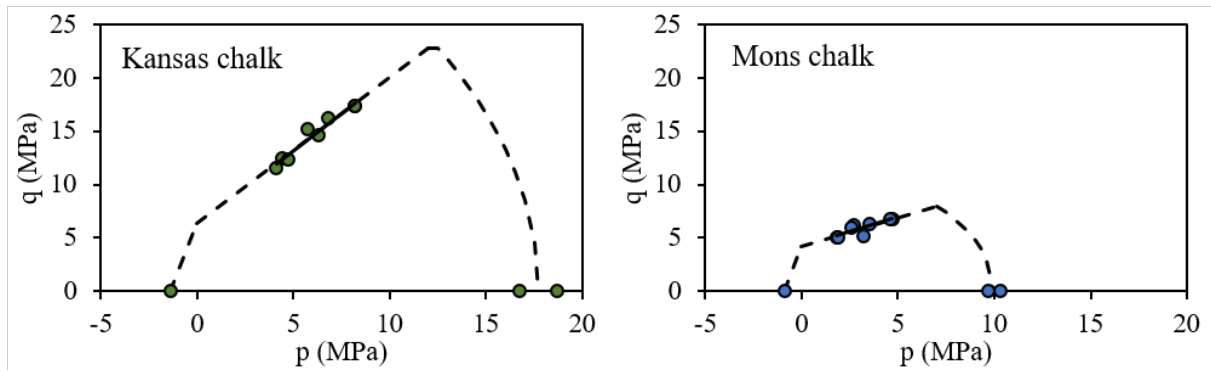
Figure 3. $p - q$ failure envelopes for Kansas and Mons chalks saturated with calcite equilibrated water at 30°C.

4.2 Temperature effects on K modulus

The test history for the hydrostatic tests is presented in **Figure 4**, and one can see cooling and heating rates as well as how the volumetric strain ε_{vol} responds to temperature and hydrostatic stress changes. We found that Kansas chalk has a higher bulk modulus than Mons chalk (**Figure 5**), and we found no significant impact of temperature cycling on Kansas chalk, while there is a decrease of the bulk modulus with additional temperature cycles for Mons chalk (**Table 5** and **Figure 6**). **Table 5** also demonstrates elastic modulus measured during hydrostatic loading, as well as the initial loading which was performed without any temperature treatment. For all samples K_{int} has lower value than moduli measured after temperature cycling. In all samples the loading modulus is marginally higher than unloading modulus.
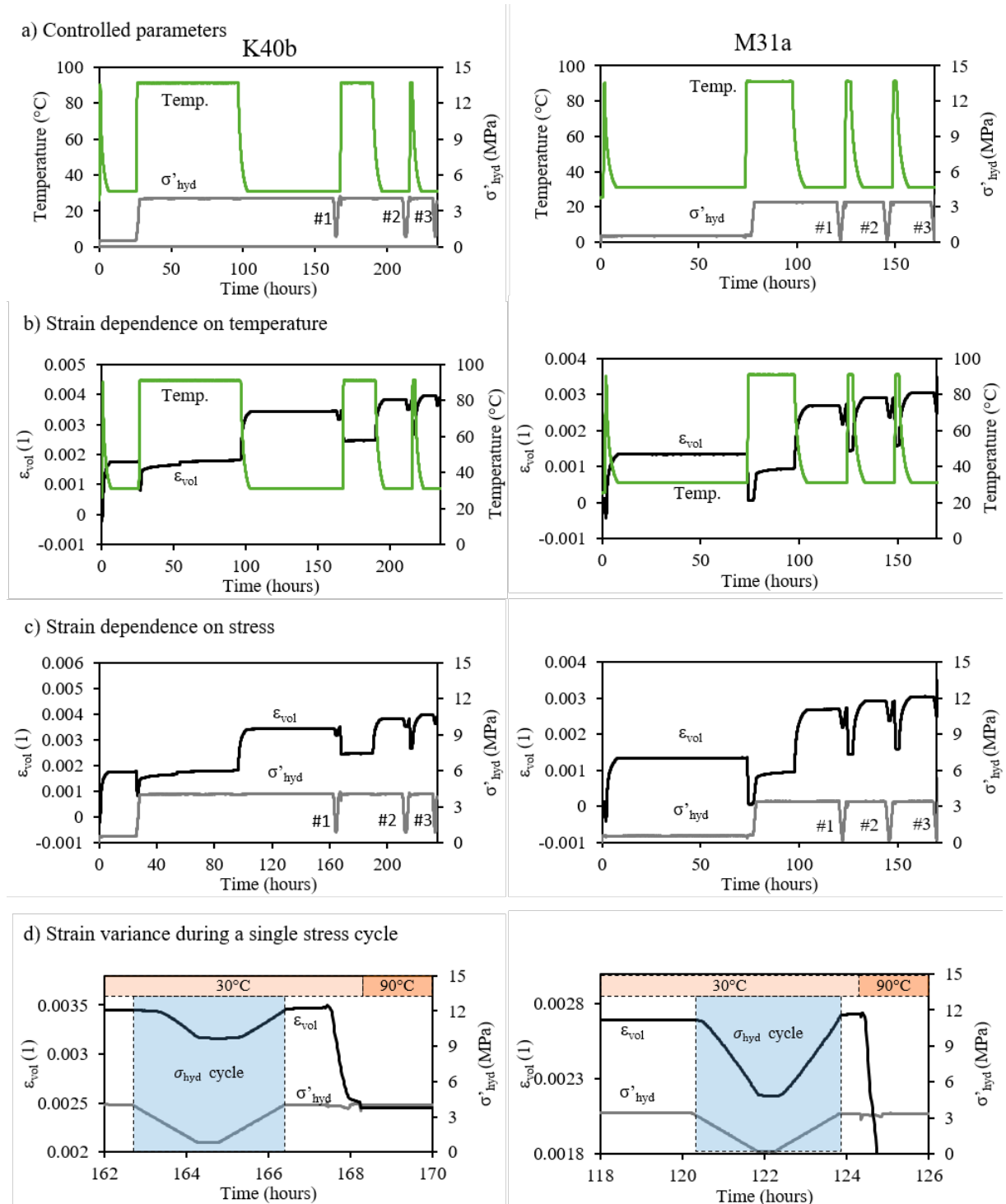
Figure 4. Test history for hydrostatic testing of Kansas chalk (left) and Mons chalk (right). (a) Controlled parameters during testing are temperature and σ_{hyd}. (b) The volumetric strain response (black line) is compared to temperature changes. (c) The volumetric strain response (black line) is compared to stress changes. (d) A zoom in of a single stress/temperature cycle compares how strain react to both temperature and stress changes.
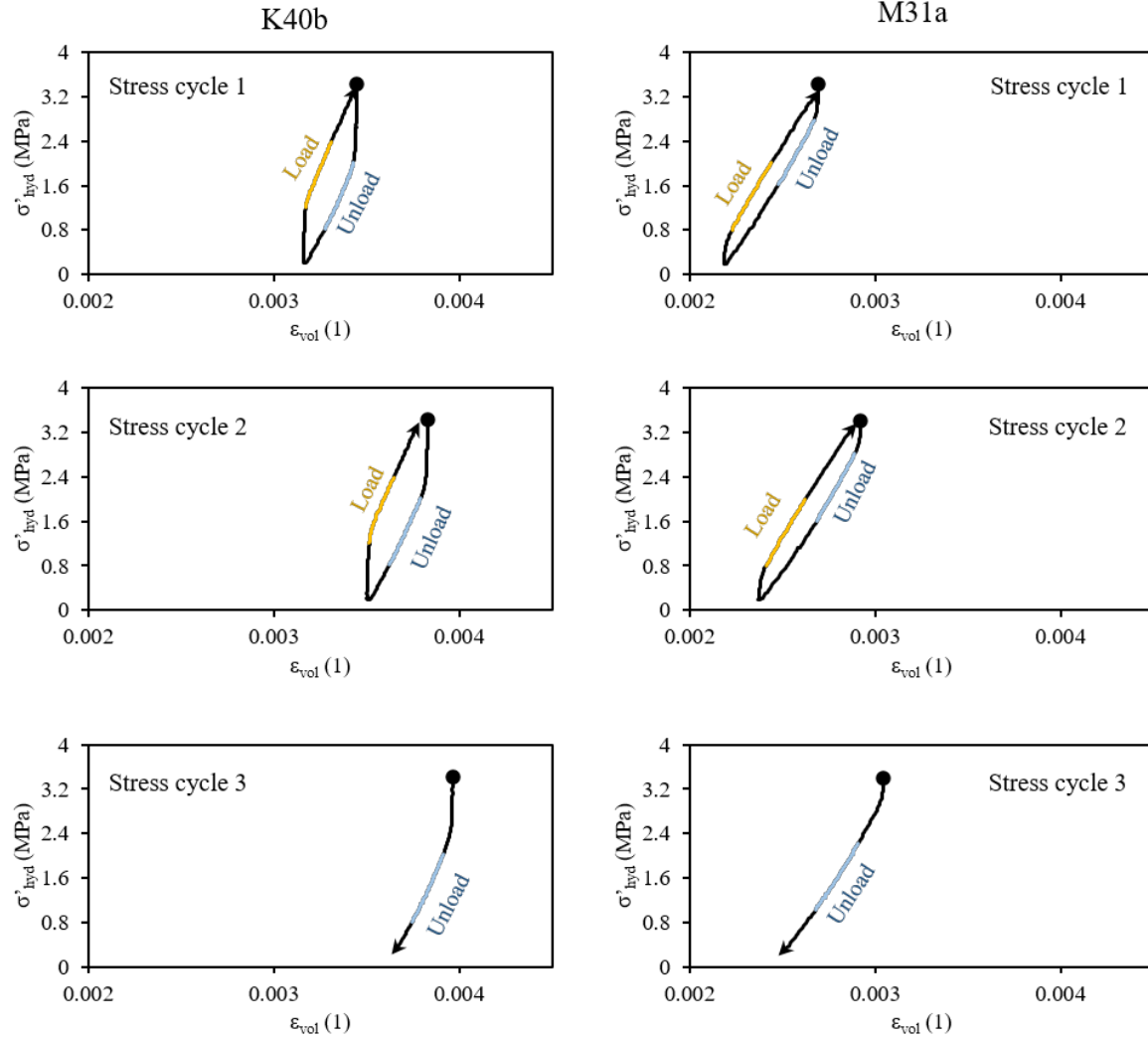
Figure 5. Stress- strain relationship during the three stress cycles for Kansas chalk (left) and Mons chalk (right), highlighting the intervals at which K was measured.

Table 5. Elastic bulk modulus K for samples measured during unloading, along with elastic moduli acquired during hydrostatic loading.

Sample	Initial loading (GPa) K_{int}	Stress cycle 1 (GPa) K	K_{load}	Stress cycle 2 (GPa) K	K_{load}	Stress cycle 3 (GPa) K
K40b	3.5 ± 0.7	6.8 ± 0.7	7.6 ± 0.3	6.8 ± 0.5	7.4 ± 0.2	6.7 ± 0.7
K41b	6.0 ± 0.3	8.7 ± 0.9	8.8 ± 0.8	8.7 ± 0.9	9.7 ± 0.4	7.6 ± 0.9
M31a	3.8 ± 0.2	5.3 ± 0.4	5.4 ± 0.2	5.1 ± 0.3	5.7 ± 0.4	4.9 ± 0.3
M32b	3.9 ± 0.2	6.0 ± 0.3	6.7 ± 0.3	5.7 ± 0.3	6.5 ± 0.5	5.5 ± 0.3
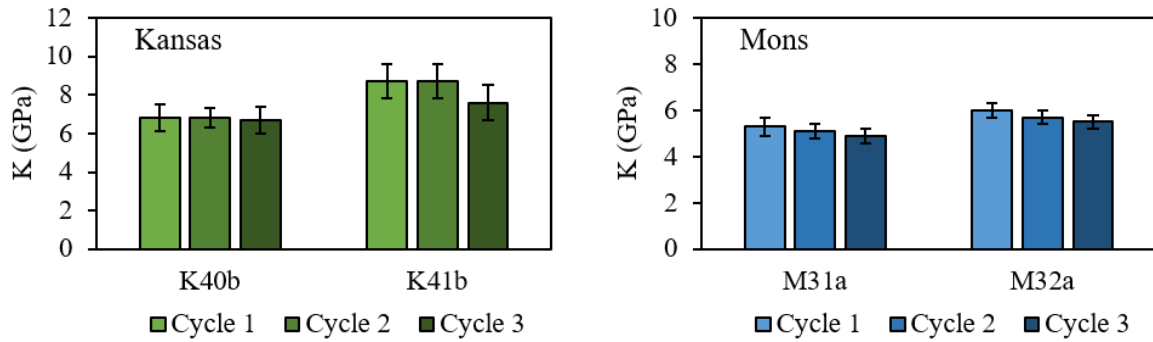
Figure 6. Elastic bulk modulus K estimated from hydrostatic stress reduction. The light color represents the first stress unloading which is followed by temperature cycling, the intermediate color second stress unloading, and the dark color represents the third stress unloading.

4.3 Temperature effects on E modulus and ν

During constant overburden tests, changes of radial stress and temperature had an effect on strain of the samples. The test history is presented in **Figure 7** and the data for Poisson's ratio is highlighted (**Figure 8**). In almost all cases, apparent Poisson's ratio significantly drops after the first unloading (**Table 6**). This could be due to the increase in q, and that the stress path almost reaches shear failure (**Figure 9**). Small axial strain during subsequent loading indicates that the sample lost strength to push back against the overburden and has been permanently damaged. If the strain is only observed in the lateral direction, and not in axial, the apparent Poisson's ratio is significantly reduced, and therefore we represent the elastic modulus as uniaxial compaction modulus (**Table 7** and **Figure 10**). In all cases loading moduli is higher than the unloading moduli, but this could be due to the experimental set up, as unloading was performed on a stabilized sample, and loading was performed right after unloading, so possible hysteresis is present. There is no clear trend of the moduli changing with additional temperature cycles.

331
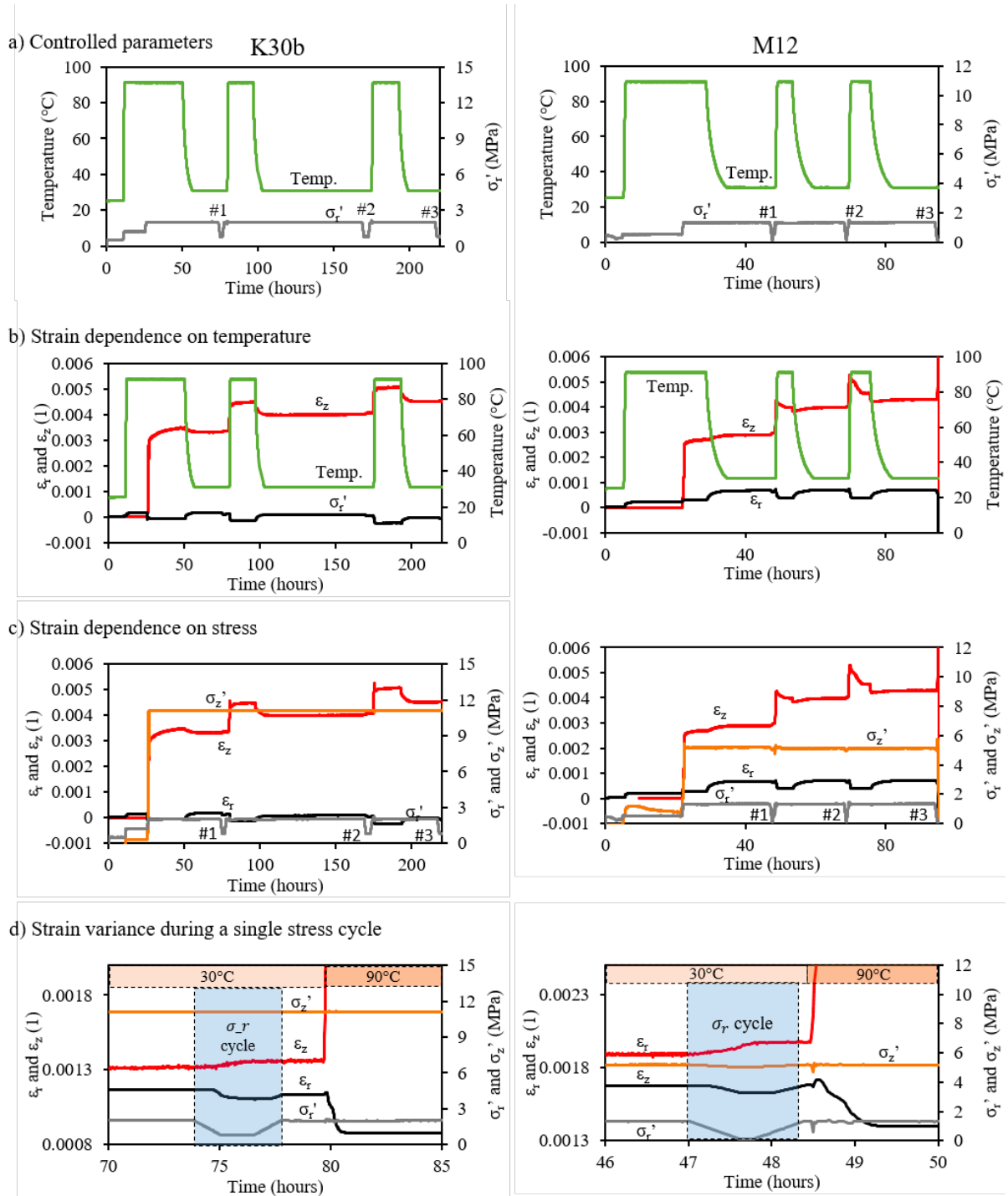
Figure 7. Test history for Kansas chalk (left) and Mons chalk (right). (a) Controlled parameters during testing are temperature and σ_{hyd}. (b) The radial strain response (black line) and axial strain response (red line) are compared to temperature changes. (c) The radial strain response (black line) and axial strain response (red line) are compared to stress changes. (d) A zoom in of a single stress/temperature cycle compares how strain reacts to both temperature and stress changes.

338
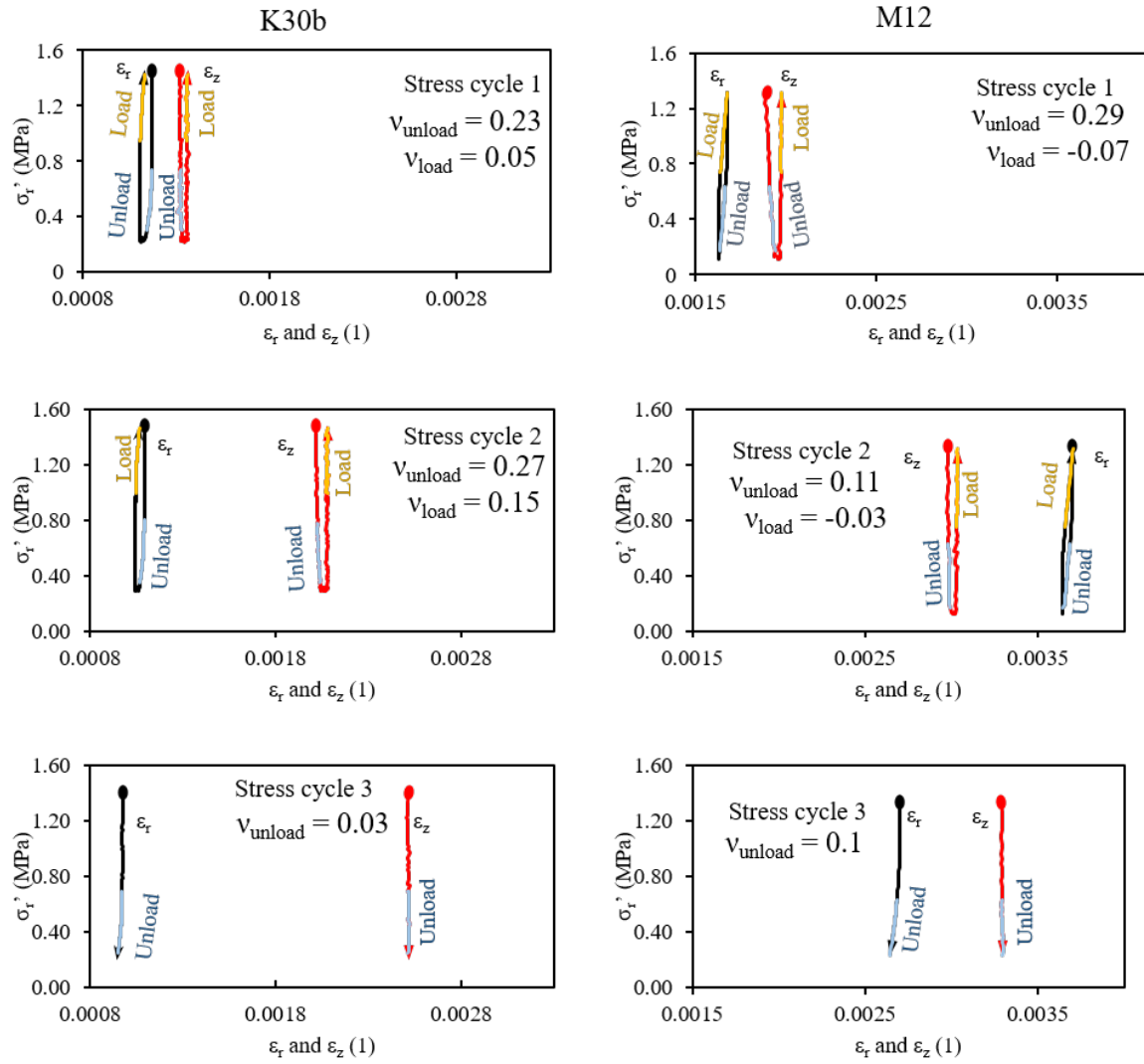
Figure 8. Stress- strain relationship during the three stress cycles for Kansas chalk (left) and Mons chalk (right), highlighting the intervals at which ν was measured.

Table 6. Apparent Poisson's ratio estimated during side stress reduction ν_{unload}, and during side stress increase ν_{load}, after additional temperature cycling.

Sample	Stress cycle 1 (GPa)		Stress cycle 2 (GPa)		Stress cycle 3 (GPa)
	ν_{unload}	ν_{load}	ν_{unload}	ν_{load}	ν_{unload}
K30b	0.15 ± 0.03	0.04 ± 0.05	0.25 ± 0.02	0.13 ± 0.06	0.03 ± 0.03
M12	0.26 ± 0.02	-0.06 ± 0.02	0.08 ± 0.02	-0.03 ± 0.02	0.08 ± 0.02
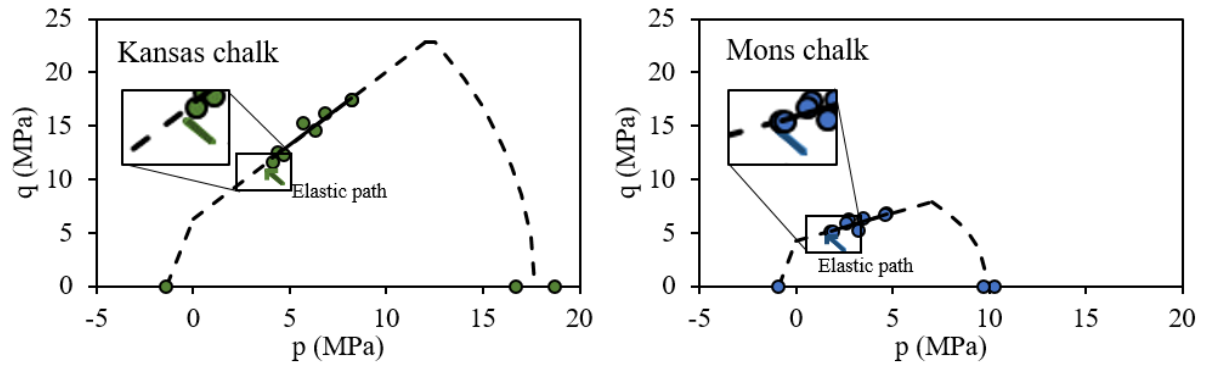
Figure 9. Elastic path of the two chalks during unloading, indicates that the deviatoric stress gets almost high enough to induce shear failure of the sample and potentially permanently damages it.

Table 7. Elastic moduli E and H estimated when the side stress is unloaded and re-loaded, and after additional temperature cycling.

| Sample | Stress cycle 1 (GPa) | | Stress cycle 2 (GPa) | | Stress cycle 3 (GPa) |
	Unload	Load	Unload	Load	Unload
K30b	E=11.6 ± 1.0	H=19.1 ± 1.1	E=12.3 ± 0.7	E=18.8± 1.7	H=16.9 ± 1.0
M12	E=10.9 ± 0.3	H=15.9 ± 0.3	E=11.9 ± 0.7	H=13.1 ± 0.3	E=9.2 ± 0.4
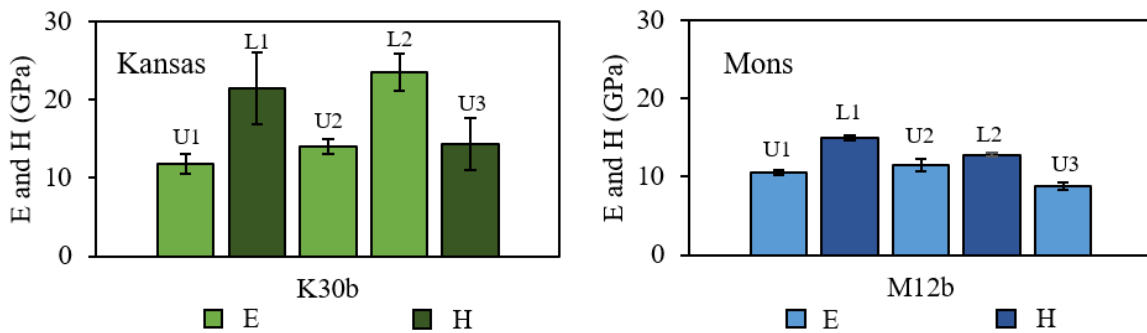
Figure 10. Young´s modulus E (lighter colour) and uniaxial compression modulus H (darker colour) measured during unloading (U) and loading (L) constant overburden experiments.

4.4 Temperature effects on thermal expansion coefficient

The coefficient of linear thermal expansion α was calculated using radial strain during hydrostatic tests when cooling from 90 to 30°C (Figure 11). The values measured are similar between the two chalk types and in line with an average thermal expansion of calcite (Table 1). However, there is a decreasing trend in thermal expansion coefficients seen for all samples tested with an increasing number of temperature cycles.
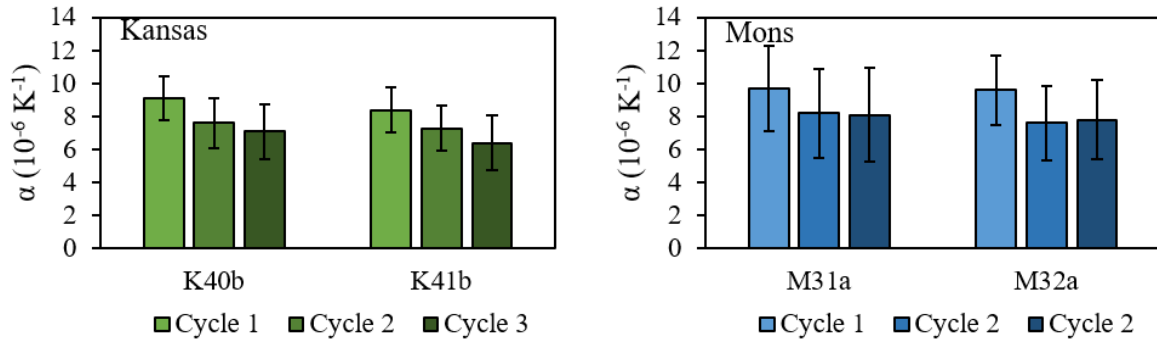
Figure 11. Thermal expansion coefficient α evolution through temperature cycles for Kansas chalk samples (green) and Mons chalk samples (blue).

5. Discussion

When tested under hydrostatic stress, the thermal expansion coefficient of Kansas and Mons chalk were found to be similar to an average of the two thermal expansion axis of calcite ($\sim$6.3 x 10^{-6} K^{-1}, **Table 1**). Temperature cycling had an impact on the thermal expansion coefficient, where both chalks demonstrated a decrease by approximately 10% by the third cycle (**Figure 11**). When tested under constant overburden conditions, hence confined and not allowed to move freely in all directions, the thermal expansion of Kansas and Mons chalk differ, where the thermal expansion of Mons chalk is almost double that of Kansas chalk (**Figure 12**). As the thermal expansion was measured by the change in diameter during cooling from 90°C to 30°C, this would mean that the Kansas chalk only contracted half as much as Mons chalk. This could correlate to the fact that the axial load applied on Kansas chalk samples is almost twice that applied on the Mons samples, σ_z'=11.8 MPa for Kansas chalk and σ_z'=5.3 MPa for Mons chalk (70% of the shear failure strength). In addition, the thermal expansion of Kansas chalk under uniaxial stress did not demonstrate a dependence on temperature cycling, while thermal expansion for Mons chalk demonstrates a decrease with increasing numbers of temperature cycles.
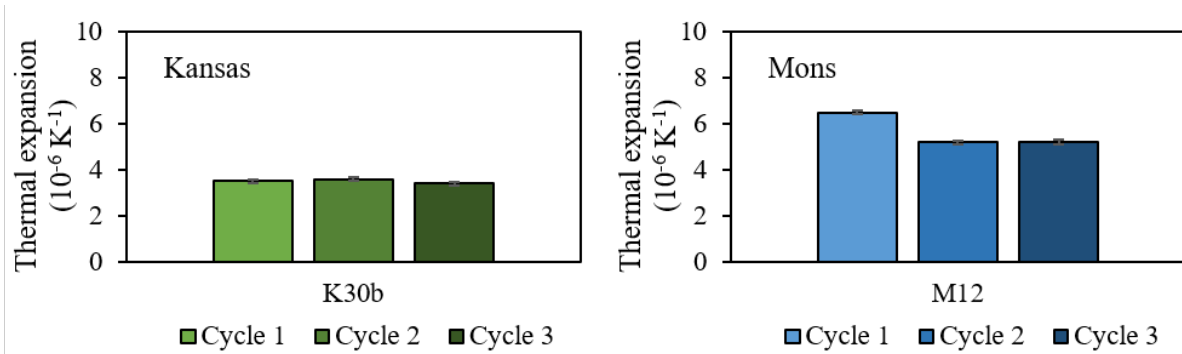
Figure 12. Thermal expansion through temperature cycles under constant overburden stress for Kansas chalk samples (green) and Mons chalk samples (blue), where σ_z'=11.8 MPa for Kansas chalk and σ_z'=5.3 MPa for Mons chalk.

Bulk modulus is higher for Kansas chalk than for Mons chalk. Bulk modulus was not influenced by temperature cycling for Kansas chalk, while it had a decreasing trend for Mons chalk. No trend was observed in the elastic moduli tested under constant overburden condition. Generally, after the first unloading the axial strain was minimum and the Poisson´s ratio was significantly

387   reduced. We believe the reason is that the samples approach close to shear failure line in $p - q$
388   diagram and potentially experience permanent damage (**Figure 9**). This could be applicable to
389   reservoir conditions during water injection and cooling. In a reservoir, the weight of the
390   overburden is constant, but the reservoir is able to be deformed axially. However, the reservoir
391   is constrained laterally, allowing no horizontal strain. During water injection, the reservoir is
392   cooled and therefore experiences contraction. In order to maintain constant horizontal strain,
393   horizontal stress must be reduced. This leads to increased deviatoric stress, and as seen in this
394   paper, increased deviatoric stress could lead to permanent damage of a rock.

395 **6. Conclusion**

396   In this study, a dependence of elastic moduli on temperature cycling was tested using two chalks
397   with differing degrees of contact cementation, the more indurated Kansas chalk and less
398   indurated Mons chalk. Under hydrostatic conditions, the bulk modulus of Mons chalk
399   demonstrated a decrease with increasing numbers of temperature cycles, while Kansas chalk
400   did not seem to be influenced. Similarly, there was no dependence of additional temperature
401   cycles observed on Young´s modulus and compression modulus on either of the chalks. Linear
402   thermal expansion coefficient measured was similar to those of calcite, but demonstrated a
403   decreasing trend with increasing temperature cycling.

409 **References:**

410   Austad T, Strand S, Madland MV, Puntervold T and Korsnes RI. Seawater in chalk: An EOR
411   and compaction fluid. Spe Reserv Eval Eng 2008; 11 (4): 648-54.
412   Becattini V, Motmans T, Zappone A, Madonna C, Haselbacher A and Steinfeld A.
413   Experimental investigation of the thermal and mechanical stability of rocks for high-
414   temperature thermal-energy storage. Appl Energ 2017; 203: 373-89.
415   Dos Reis JML. Effect of Temperature on the Mechanical Properties of Polymer Mortars.
416   Mater Res-Ibero-Am J 2012; 15 (4): 645-49.
417   Fathi SJ, Austad T and Strand S. Water-Based Enhanced Oil Recovery (EOR) by "Smart
418   Water": Optimal Ionic Composition for EOR in Carbonates. Energ Fuel 2011; 25 (11): 5173-
419   79.
420   Goncalves TD and Brito V. Differential thermal expansion as a cause of salt decay: literature
421   review, experiments, and modelling of micro and macro effects on Anca limestone. Stud
422   Conserv 2017; 62 (6): 310-28.
423   Hansen KK, Leksø H and Grelk B. Assessment of the Durability of Marble Cladding by
424   Laboratory Exposure compared to Natural Exposure. 2003:
425   Harvey R. Thermal expansion of certain Illinois limestones and dolomites. Illinois State
426   Geological Survey Circular 1967:
427   Johnson WH and Parsons WH. Thermal expansion of concrete aggregate materials,
428   Washington,: U. S. Govt. print. off., 1944.

429 Madland MV, Korsnes RI and Risnes R. Temperature Effects In Brazilian, Uniaxial And
430 Triaxial Compressive Tests With High Porosity Chalk. Society of Petroleum Engineers 2002:
431 SPE77761.
432 Markgraf SA and Reeder RJ. High-temperature structure refinements of calcite and
433 magnesite. American Mineralogist 1985; 70 (5-6): 590-600.
434 Olsen C, Christensen HF and Fabricius IL. Static and dynamic Young's moduli of chalk from
435 the North Sea. Geophysics 2008; 73 (2): E41-E50.
436 Puntervold T and Austad T. Injection of seawater and mixtures with produced water into
437 North Sea chalk formation: Impact of fluid-rock interactions on wettability and scale
438 formation. J Petrol Sci Eng 2008; 63 (1-4): 23-33.
439 Rao KVK, Naidu SVN and Murthy KS. Precision lattice parameters and thermal expansion of
440 calcite. Journal of Physics and Chemistry of Solids 1968; 29 (2): 245-48.
441 Rosenholtz JL and Smith DZ. Linear thermal expansion of calcite, var. Iceland spar and
442 Yule marble. American Mineral 1949; (34): 846–54.
443 Voake T, Nermoen A, Korsnes RI and Fabricius IL. Temperature cycling and its effect on
444 mechanical behaviours of high-porosity chalks. J Rock Mech Geotech 2019a; 11 (4): 749-59.
445 Voake T, Nermoen A, Ravnas C, Korsnes RI and Fabricius IL. Influence of temperature
446 cycling and pore fluid on tensile strength of chalk. J Rock Mech Geotech 2019b; 11 (2): 277-
447 88.
448 Weiss T, Siegesmund S and Fuller ER. Thermal degradation of marble: indications from
449 finite-element modelling. Build Environ 2003; 38 (9-10): 1251-60.
450 Wu TC, Shen AH, Weathers RS, Bassett WA and Chou IM. Anisotropic Thermal-Expansion
451 of Calcite at High-Pressures - an in-Situ X-Ray-Diffraction Study in a Hydrothermal
452 Diamond-Anvil Cell. American Mineralogist 1995; 80 (9-10): 941-46.
453

Paper IV: Induced shear failure by temperature reduction at uni-axial strain conditions

Voake, T., Nermoen, A., Korsnes, R.I., Fabricius, I.L. (2017)

Tu P027

Induced Shear Failure by Temperature Reduction at Uni-axial Strain Conditions

T. Voake* (University of Stavanger, IOR Centre of Norway), A. Nermoen (University of Stavanger, IOR Centre of Norway), R.I. Korsnes (University of Stavanger) & I.L. Fabricius (Technical University of Denmark)

SUMMARY

This study improvises uniaxial strain condition during cooling by keeping constant overburden, and adjusting radial stress at cooler temperatures in order to re-establish the same radial dimensions prior to cooling. The amount of radial stress reduction by thermal contraction could be sufficient to trigger shear failure. Experiments are performed on Mons chalk and Kansas chalk so the role of induration can be assessed. Calcite thermal expansion is highly anisotropic. Weakening caused by temperature fluctuation could give insight to what gives chalk its strength, cementation, or repulsive electrostatic forces. For each chalk type, shear failure line is determined. The samples are heated to 90oC and loaded to 70% of the axial stress required to induce shear failure. Then the temperature is reduced by 60°C. The change in confining pressure necessary to restore zero radial strain is estimated. The two chalks show different behaviour. Mons demonstrates this cooling would induce shear failure, but has no significant effect on its strength. Kansas, is able to restore uniaxial strain conditions without shear failure. The strength of the Kansas sample was unaffected, however the change in confining pressure needed to restore the uniaxial strain condition decreased with each additional cycle, indicating changing elastic properties.

Introduction

This project aimed at to better understand chalk reservoir stability during water injection. Enhanced oil recovery techniques (EOR) increase the amount of oil that can be extracted from an oil field. New discoveries are becoming harder and more costly to find (Sahrabi et al., 2011), and therefore a lot of research has focused on the recovering techniques to make better use of the discovered reserves by increasing recovery factors. However, sometimes the EOR methods and injected fluid can destabilize reservoirs. A well-known example is the Ekofisk field in the North Sea. Ekofisk is a chalk reservoir that was compacted during production and water flooding, leading to sea floor subsidence (Nagel, 2000). Chalk is a carbonate rock whose particles originate from skeletons of coccoliths algae, mostly made of calcite grains. The grains are held together by contact cement at short distances counteracted by electrostatic repulsion at intermediate distance that is dependent on temperature and brine composition (Nermoen et al., 2016). One factor that could lead to reservoir destabilization, that may have been overlooked so far, is the effect of temperature variation. As cold water is injected into a hot reservoir during water flooding, calcite crystals will be subjected to thermal contraction, and conversely to expansion when reservoir temperature is re-established. Because the thermal expansion coefficient of calcite crystals is strongly anisotropic ($23.6 \cdot 10^{-6}$ K^{-1} along the c-axis and $-5.2 \cdot 10^{-6}$ K^{-1} along a-axes (Rosenholtz and Smith, 1950)), temperature fluctuations can cause considerable deformation of calcitic rocks. Many common examples include the degradation of marble cladding of buildings and monuments which are mineralogically equivalent to chalk but with a different chemical micro-structure, such as the Finlandia Hall in Helsinki which consists of Carrara marble (Royer-Carfagni, 1999).

Many studies have been conducted on how the injected EOR fluid composition which can, for example alter reservoir wettability, a property that defines which fluid preferentially stick to rock surfaces and thereby control the flow of oil and water. The aim of these studies was to extract the previously immobile oil. Other EOR studies focus on enhancing the volumetric sweep by diverging fluids to unswept regions of the reservoirs. Our focus is on understanding how the mechanical properties of chalks are sensitive to temperature changes. Lee et al., 1996 observed that the compressive strength of igneous and metamorphic rocks, as well as Young's and bulk modulus decrease with increasing temperature. These authors conducted experiments on granite and gneiss with increasing temperatures from 25°C to 200°C and report rock strength reduction in both uniaxial and triaxial tests. Similar results were obtained by dos Reis (2012) who studied Polymer mortars, which are used as building materials, and where increasing temperature from room temperature to 90°C resulted in decrease of material compressive strength. Results from Huang and Xia (2015) and Yu et al. (2015) on sandstone mechanical properties suggest strength increase with temperature rise from 20°C to 200°C as a result of original crack closures, but upon further heating to 600°C, weakening was observed. Finally, a study by Madland et al. (2002) on strength comparison of high porosity chalk at 20°C and 90°C was conducted using Brazilian, uniaxial, and triaxial tests, and reported strength reduction, along with 30% reduction of elastic modulus with temperature increase from 20 to 90°C.

This paper concentrates on quantifying how the radial stress was affected by decreased temperature for two different types of chalk. The purpose was to find to what degree Lame's parameter λ decrease upon cooling. This is done by measuring how much the horizontal side stress has to be reduced to keep a constant diameter when a chalk sample was cooled from 90°C to 30°C. The reduction of side stress was performed at constant overburden axial stress and pore pressure. The tests were performed with an overburden stress equal to 70% of the stress required to induce shear failure.

The strength of a rock is commonly defined from the relation between stress and strain and the stress level at which it fails. To calculate a shear failure line, a series of triaxial compression tests were performed at different confining pressures. The effective radial stress $\sigma_r{'}$ relates to the effective confining pressure P_{conf}, as:

$$\sigma_r' = P_{conf} - \alpha P_{pore}, \tag{1}$$

where P_{pore} is pore pressure and α is the Biot coefficient which in the absence of shear velocity data can be estimated from P-wave velocity of the dry sample, v_p and frame density, ρ_{dry}, as:

$$\alpha \approx 1 - \frac{M_{dry}}{M_{min}}, \tag{2}$$

$$M_{dry} = v_{p\_dry}^2 \rho_{dry}, \text{ and} \tag{3}$$

$$M_{min} = K_{calcite} + \frac{4G_{calcite}}{3}, \tag{4}$$

where $K_{calcite} = 70.8$ GPa and $G_{calcite} = 30.3$ GPa (Citations in Mavko et al. 2008).

The effective axial stress is calculated using,

$$\sigma_z' = \sigma_r + f(P_{pist} \cdot m) - \alpha P_{pore}, \tag{5}$$

where f is an area factor relating the cross sectional area of the chamber providing the hydraulic pressure, P_{pist}, of the piston to the cross sectional area of the sample and P_{fric} which is measured during initial piston movement and is round 0.3 MPa. The strain, ε, of a rock is calculated form the original length (L_0) and diameter (D_0) of the sample, and the resulting length L and diameter D during the test,

$$\varepsilon_z = -\frac{L - L_0}{L}, \text{ and } \varepsilon_r = -\frac{D - D_0}{D}. \tag{6}$$

For cylindrical coordinate system of linearly elastic, homogeneous and isotropic materials, Hooke's law describes the relation between stress and strain by,

$$E\varepsilon_r = (1 - v)\sigma_r' - v\sigma_z', \text{ and} \tag{7}$$

$$E\varepsilon_z = \sigma_z' - 2v\sigma_r'. \tag{8}$$

Hence, the stress changes would lead to changes in strain, so **Eq. 7-8** can be rewritten as,

$$E\delta\varepsilon_r = (1 - v)\delta\sigma_r' - v\delta\sigma_z', \text{ and} \tag{9}$$

$$E\delta\varepsilon_z = \delta\sigma_z' - 2v\delta\sigma_r'. \tag{10}$$

Further, if constant overburden is assumed, and hence $\delta\sigma_z' = 0$, the equations can be further simplified, and the change in radial stress $\delta\sigma_r'$ calculated as following,

$$\delta\sigma_r' = \frac{E\delta\varepsilon_r}{(1 - v)}, \text{ and} \tag{11}$$

$$\delta\sigma_r' = -\frac{E\delta\varepsilon_z}{2v}. \tag{12}$$

The strain induced by cooling depends on linear thermal expansion coefficient K_T, and the quantity of temperature change ΔT,

$$\varepsilon_r = K_T^r \Delta T \tag{13}$$

During axial loading with constant side stress, the Poisson's ratio v relates the observed axial and radial strains through,

$$v = -\frac{\varepsilon_r}{\varepsilon_z} \tag{14}$$

From the stress-strain diagram, one can obtain elastic property using **Eq. 15**. Bulk modulus K_{bulk} is measured during hydrostatic loading $\sigma_{hyd} = \sigma_r = \sigma_z$ (only confining pressure acting on the sample, i.e. $P_{pist} = P_{fric}$),

$$K_{bulk} = \frac{\sigma_{hyd}}{\varepsilon_{vol}}, \tag{15}$$

whereas, for cylindrical samples $\varepsilon_{vol} \simeq 2\varepsilon_r + \varepsilon_z$, when higher order terms are omitted.

Similarly, Young's modulus E, is estimated from the slope in the overburden stress as a function of axial strain during axial loading with constant radial stress,

$$E = \frac{\sigma_z'}{\varepsilon_z}. \tag{16}$$

The *p-q* diagram (**Figure 1**) is conventionally used to display sample failure data, which compares maximum shear stress q with mean effective stress p (**Eq. 17-18**). A stress path can be traced as a line in the *p-q* plot, and failure occurs once a failure line is crossed. The combinations of p and q are particularly useful since both are invariant properties of stress tensor such that the position of the failure line can be used in any geotechnical calculation (see discussion in Fjær et al., 2008). Multiple shear failure tests at different confining stresses were performed in order to plot the shear failure line.
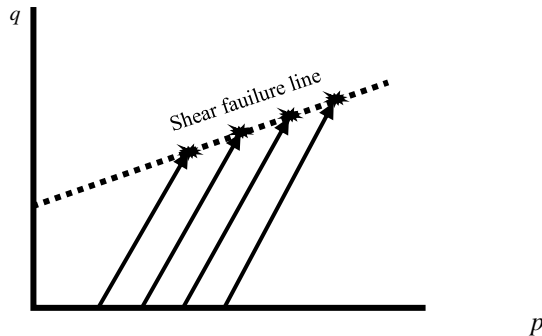
Figure 1 *p-q diagram and direction of deviatoric loading at different confining pressures until shear failure line is reach and the sample fails.*

$$q = \sigma_z' - \sigma_r' \tag{17}$$

$$p = \frac{1}{3} \left(2\sigma_r' + \sigma_z' \right) \tag{18}$$

This project investigates how, after contraction due to cooling from reservoir temperatures, the amount by which side stress acting on the tested material must be reduced in order to re-establish the diameter of the sample prior to cooling, and whether the change of temperature would be sufficient to cause crossing of the failure line. In addition, the project compares how two different chalks behave for the same given conditions.

Material

Two different outcrop chalks with different degrees of induration were used. Properties of the two test samples are listed in **Table 1**. Porosity and solid density were calculated from dry weight and wet weight obtained from saturating the samples with distilled water in a vacuum chamber. Permeability was determined by Darcy's law, using transducers at the triaxial cell to measure pore pressure gradients.

Table 1 *Physical properties of samples tested in this study.*

Sample	Chalk type	Diameter (mm)	Length (mm)	Porosity (%)	Solid density	Permeability (mD)	v_{p_dry} (m/s)	Biot coef.
M-10b	Mons	38.10	73.41	41.1	2.69	0.53	2225	0.93
K-21a	Kansas	38.11	76.20	35.8	2.71	0.48	3060	0.85

The Mons chalk sample from Trivières quarry has a calcite content of approximately 99% and a coccolith mudstone texture. Richard et al. (2005) described Mons chalk as more coccolith fragments than intact coccoliths, and prominent "point-contact fabric" (contact cement) corresponding to the observed induration of H2.

The sample of Kansas chalk has a carbonate content of 97%, and wackestone texture. Cementation and recrystallization are common, which gives grains angular shapes (Megawati et al., 2015) and an induration of H3.

The fluid used in the reported experiments was calcite equilibrated water. The equilibrium water was made by dissolving chalk pieces in distilled water, and then allowed to settle for a day at room temperature. Finally, the solution was filtered using a 0.65 μm filter.

Method

Mechanical testing of the samples was performed in a triaxial cell (**Figure 2**). The cell is equipped with a 1000 W heating jacket controlled by a Omron E5CN PID connected to a Pt-100 RDT resistance temperature detector inside the cell. The precision of the temperature control is approx. ±0.1°C. Three different pumps were connected to the cell, so injection flow rate, confining and piston pressure can be controlled individually through a LabVIEW routine. A back pressure regulator connects on the outlet side of the sample to ensure constant pore pressure, which was set to 0.7 MPa. Confining and piston pressures were applied using hydraulic pumps (Teledyne Isco Syringe Pump model 260D and Quizix model QX-20000 HC pump), while injection flow rate used a Gilson Pump (model 307 HPLC). Vertical displacement of the axial length of the core was measured both externally and internally by two different LVDT's (Low Voltage Displacement Transducer, MHR 500 for external and MHR 250 for internal from Measurments Specialties™). Radial deformation was measured using an extensometer (the circumference changes were detected by LVDT MHR 100 from Measurments Specialties™).
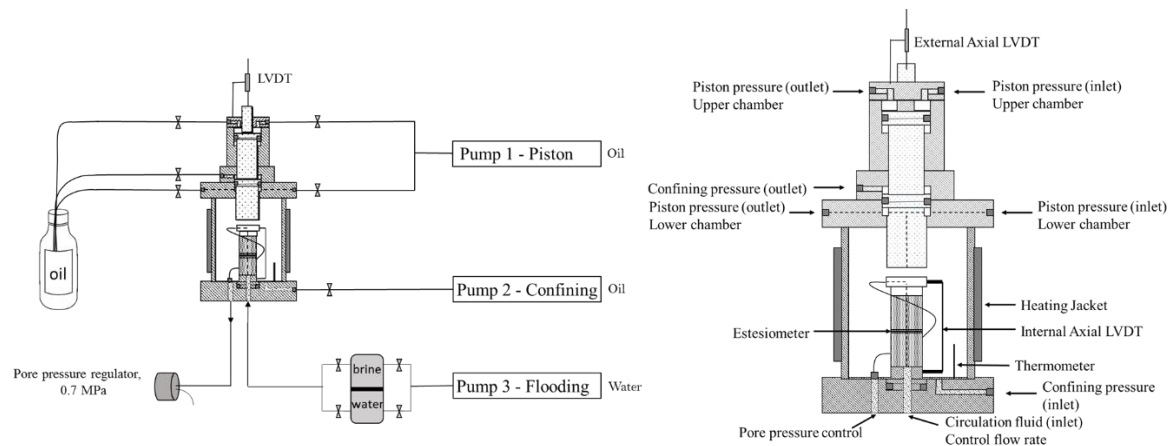
Figure 2 Equipment set up.

Tests determining the shear failure line

Shear failure tests were performed on samples from the same chalk block at different confining pressures. Four different confining pressures were used and the axial stress was increased to failure. Each side stress was tested twice to ensure repeatability of the results. In total, the results of eight individual core tests were used to obtain the shear failure line. The tested confining stresses were 0.8 MPa, 1.2 MPa, 2 MPa, and 3 MPa. All tests were performed at 30°C. Each experiment was performed according to following procedure:
  - Confining pressure was loaded to 0.5 MPa (apart for the tests at 0.8 MPa confining pressure, where the initial loading was set to 0.1 MPa).
  - Samples were flooded with calcite equilibrium water to measure permeability.

- Simultaneously, confining and pore pressure were increased to 1.2 MPa and 0.7 MPa respectively (apart the tests at σ_r =0.8 MPa, where confining and pore pressure was increased to 0.8 and 0.3 MPa).
- The temperature was set to 30˚C and the samples were left until the extensometer obtained a stable reading.
- Piston lowered to touch the sample providing piston friction (P_{fric}) measurement.
- Tests at 0.8 MPa and 1.2 MPa were already at the desired confining pressures. For the tests at 2 MPa and 3 MPa, the confining pressure was loaded to 2 MPa and 3 MPa at the rate of 0.03 MPa/min.
- Deviatoric loading was performed by increasing the piston pressure at a rate of 0.03 MPa/min from zero hydraulic pressure until failure. The *p* and *q* values were calculated using the confining pressure at which the loading was performed and axial pressure which the core failed.

Induced shear failure by cooling test

The aim of this experiment was to measure how much side stress needs to be reduced in order to maintain the same diameter of the sample once temperature was decreased from 90°C to 30°C. The side stress reduction occurred with constant overburden weight (i.e. σ_z const), and to evaluate if this stress would be sufficient to induce shear failure. The deviatoric tests were chosen to be performed at $\sigma_r = 2$ MPa. Before the temperature reduction from 90 to 30°C, the axial stress was chosen to be set to 70% of the value required to induce shear failure. This yield overburden value of σ_z' =5.3 MPa for Mons chalk and σ_z' =11.8 MPa for Kansas chalk. The experimental steps were:
- Confining pressure loaded to 0.5 MPa.
- Saturated samples flooded with calcitic water to measure the differential pressure.
- Simultaneous increase of confining and pore pressure to 1.2 MPa and 0.7 MPa, respectively.
- Set temperature to 90˚C and the experiments were left until the diameter stabilised (between 1-2 days).
- Piston was lowered to touch the sample. During lowering of the piston friction (P_{fric}) could be measured.
- Hydrostatic loading was performed from 1.2 to 2 MPa confining pressure at a rate of 0.03 MPa/min.
- The axial stress was increased to 70% of the shear strength.
- A Labview program that ensures pump control, monitoring and data save, was set up to constant overburden mode such that the piston pressure varied according to σ_r using **Eq. 5**. The test was left to rest for approximately 24 hours, such that a stable diameter was attained.
- Reduced temperature from 90°C to 30°C.
- Confining pressure lowered from 2 MPa to 0.8 MPa in 36 minutes for Mons and 72 minutes for Kansas, or until the target diameter was reached.
- Confining pressure raised from 0.8 MPa to 2 MPa in 36 minutes and temperature increased back to 90°C.
- Last three steps were repeated two more times to investigate the impact of how the mechanical properties of the core reacted to the temperature and stress cyclic behaviour.
- After the last cycle, the sample was deviatoric loaded by increasing the axial stress until failure at $\sigma_r = 0.8$ MPa.
-

Results

The results section is divided into two parts. First, with the aim of loading the sample to 70% of the axial stress required to induce shear failure requires the shear failure line to be known. The results of

eight samples at four different confining pressures for each chalk type are shown here. Second, the dependence of side stress on temperature is initially calculated theoretically using Hooke's law and elastic properties of the sample. Then the experimental results are reported.

Shear failure line

The shear failure line was obtained from eight tests for each chalk type. Samples used for this calculation were from the same blocks as the samples used for the side stress reduction test. The results of eight different samples for each chalk type are presented in **Table 2** and the shear failure lines are visualized at **Figure 3**. Both p and q values are representative of the peak stress points.

Table 2 *Mechanical test results for samples used to plot shear failure lines for Mons and Kansas chalks*

Conf. pressure	Mons chalk			Kansas chalk		
	Sample	*p*	*q*	**Sample**	*p*	*q*
0.8	M-10a	1.8	5.1	K-20a	4.4	12.5
0.8	M-8	1.9	5.1	K-21b	4.1	11.6
1.2	M-4b	2.7	6.2	K-30a	4.7	12.3
1.2	M-9b	2.6	5.9	K-29b	5.7	15.2
2.0	M-5a	3.5	6.3	K-19b	6.8	16.2
2.0	M-5b	3.2	5.2	K-25a	6.3	14.6
3.0	M-3	4.7	6.8	K-25b	8.2	17.4
3.0	M-7	4.6	6.7	K-29a	8.2	17.4
			Stan. dev			Stan. dev
	Slope	0.534	0.144	Slope	1.375	0.128
	Cohesion	4.236	0.471	Cohesion	6.344	0.796
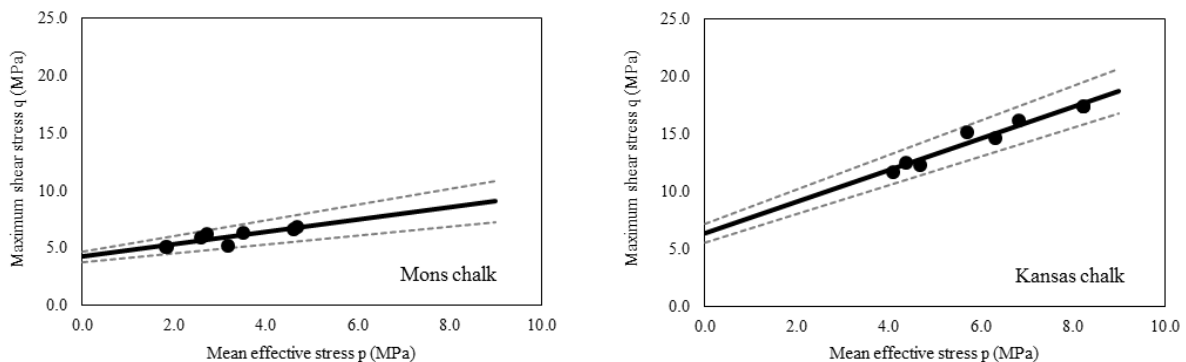
Figure 3 *p-q shear failure line diagram for Mons and Kansas chalk.*

Induced shear failure by cooling test

Three cooling cycles were performed on each of the two cores. The experiments had to be performed in steps and stable readings had to be gained, since significant transient temperature dependent behaviour of the radial strain was observed. After the core diameter had stabilized at 30˚C, confining pressure was lowered in order to match the core diameter reduction due to cooling. **Figure 4** displays the test history of the two core tests and how temperature and side stress was varied along with radial strains (black line in **Figure 4**). The Mons sample almost accumulates zero strain with temperature cycles, while Kansas sample keeps accumulating strain with diameter increasing after each heating and cooling cycle.

Figure 4 *Test history for Mons (a,c) and Kansas (b,d), radial strain (black) is compared with temperature changes (a,b) and stress changes (c,d).*

Within the elastic domain, the amount of side stress reduction required to regain the circumferential diameter relied on the stiffness parameters. Young's modulus of the samples was measured during experimental loading to 70% of the axial stress required to induce shear failure. Bulk modulus was obtained from literature (Megawati et al., 2015), and Poisson's ratio was calculated using
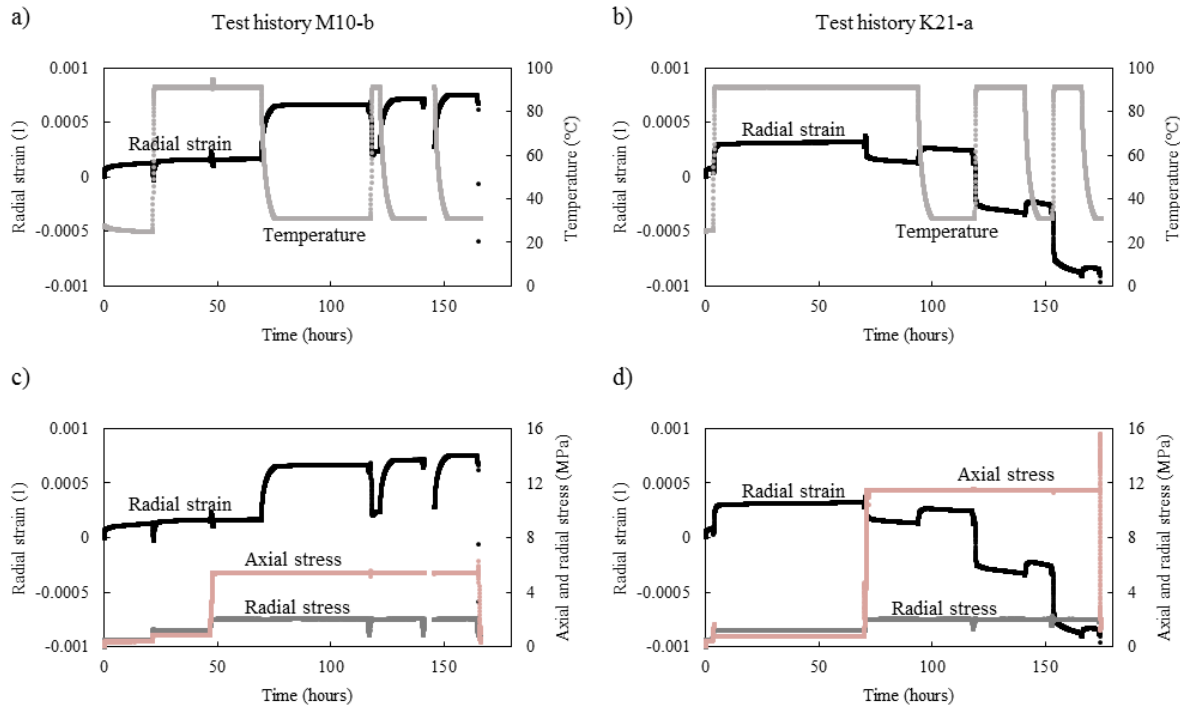
$$E = 3K\,(1 - 2v). \tag{19}$$

In **Table 3** the theoretical value of the confining stress reduction was calculated using a combination of **Eq. 11** and **Eq. 13**. Using the experimental data, thermal contraction K_T^r for Mons chalk was calculated to be $8.4 \cdot 10^{-6}, 8.0 \cdot 10^{-6}$ and $7.9 \cdot 10^{-6} \mathrm{K}^{-1}$ for the three cycles. However, for Kansas chalk the thermal coefficient varied from $1.8 \cdot 10^{-6}$, to $1.2 \cdot 10^{-7}$, and finally $5.5 \cdot 10^{-7}$ K⁻¹ for cycle 1, 2 and 3, respectively. With the given values of E, v and the measured values of K_T^r, stress reduction calculated for Mons were 1.06, 1.01, and 1.0 MPa. For the Kansas core, the thermo-elastic coefficients were not constant for each cycle such that the predicted values of the necessary side stress reduction were 0.36, 0.24 and 0.11 MPa.

Table 3 *Strain and thermal expansion coefficient measured from diameter changes during temperature reduction. *value from (Megawati et al., 2015) for Mons sample saturated with 0.657 M NaCl , as that sample demonstrated the least dissolution. **value from (Megawati et al., 2015) for Kansas sample saturated with distilled water.*

Sample	E (GPa)	K_{bulk} (GPa)	v		ε_r ($\times 10^{-4}$)	K_T^r (K⁻¹)	$\delta\sigma_r'$ (MPa)
M-10b	1.9	0.8*	0.10	Cooling 1	5.0	$8.4 \cdot 10^{-6}$	-1
				Cooling 2	4.8	$8.0 \cdot 10^{-6}$	-1
				Cooling 3	4.7	$7.9 \cdot 10^{-6}$	-1
K-21a	2.7	1.5**	0.20	Cooling 1	1.1	$1.8 \cdot 10^{-6}$	-0.4
				Cooling 2	0.73	$1.2 \cdot 10^{-7}$	-0.2
				Cooling 3	0.33	$5.5 \cdot 10^{-7}$	-0.1

The experimental results of the side stress reduction cycles are presented in **Table 4**. To reach the target diameters at 30°C, the side stress was reduced. For Mons, the side stress was reduced from 2 to the minimum value of 0.8 MPa. Within this stress window the diameter did not regain its value at 90°C. As such, a linear relationship was used between diameter and side stress that enabled to predict side stress reductions of between -8.2 and -8.9 MPa to reach the target diameter (**Table 4**). **Figure 5** is used to represent the corresponding results with respect to stress cycle values of q and p in relation to the shear failure line. For these experiments, the extrapolated values cannot be meaningful because shear failure would occur before zero radial strain is reached, and so the linearity between diameter and side stress would not longer apply (**Figure 5** left).

Kansas chalk however, required less side stress reduction to reach the target diameter. Here, the side stress reduction could be measured directly. It was found that the side stress reduction needed was decreasing with each cycle from $-0.72, -0.44$ to $-0.20 \ MPa$. The experimental values of side stress reduction for Kansas chalk are relatively close to the calculated values in **Table 3**. On the other hand, Mons chalk experimental values were much higher than theoretically predicted.

Table 4 *Extrapolated (*) and measured radial stress change needed to restore diameter prior cooling. For Mons, radial stresses reduction was projected for the desired diameter using linear relationship between side stress changes from 1.2 to 0.8 MPa and diameter change*

	Cooling 1	Cooling 2	Cooling 3
Sample	$\boldsymbol{\delta\sigma_r}$ **(MPa)**	$\boldsymbol{\delta\sigma_r}$ **(MPa)**	$\boldsymbol{\delta\sigma_r}$ **(MPa)**
M-10b	-8.9 (*)	-8.2 (*)	-8.4 (*)
K-21a	-0.72	-0.44	-0.20

The last part of the experiment was to investigate if the maximum shear strength of the sample was affected by the stress and temperature cycles. The red dot in **Figure 5 (left)** displays the shear strength required for the Mons sample. The Kansas chalk (**Table 4**) reaches the target diameter within the allowed confining pressure reduction. The maximum strength at which the sample fails is shown by the red dot in **Figure 5 (right).** Similar to Mons, the maximum shear strength is within the calculated error of the shear failure line (**Figure 3**). This indicate that the combined stress and temperature cycling had no significant effect on strength.
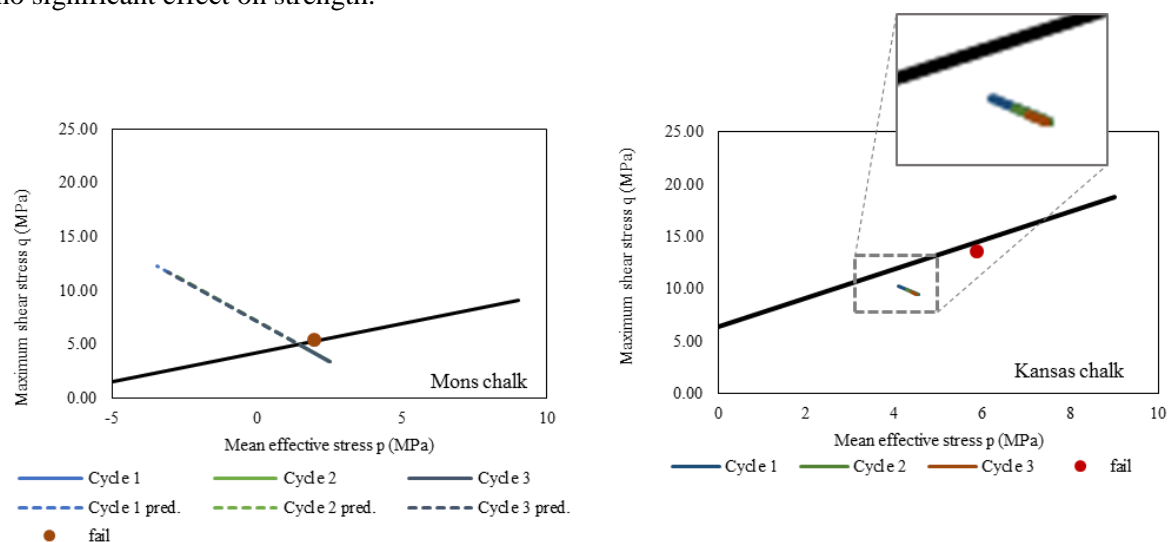

Figure 5 *p-q diagram for Mons chalk (left) and Kansas chalk (right) at uniaxial strain conditions. Mons chalk experience much greater confining pressure reduction than Kansas to reach the target diameter, and hence crosses the shear failure line in order to maintain uniaxial strain condition. Kansas chalk did not cross the shear failure line before the target diameter was reached.*

Discussion

Uniaxial strain tests mimic reservoir behaviour, where the reservoir is free to deform vertically, but is constrained horizontally. During cooling, thermal contraction takes place, and to maintain the constant horizontal dimensions the radial stress must be reduced. This study examined if this change in radial stress was sufficient to cause chalk core failure, and if the behaviour changed as the chalk was repeatedly heated and cooled.

Two chalk types, Mons and Kansas were tested using the same set up and procedure. The impact of temperature was investigated at 70% of yield failure, keeping the side stress at 2 MPa. The axial yield stresses were higher for Kansas than for Mons, and thus were the axial overburden stresses, 11.8 and 5.3 MPa respectively. This lead to a lower stress ratio in Kansas (0.17) than Mons (0.37). This could explain why more permanent strain was accumulated in Kansas during the experiment, and the Mons sample behaved more elastically.

The side stress could only be lowered to 0.8 MPa (0.1 MPa above pore pressure). In order to restore the same diameter after temperature reduction from 90°C to 30°C, the side stress had to be extrapolated for the Mons chalk, and it was sufficient to cross the shear failure line. Kansas chalk, on the other hand, was able to reach uniaxial strain conditions without crossing the shear failure line. The thermal radial contraction reduced from 1.8 to $0.55 \cdot 10^{-6}$ K^{-1} for each cycle. Consequently, the amount of confining pressure reduction decreases with each temperature cycle.

For both samples, the shear strength was not significantly different compared to the samples used to plot the shear failure, which were not exposed to temperature nor stress cycles.

The difference in behaviour of the two chalks may also be due to differing degrees of induration, and the different contributions from the forces that bind the grains together. Potentially, Mons stiffness and strength comes from electrostatic forces, as the temperature cycling does not seem to influence the stiffness and strength of the sample through the test. On the contrary, the contact cementation is more important for the H3 indurated Kansas chalk, as can be seen from the larger change in material property and accumulated strain for each cycle. This could indicate that once cementation is broken it cannot be re-established, resulting in permanent changes.

Conclusion

Two different chalks with different carbonate content and induration were tested in order to examine if temperature reduction could trigger shear failure. The extrapolated value of radial stress reduction for Mons indicates that 60°C temperature decrease was sufficient to cause shear failure while restoring the uniaxial strain conditions. The Mons sample did not demonstrate any change in either the thermal expansion coefficient, elastic stress-strain behaviour or strength due to three temperature and stress cycles. This could indicate that the forces that bind its grains together are at greater distance than the thermal expansion of each grain, and would not play any role in how the chalk is held together. On the contrary, the temperature reduction was not sufficient to cause the Kansas sample to fail, but the temperature cycles caused permanent deformation. This could indicate that the behaviour of Kansas chalk is dictated by forces at shorter distance ranges, such as cementation, and once those bonds were broken due to thermal expansion and contraction, and they did not re-establish.

Acknowledgment

Reference

dos Reis, J.M.L. (2012) Effect of temperature on mechanical properties of polymer mortars. *Materials Research*, **15(4)**, 645-649

Fjær, E., Holt, R.M., Horsrud, P., Raaen, A.M. and Risnes, R. (2008) Petroleum Related Rock Mechanics, volume Developments in Petroleum Science 53. Elsevier Science, 2nd edition.

Huang, S. and Xia, K. [2015] Effects of heat-treatment on the dynamic compressive strength of Longyou sandstone. *Engineering Geology*, **191**, 1-7.

Lee, H.S, Lee, H., Park, Y. and Kwon, K. (1996) The mechanical and hydraulic characteristics of granite and gneiss under temperature variation. *Eurock '96 Barla*, 1371-1377.

Madland, M., Korsnes, R.I. and Risnes, R. (2002) Temperature effects in Brazilian, uniaxial and triaxial compressive tests with high porosity chalk. *SPE Reservoir Evolution and Engineering*, 74711.

Mavko, G., Mukerji, T., Dvornik, J. (2009) The Rock Physics Handbook, Tools for Seismic Analysis of Porous Media. Cambridge University Press, 2nd edition.

Megavati, M., Madland, M.V. and Hiorth, A. (2015) Mechanical and physical behaviour of high-porosity chalks exposed to chemical perturbation. *Journal of Petroleum Science and Engineering,* **133**, 313-327.

Nagel, N.B. (2000) Compaction and subsidence issues within the petroleum industry: Wilmington to Ekofisk and beyond. *Physics and Chemistry of the Earth, Part A: Solid Earth and Geodesy*, **26**, 3-14.

Nermoen, A., Korsnes, R.I., Fabricius, I.L. and Madland, M.V. (2016) Extending the effective stress relation to incorporate electrostatic effects. *Society of Exploration Geophysicists*, 5891149.

Richard, J., Suzun J.-P. and Machhour, L. (2005) Environmental and diagenetic records from a new reference section for Boreal realm: The Campanian chalk of the Mons basin (Belgium). *Sedimetary Geology*. **178**, 99-111.

Rosenholtz, J.L. and Smith, D.T. (1949) Linear thermal expansion of calcite, var. Iceland Spar, and Yule marble. *American Mineralogist*, **34**, 846-854.

Royer-Carfagni, G. (1999) Some considerations on the wrapping of marble facades: the example of Alvar Aalto's Finlandia Hall in Helsinki. *Construction and Building Materials*, **13**, 449-457.

Sahrabi, M., Kechut, N.I., Riazi, M., Jamiolahmady, M., Ireland, S. and Robertson, G. (2011) Safe storage of CO-2 together with improved oil recovery by CO-2 enriched water injection. *Chemical engineering research and design*, **89**, 1865-1872.

Yu, J., Chen, S., Chen, X., Zhang, Y. and Cai, Y. (2015) Experimental investigation on mechanical properties and permeability evolution of red sandstone after heat treatment. *Journal of Zhejiang University - SCIENCE A (Applied Physics and Engineering)*, **16** (9), 749-759.

Paper V: To what degree thermal cycles affect chalk strength

Voake, T., Nermoen, A., Korsnes, R.I., Fabricius, I.L. (2016).

TO WHAT DEGREE THERMAL CYCLES AFFECT CHALK STRENGTH

Tijana Livada[1,3], Anders Nermoen[1,3], Reidar Inger Korsnes[1], Ida Lykke Fabricius[1,2]

[1] University of Stavanger, [2] Technical University of Denmark
[3] The National IOR Center of Norway

This paper was prepared for presentation at the International Symposium of the Society of Core Analysts held in Snow Mass, Colorado, USA, 21-26 August 2016

ABSTRACT

Chalk reservoirs could potentially undergo destabilization as the result of repeated cold water injection into a hot reservoir during water flooding. Preliminary results of an ongoing study are presented in this paper, which compare the impact of temperature cycling on mechanical behavior on dry and water saturated chalk. Sixty disks of dry Kansas chalk exposed to different number of temperature cycles were tested for tensile strength using a Brazilian test. Changes in elastic properties as function of number of temperature cycles of the same chalk, but now saturated in water, were studied using triaxial cell experiments. For dry rock, no significant effects of temperature cycling was found on average tensile strength, however the range of the tensile failure stress is doubled for the samples exposed to 50 temperature cycles, as opposed to those to none. For water saturated cores, the temperature cycling had a significant effect and a significant accumulative irreversible deformation was seen for the core exposed to cyclical temperature variations, so that the elastic bulk modulus consequently increased more than for a core that had been tested at constant temperature. The inconsistency of the results from the two tests suggests the importance of the pore fluid.

INTRODUCTION

Thermal cycling effects are observed on (calcitic) marble cladding, which after being exposed to repeated seasonal change, experience considerable deformation. A famous example is the degradation of marble cladding on the Finlandia Hall in Helsinki [1]. Similar to marble, chalk is mostly composed of calcite. The thermal expansion of calcite is temperature dependent, and very anisotropic [2], so when temperature is increased the grain expands parallel to the c-axis, but also contracts in the perpendicular direction. The deformation observed in marble probably arises due to the combined effect of the expansion of single calcite crystals, the difference in the thermal expansion coefficient and the angle between neighboring crystals. Decoupling of reversible and irreversible processes is another important factor to consider when rock is exposed to stress. The total strain is defined as the sum of the irreversible ε_{irr} and reversible ε_{rev} strain,

$$\varepsilon_{tot} = \varepsilon_{irr} + \varepsilon_{rev}. \tag{1}$$

As plastic deformation accumulates the rock becomes stiffer and harder to further deform, such that the rock is hardened by plastic deformation. This phenomenon is called work hardening.

PROCEDURE

Material

Chalk is a carbonate rock mostly composed of calcitic coccoliths originating from skeletons of algae. The grains in chalk are held together by contact cement and attractive van der Waals forces at short distances between the particles, counteracted by electrostatic repulsion at intermediate distance. These forces are dependent on temperature and brine composition [3-5].

Chalk from Kansas (USA) was used in this study. It is an indurated chalk with wackestone texture. Petrophysical properties of selected samples are listed in Table 1. The average porosity ϕ was calculated to be 34%, permeability was measured to be 0.3 and 0.9 mD, and elastic wave velocity, V_p, around 3000 m/s. The samples thus resemble North Sea reservoir chalk with respect to porosity, permeability, and induration.

Table 1. Petrophysical properties of selected samples for the Brazilian test.

Sample number	# of cycles	ϕ-sat. (%)	Diameter (mm)	Length (mm)	V_p (m/s)	He-gas (g/cm^3)	ϕ-He gas (%)
K1-3	0	35.1	38.09	26.28	2857	2.71	35.7
K1-4	30	33.9	38.10	27.51	3057	2.72	34.9
K2-1	50	34.7	38.09	26.95	2929	2.70	34.7
K2-5	15	30.9	38.09	23.21	3179	2.70	31.2
K4-2	0	34.9	38.10	26.04	2504	2.69	35.0
K5-3	30	34.6	38.10	22.83	2890	2.69	34.6
K6-3	15	33.8	38.08	30.09	2812	2.71	34.4
K7-1	8	34.8	38.08	25.26	2476	2.71	36.0
K8-5	8	32.6	38.10	19.59	3160	2.69	32.5
K10-6	50	33.4	38.13	22.63	2487	2.69	34.4

Brazilian test

Precautions were taken to keep track of the spatial directions in the block to remove any anisotropy effects that would affect direct comparison. Long cores were shaped and cut into disks with diameters double the length. 60 samples were prepared. After drying at 120ºC overnight, each sample was weighed and saturated in a vacuum chamber with distilled water to estimate porosity and solid density. He-gas pycnometry was used to confirm measures of the solid density and porosity. The dried samples were then repeatedly heated and cooled and the effect on the tensile strength in Brazilian tests were investigated. Dry samples were used to single out the effects of temperature fluctuations, without the influence that pore fluids might have.

In Brazilian tests, the tensile strength (T_0) at failure is estimated from the critical force (F) applied by two parallel plates, $T_0 = 2F/\pi DL$, where D and L are diameter and length of the sample. 10 samples were tested directly before any temperature cycling was performed. The other 50 specimens were put in an oven at 135°C for 8h, and then switched off for 16h, allowing the samples to cool. After eight temperature cycles 10 samples were tested, and the rest of the samples were tested after 15, 30 and 50 cycles (see Table 2).

Hydrostatic test

Two cores from the same chalk block were prepared for testing in a triaxial cell, and saturated with calcite equilibrated brine that was prepared by placing chalk pieces in distilled water. The average pH of the brines were 8.7 and the salinity were approx. 300 ppm (ion chromatography). The triaxial cell has two pumps to control the confining pressure (P_c) and fluid pressure (P_f). The cell is additionally equipped with a heating jacket which allows temperature control, as well as with extensimeter and internal LVDT to measure radial and axial deformation of the core. The elastic bulk modulus (K_b) is measured using Equation 3. For both cores, the modulus is calculated for both the loading phase and unloading phase.

$$K_b = \frac{P_c}{\varepsilon_{vol}},\qquad(2)$$

Each core was mounted into the triaxial cell, followed by increasing the P_c to 0.5 MPa. Next, P_f and P_c were increased to 0.7 and 1.2 MPa respectively. Then each core was tested: one was subjected to confining pressure cycling alone, where the temperature was kept constant at 30ºC throughout the test. The second experiment included a temperature cycle for each stress cycle that could be compared to the constant temperature experiment. Each morning, at 30ºC, a confining stress cycle was performed to measure stress-strain behavior and to quantify the elastic bulk modulus. The stress cycle is characterized by a loading phase (1.2→5.2 MPa) and unloading (5.2→1.2 MPa), 30 minutes each way. The bulk modulus was measured as an average during both loading and unloading phase of each cycle, along with the reversible and irreversible strain components. Directly after each stress cycle, the cell-temperature was increased to 130ºC, and six hours later the temperature was reduced back to 30ºC. This procedure was repeated daily to explore the evolution in the strain and bulk modulus for 10 days. An additional 11th cycle was performed on the core, however this cycle did not include the temperature variation. This was done in order to confirm if the effects observed were temperature and not sample dependent.

RESULTS

The results of the Brazilian tests for tensile strength T_0 and the dynamic evolution of the stress-strain behavior during hydrostatic loading are shown here.

Brazilian Test

Average tensile strength for each temperature cycling procedure is presented in Table 2. The average tensile strength does not show any significant response to temperature cycling, however the distribution of the data is significantly broader when the samples have been exposed to temperature cycling. The standard deviation is doubled for samples

Table 2. Average tensile strength failure for the Brazilian tests and their std. dev.

# of cycles	# of tests	T_0 (MPa)	Std. dev (MPa)
0	10	3.10	0.40
8	10	3.07	0.62
15	15	3.30	0.50
30	10	3.32	0.58
50	15	3.08	0.82

exposed to 50 temperature cycles as opposed to those unaged. Figure 1 (a) illustrates the distribution of tensile strengths at which chalk fails. Figure 1 (b) shows that there is no

obvious trend between porosity and the failure strength, indicating that the results obtained are not porosity dependent.
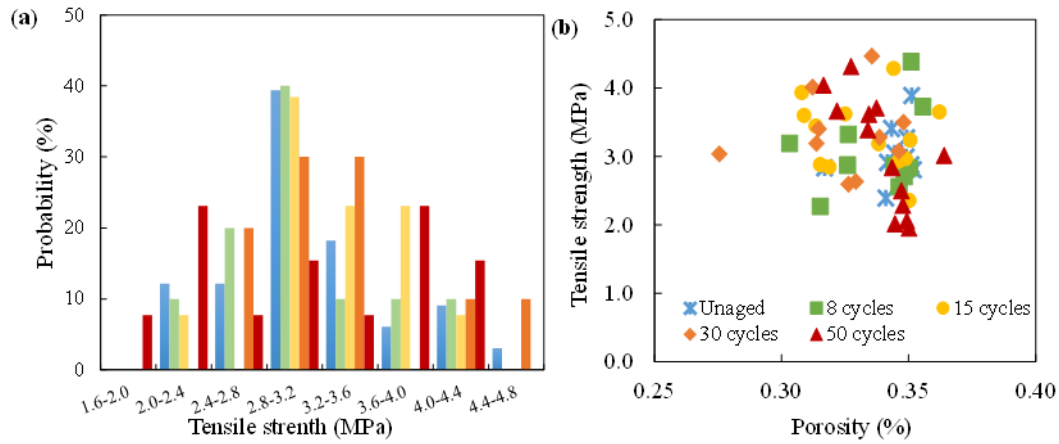

Figure 1. Results from the Brazilian test: (a) probability of the sample to fail within a tensile strength range; (c) Tensile strength shows no dependency on porosity.

Hydrostatic test

The results of the two experiments are presented in Table 3 and Figure 2 (for all values in the figures, but every second in the table). The irreversible fraction of the total strain during each stress cycle $\varepsilon_{irr}/\varepsilon_{tot}$ was calculated by modifying Equation 1, and is shown in Table 3. To ensure the comparability of the results, the first cycle for both experiments was completed without any temperature variation. K_b and the strain fraction for both experiments during loading and unloading phase have similar values. But once the temperature cycling was applied to one of the cores, the fraction is much higher for cycles in the experiment where temperature is varied (Figure 3). The additional 11th cycle proves this effect does not depend on the strain but on the temperature cycling. The K_b of the core with constant temperature increases slightly during loading and decreases slightly during unloading. However, for the core treated with heating/cooling cycles, K_b increases more significantly during loading and unloading as irreversible strain increase.

Table *3*. K_b and irreversible fraction of strain (*additional cycle with const. temp.)

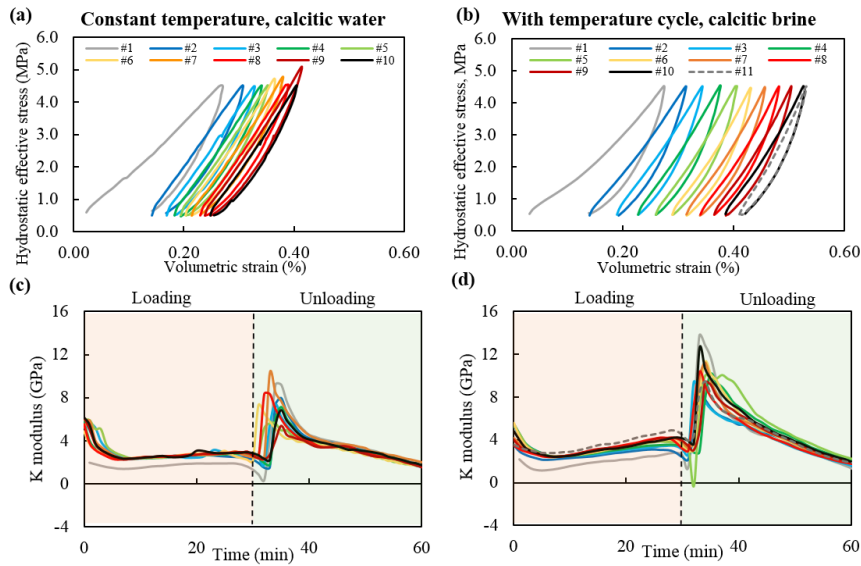| # of cycles	Constant temperature			Temperature cycling		
	K_b load (GPa)	K_b unload (GPa)	$\varepsilon_{irr}/\varepsilon_{tot}$ (%)	K_b load (GPa)	K_b unload (GPa)	$\varepsilon_{irr}/\varepsilon_{tot}$ (%)
1	1.60	3.07	48.2	1.64	2.91	44.1
2	2.44	2.77	14.7	2.26	2.95	28.3
4	2.48	2.71	7.2	2.67	3.40	21.6
6	2.47	2.64	7.0	2.74	3.37	18.0
8	2.50	2.66	5.5	2.79	3.28	17.5
10	2.52	2.55	4.0	2.79	3.58	17.8
11	/	/	/	3.23*	3.43*	2.55*

Figure 2. Hydrostatic test results for constant temperature in the left column (a and c) and with temperature cycling in the right column (b and d). Stress versus volume strain in (a) and (b). Slopes during loading and unloading in (c) and (d).
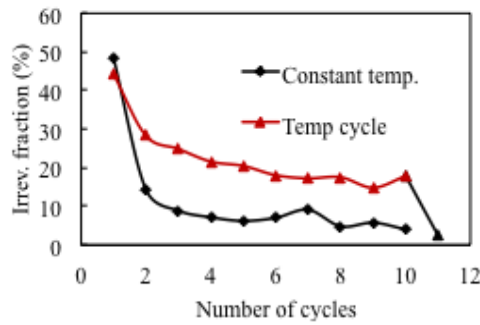

Figure 3. Irreversible strain fraction, $\varepsilon_{irr}/\varepsilon_{tot}$, for individual hydrostatic cycles.

DISCUSSION

Brazilian tensile failure of dry chalk displays no weakening of tensile strength for increasing numbers of temperature cycles, except an increased spread in the tensile strength after 50 cycles (Table 2). For the saturated cores in the hydrostatic tests, the fraction of irreversible strain, $\varepsilon_{irr}/\varepsilon_{tot}$, is significantly higher when temperature has been cycled between each stress cycle (Figure 3). After 10 stress cycles the temperature exposed core accumulates 0.40% total volumetric strain as opposed to the constant temperature core that only accumulated 0.25% (Figure 2 a and b). In fact, the core exposed to the temperature cycling reaches 0.25% irreversible deformation after only 4 cycles. The 11th cycle that was performed with constant temperature, shows that the irreversible fraction drops down to 2.5%, which is comparable to the constant temperature experiment (Figure 3). This shows that the magnitude of the irreversible component is due to the temperature cycling. The evolution of the elastic stiffness during loading and unloading (K_b) with respect to number of cycles is different between the constant temperature and temperature cycle tests (Table 3). K_b during unloading is reduced for the constant temperature while increases for the temperature exposed cores, while K_b during loading increases independent of temperature exposure. In reservoirs,

the accumulation of irreversible deformation alters the pore volume and thus the reservoir permeability. Variations in temperature and effective stresses are expected since injection rates may vary, thus impacting the irreversible strain component. The results from the Brazilian tests and hydrostatic test seem not to show a clear relation between temperature variations and mechanical strength. This may indicate the importance of either the pore fluid, or inconsistencies of mechanical properties tested (tensile vs compaction).

CONCLUSION
Two different tests procedures were performed on Kansas chalk to determine if temperature cycling has an effect on chalk mechanical strength. The Brazilian test on dry samples reveals no significant weakening observed with temperature cycling. Hydrostatic tests show that temperature cycling on water saturated samples has an effect on the reversible and irreversible strain partitioning, and the bulk modulus during loading and unloading. At this point, presented evidence does not univocally show if thermal expansion coefficients play a role in dictating the mechanical strength of chalk.

NOMENCLATURE
ϕ	Porosity	L	Length	K_b	El. bulk modulus
V_p	P wave velocity	D	Diameter	ε_{vol}	Vol. strain
F	Force	P_c	Confining pres.	ε_{irr}	Irr. strain comp.
T_o	Tensile strength	P_f	Pore fluid pressure	ε_{tot}	Total strain

ACKNOWLEDGEMENTS

REFERENCES

[1] Royer-Carfagni, G., "Some considerations on the wrapping of marble façades: the example of Alvar Aalto's Finlandia Hall in Helsinki," *Construction and Building Materials*, (1999), **13**, 449-457.

[2] Rosenholtz, J. L. and D. T. Smith, "Linear thermal expansion of calcite, var. Iceland Spar, and Yule marble," *Am. Mineralogist*, (1949) **34**, 846-854.

[3] Nermoen, A., R. I. Korsnes, I. L. Fabricius, and M. V Madland, "Extending the effective stress relation to incorporate electrostatic effects," *Society of Exploration Geophysicists*, (2015), 5891149.

[4] Megawati, M., A. Hiorth, M. V. Madland, "The impact of Surface Charge on the Mechanical Behavior of High-Porosity Chalk", *Rock Mech. and Rock Eng.* (2013), **46**, 5, 1073-1090.

[5] Røyne, A., K. N. Dalby, T. Hassenkam, "Repulsive hydration forces between calcite surfaces and their effect on the brittle strength of calcite-bearing rocks", *Geophys. Res. Lett.,* (2015), **42**, 4786-4794.